UNIWERSYTET JAGIELLOŃSKI
INSTYTUT FIZYKI

Quantum Fluctuations in Bose Einstein Condensates

Bartłomiej Oleś

PhD Dissertation

Supervisor: **dr hab. Krzysztof Sacha**

Kraków, 2009

Contents

Part I
Introduction

When describing a many body system forming a condensate a product state is usually assumed which reveals all atoms described by the same single particle wavefunction [1, 2, 3, 4]. The fraction of non-condensed atoms is, however, always present [5]. It can be due to a nonzero temperature of the sample, but also at zero temperature interparticle interactions can be responsible for it. We will study only quantum fluctuations neglecting all thermal effects.

All chapters except for the first one discuss systems where quantum fluctuations are included in the many body description, and in fact are pronounced. Those systems are first of all two component condensates where the interplay between the interactions results in reach behaviour [6]. Quantum fluctuations occur close to a quantum phase transition [7, 8]. A critical point marking occurrence of mean field solutions that break symmetry of a trap will be investigated for a condensate with attractive interactions trapped in a one-dimensional symmetric double well potential [9]. Phase transition of a similar origin will be discussed for a condensate in a three dimensional homogeneous case [10] and for a two component system in the double well. In the last chapter self-localized states of impurity atoms immersed in a large condensate are investigated. Only the first chapter is based purely upon the mean field approximation, and deals with a Feshbach resonant molecule production [11], ground state properties and their dynamical production.

Each of the chapters begins with an introduction that presents the state of research in the system under study, motivations and main goals. Conclusions from all the chapters are gathered together at the end of the thesis.

Part II
Atomic - molecular solitons in the vicinity of a Feshbach resonance

A set of quantum numbers defining an internal state of two scattering atoms defines a scattering channel. If a dissociation threshold of an interatomic interaction potential is at lower energy than the energy of two scattering atoms, the atoms are in an open scattering channel. A Feshbach resonance occurs when the energy of a bound state in a closed channel approaches the energy of the scattering atoms. Due to a coupling between the two channels a resonant formation of the bound state takes place [12, 13]. The coupling can be realized by means of optical transitions (*optical* Feshbach resonances [14]) or by atomic hyperfine interactions (*magnetically tunable* Feshbach resonances, see [15]). In the latter, interaction potentials associated with different scattering channels can be shifted with respect to one another by means of an external homogeneous magnetic field, due to the Zeeman effect [16]. It requires a difference in magnetic moments of a bound state and a pair of free atoms.

A signature of resonant pair formation is divergent behaviour of the scattering length which is a relevant parameter of interactions in cold atom collisions

$$a(B) = a_{bg}\left(1 - \frac{\Delta B}{B - B_r}\right), \tag{1}$$

where a_{bg} is an off-resonant value of the scattering length and ΔB is the resonance width. Note that usually the magnetic field value where the scattering length has singularity B_r is different than B_0, magnetic field for which the scattering energy is degenerate with an energy of the bound state [16]. The bound state exists for positive values of the scattering length. In experiments Feshbach resonance position is determined from enhanced atom losses, due to bound state formation and inelastic collisions maximal for the divergent scattering length [17] or from the size variation of the trapped cloud [18].

In some cases tuning of the scattering length is necessary either to produce large condensates or to achieve BEC at all [18, 19, 20]. Feshbach resonance techniques are now widely used as a tool to tune interatomic interactions, from an ideal gas [19] to strongly interacting systems with even an attractive nonlinearity leading to a condensate collapse [21, 22]. Control over interaction strengths made it possible to observe long lived Bloch oscillations in an optical lattice potential [23, 24]. Feshbach resonances in ultracold Fermi gases [25] led to observations of BEC of molecules that are remarkably stable against three body decay [26, 27]. In two component Fermi gases a transition region from fermionic superfluidity $a < 0$ to a molecular condensate $a > 0$ can be studied, and in the so-called BEC-BCS crossover the gas is strongly interacting [28].

In bosonic species coherent oscillations between atom pairs and Feshbach molecules were first observed in a BEC of ^{85}Rb atoms [29]. Molecules were more directly observed in experiments

using magnetic field ramps towards a resonance [30] together with, however, significant inelastic losses [31].

Based upon the mean field description of a Bose Einstein condensate many nonlinear phenomena can be investigated in BEC, for instance vortices [32, 33, 34], four-wave mixing [35, 36], Josephson-like oscillations [37, 38] or solitons. The latter have been realized experimentally in a quasi one-dimensional condensate with effectively attractive interactions (bright solitons) [39, 40] and with repulsive interactions (dark solitons) [41, 42]. There are studies of solitons in BEC with a time-dependent scattering length [43, 44], in condensates confined in an effectively two- or three-dimensional trap [45, 46] or in Bose Fermi mixtures [47]. In periodic optical lattice potentials gap solitons were prepared [48].

In the context of nonlinear optics there exists another type of solitonic solutions. It is a parametric soliton which is formed due to a coupling between electromagnetic fields propagating in a nonlinear medium [49] so that the fields propagate as solitons. In the present chapter we will consider parametric solitons occurring as a result of the coupling between atoms and molecules close to a Feshbach resonance.

Analytical solitonic solutions exist in a free one dimensional Feshbach resonance system of noninteracting atoms. We will show that bright, as well as dark soliton solutions can be found numerically in a quasi-1D trapped interacting system. We will simulate production of soliton-like states in a magnetic field ramp experiment and discuss their subsequent detection [11]. We will qualitatively discuss the problem of atom losses close to the Feshbach resonance.

1 Model

We will use a model commonly applied to the association of atoms into molecules in Bose Einstein condensates, and based upon a description of atoms and molecules in terms of two separate quantum fields [16, 50], $\hat{\psi}_a$ and $\hat{\psi}_m$, respectively,

$$\begin{aligned}\hat{H} &= \int \mathrm{d}^3 r \left(\hat{\psi}_a^\dagger \left[-\frac{\hbar^2}{2m}\nabla^2 + U_a(\vec{r}) + \frac{\lambda_a}{2}\hat{\psi}_a^\dagger\hat{\psi}_a \right] \hat{\psi}_a + \hat{\psi}_m^\dagger \left[-\frac{\hbar^2}{4m}\nabla^2 + U_m(\vec{r}) + \mathcal{E} + \frac{\lambda_m}{2}\hat{\psi}_m^\dagger\hat{\psi}_m \right] \hat{\psi}_m \right. \\ &+ \left. \lambda_{am}\hat{\psi}_a^\dagger\hat{\psi}_a\hat{\psi}_m^\dagger\hat{\psi}_m + \frac{\alpha}{\sqrt{2}} \left[\hat{\psi}_m^\dagger\hat{\psi}_a\hat{\psi}_a + \hat{\psi}_m\hat{\psi}_a^\dagger\hat{\psi}_a^\dagger \right] \right). \end{aligned} \quad (2)$$

In ultra-cold collisions real interatomic potentials that are often unknown precisely can be replaced by a model potential correctly reproducing their crucial properties. We will use a contact pseudopotential parameterized only by the scattering length [51]. Consequently the strength of the atomic, molecular and atomic-molecular interaction is given by the coupling constants proportional to respective scattering lengths

$$\lambda_a = 4\pi\hbar^2 a/m, \quad \lambda_m = 2\pi\hbar^2 a_m/m, \quad \lambda_{am} = 4\pi\hbar^2 a_{am}/m_r. \quad (3)$$

Here m and m_r stand for the atomic and reduced mass, respectively. The scattering lengths a, a_m, a_{am} refer to so-called background scattering lengths, i.e. scattering lengths in an open channel

far from resonances [16]. Since precise values of the molecular and atomic - molecular scattering lengths are known only for very few resonances, we will assume $\lambda_m = \lambda_{am} = \lambda_a$. The trapping potentials for atoms and molecules are $U_a(\vec{r})$ and $U_m(\vec{r})$, respectively. The Hamiltonian (2) contains also a term describing the association and decay of molecules, whose strength depends on the resonance width ΔB, difference between molecular and atomic magnetic moments, $\Delta\tilde{\mu} = \tilde{\mu}_m - 2\tilde{\mu}_a$ and the background scattering length a,

$$\alpha = \sqrt{\frac{4\pi\hbar^2 a \Delta\tilde{\mu}\Delta B}{m}}. \tag{4}$$

In case of a magnetically tunable Feshbach resonance, the magnetic field dependence of the Hamiltonian comes only from the detuning $\mathcal{E}$, the difference between a bound state energy and the energy of a free atom pair. Note that the magnetic field B_0 corresponding to $\varepsilon = 0$ is in general shifted with respect to the magnetic field B_r which reveals the divergent value of the scattering length [16].

In the following we will focus on a Feshbach resonance observed in a ^{87}Rb condensate at the magnetic field $B_r = 685.43$ G. The resonance width is $\Delta B = 0.017$ G, the background scattering length $a = 5.7$ nm and $\Delta\tilde{\mu} = 1.4\mu_B$ [52], where μ_B is the Bohr magneton. Atoms are prepared in an $|f, m_f\rangle = |1, 1\rangle$ entrance channel which is the hyperfine ground state of ^{87}Rb.

We assume a quasi one-dimensional trap, i.e. the transverse confinement so strong that transverse dynamics is reduced to the lowest state in the trap. We take harmonic trapping potentials with frequencies $\omega_{m,\perp} = \omega_{a,\perp} = 2\pi \times 1500$ Hz and $\omega_{m,x} = \omega_{a,x} = 2\pi \times 10$ Hz [1].

With the chosen trap parameters the system is effectively one-dimensional. Throughout the chapter we will apply the mean field approximation replacing the quantum fields in their equations of motion by their expectation values $\phi_a = \left\langle \hat{\psi}_a \right\rangle$, $\phi_m = \left\langle \hat{\psi}_m \right\rangle$. In the units

$$E_0 = \hbar\omega_{a,x}, \quad x_0 = \sqrt{\hbar/m\omega_{a,x}}, \quad \tau_0 = 1/\omega_{a,x}, \tag{5}$$

the dimensionless stationary mean field equations are the following

$$\begin{aligned} \mu\phi_a &= \left[-\frac{1}{2}\frac{\partial^2}{\partial x^2} + \frac{1}{2}x^2 + \lambda_a N\phi_a^2 + \lambda_{am} N\phi_m^2\right]\phi_a + \alpha\sqrt{2N}\phi_m\phi_a \\ 2\mu\phi_m &= \left[-\frac{1}{4}\frac{\partial^2}{\partial x^2} + x^2 + \varepsilon + \lambda_m N\phi_m^2 + \lambda_{am} N\phi_a^2\right]\phi_m + \alpha\sqrt{\frac{N}{2}}\phi_a^2, \end{aligned} \tag{6}$$

where μ is the chemical potential of the system that stems from the conservation of the total number of atoms N in the system. Searching only for ground states we have restricted to real

[1] The same trap frequencies for atoms and molecules are chosen for simplicity. Different frequencies in the transverse directions would lead only to modification of the effective coupling constants in the 1D equations (6). We will see that different frequencies in the longitudinal direction do not introduce any noticeable changes in shapes of solitons as long as the widths of the soliton wavepackets are much smaller than the characteristic length of the traps.

wavefunctions. The magnetic field detuning in the one-dimensional situation is modified by the trap frequencies $\varepsilon = \mathcal{E} + (\omega_{a,\perp} - 2\omega_{m,\perp})/\omega_{a,x} = \mathcal{E} - 150$. The wave-functions $\phi_a(x)$ and $\phi_m(x)$ are normalized so that

$$\int \mathrm{d}x \left(|\phi_a(x)|^2 + 2|\phi_m(x)|^2 \right) = 1. \tag{7}$$

Equations (6) constitute a Feshbach resonance version of the Gross–Pitaevskii equation [1, 2, 3, 4], commonly used for describing almost perfect condensates, i.e. condensates with negligible depletion effects [5]. The model (6) neglects also effects of particle losses due inelastic collisions. They could be introduced via imaginary loss coefficients [53], provided there is an experimental analysis of losses in the vicinity of the Feshbach resonance of interest. The dimensionless 1D coupling constants can be calculated integrating out transverse wavefunctions which were assumed to be ground states of the trapping potentials. For the present choice of the system parameters they have the values

$$\lambda_a = \lambda_m = \lambda_{am} \approx 0.505, \quad \alpha \approx 41.0. \tag{8}$$

The dynamics of the system we will study using time dependent mean field equations

$$\begin{aligned} i\frac{\partial \phi_a}{\partial t} &= \left[-\frac{1}{2}\frac{\partial^2}{\partial x^2} + \frac{1}{2}x^2 + \lambda_a N|\phi_a|^2 + \lambda_{am} N|\phi_m|^2 \right] \phi_a + \alpha\sqrt{2N}\phi_m \phi_a^* \\ i\frac{\partial \phi_m}{\partial t} &= \left[-\frac{1}{4}\frac{\partial^2}{\partial x^2} + x^2 + \varepsilon + \lambda_m N|\phi_m|^2 + \lambda_{am} N|\phi_a|^2 \right] \phi_m + \alpha\sqrt{\frac{N}{2}}\phi_a^2. \end{aligned} \tag{9}$$

2 Soliton-like solutions

A soliton is a special solution to a nonlinear equation, which preserves its shape during time evolution and reveals elastic scattering from another function of its type. Analytic solitonic solutions can be found only for a special choice of the system parameters. Wavefunctions found in other cases numerically, that do not spread in time evolution, we will call soliton-like solutions. We will not study soliton collisions. One can expect that their scattering properties will depend on an amount of the energy involved in a collision, i.e. whether it is high enough to produce also transverse excitations.

2.1 Bright soliton solutions

In the absence of trapping potentials and elastic interparticle interactions the set of equations (6) has an analytical solitonic solution

$$\phi_a(x) = \pm \frac{A}{\cosh^2\left(\frac{x}{l}\right)}, \quad \phi_m(x) = -\frac{A}{\cosh^2\left(\frac{x}{l}\right)}, \tag{10}$$

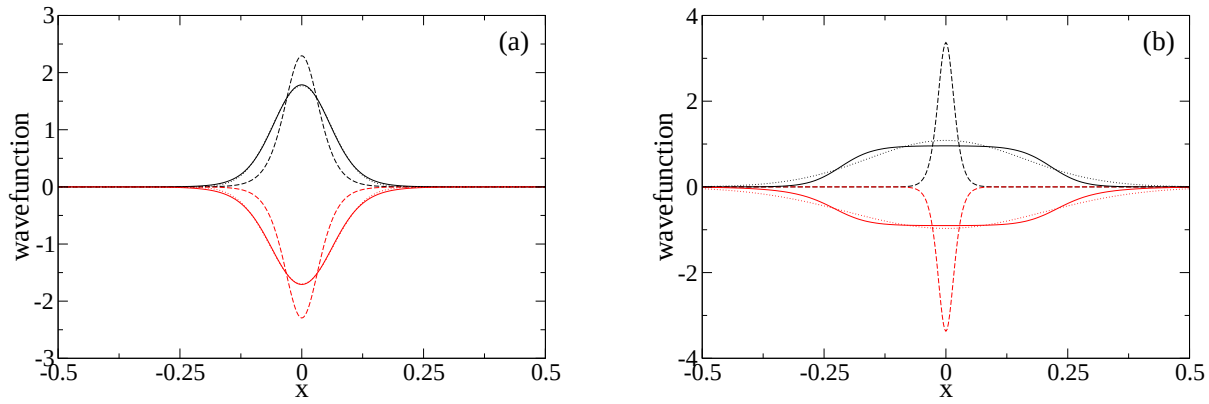

Figure 1: Ground states of the coupled system for $N = 100$ (a) and $N = 1000$ (b). In both panels ϕ_a are marked in black and ϕ_m in red. Ground states of the system (6) found numerically for $\varepsilon = -900.53$ (a) and $\varepsilon = -1505.25$ (b) are drawn with solid lines. Analytic solutions (10) are marked with dashed and variational functions (13) with dotted lines. For $N = 100$ the gaussian approximation is indistinguishable from the exact eigenstate.

where

$$A = \frac{3}{\sqrt{2N\alpha l^2}}, \quad l = \left(\frac{18}{\alpha^2 N}\right)^{1/3}, \tag{11}$$

and the chemical potential $\mu = -2/l^2$. It reveals an equal number of atoms and molecules in the system and is valid for $\varepsilon = -6/l^2$. Solitons (10) have been investigated in nonlinear optics [54] where a classification of solitonic solutions to a set of equations describing a parametric waveguide was provided [55], and it was shown that the same model can describe coupled atomic-molecular condensates [56]. Solutions (10) exist also for a problem of an impurity self-localization in a BEC [57].

Time propagating parametric solitons of width l are given by a solution to the time dependent equations (9)

$$\phi_a(x,t) = \pm\frac{Ae^{ivx}e^{-i(v^2+\mu)t}}{\cosh^2\left(\frac{x-vt}{l}\right)}, \quad \phi_m(x,t) = -\frac{Ae^{2ivx}e^{-2i(v^2+\mu)t}}{\cosh^2\left(\frac{x-vt}{l}\right)}, \tag{12}$$

where v is a propagation velocity.

We have solved the set of equations (6) and (9) numerically and found soliton-like solutions for a broad range of detuning values ε, in general having unequal atom and molecule numbers. Moreover, soliton-like solutions exist also in an interacting system in a trap. The repulsive interactions given by positive values of λ_a, λ_m and λ_{am} compete with the effectively attracting

transfer term. For small particle numbers $N = 100, 1000$ the ground states are hardly influenced by the trap. For particle numbers of the order of $N = 10000$ and higher the shape of a ground state is determined mainly by the interplay between the repulsive interactions and the trapping potential, and is modified by the transfer term. Neglecting the kinetic energy would correspond to the Thomas-Fermi approximation [4].

We have also performed a Gaussian variational analysis [45] taking into account the values (8) and minimizing the system energy for states of the form

$$\phi_a(x) = \tilde{A}e^{-\tilde{a}x^2}, \qquad \phi_m(x) = \tilde{M}e^{-\tilde{m}x^2}. \tag{13}$$

Requiring the same fraction of atoms and molecules, for $N = 100$ ($N = 1000$), we obtain $\tilde{A} = 1.77$, $\tilde{a} = 139.54$, $\tilde{M} = 1.70$, $\tilde{m} = 117.43$, $\varepsilon = -900$ ($\tilde{A} = 1.08$, $\tilde{a} = 19.58$, $\tilde{M} = 0.97$, $\tilde{m} = 12.47$, $\varepsilon = -1429$).

In Fig. 1 we compare exact ground states of the equations (6) found for coupling constants (8) with the solitonic solutions (10) and the variational functions (13). We can see that for a small particle number ($N = 100$) it is the attractive transfer term that dominates, for moderate $N = 1000$ the solitonic approximation is too crude, but the gaussian functions work reasonably well in both cases. Note that the widths of the states are much smaller than the harmonic oscillator ground state width, which indicates that even for a very small particle number the nonlinearities in Eqs. (6) determine the shapes of the states. We have verified the solitonic character of exact solutions performing time evolution in the presence of the transversal trap and with the axial one turned off.

We have taken $\lambda_m = \lambda_a = \lambda_{am}$ for simplicity. The studies of an optical resonance in ^{87}Rb atoms [58] indicate that the atomic-molecular elastic interactions strongly depend on the internal state of a molecule and can even be attractive ($\lambda_{am} < 0$). Negativity of the latter coupling constant should in fact make the solitonic behaviour even more pronounced. Gaussian variational calculation based upon (13) confirms the existence of soliton-like states for $\lambda_m \in (0, 2\lambda_a)$ and $\lambda_{am} \in (-2\lambda_a, 2\lambda_a)$ (for $N = 1000$), which shows that the choice of equal coupling constants is not essential in order to deal with soliton-like solutions.

All stationary states of the Gross-Pitaevskii equations (6) have been obtained numerically by means of the imaginary time evolution method, which implies that the obtained ground states are dynamically stable.

2.2 Two bright solitons and dark soliton solutions

In the absence of trapping potentials and interparticle interactions an asymptotic double soliton solution can be found

$$\begin{aligned} \phi_a(x) &= \frac{A}{\cosh^2\left(\frac{x-q}{l}\right)} \pm \frac{A}{\cosh^2\left(\frac{x+q}{l}\right)} \\ \phi_m(x) &= -\frac{A}{\cosh^2\left(\frac{x-q}{l}\right)} - \frac{A}{\cosh^2\left(\frac{x+q}{l}\right)}, \end{aligned} \tag{14}$$

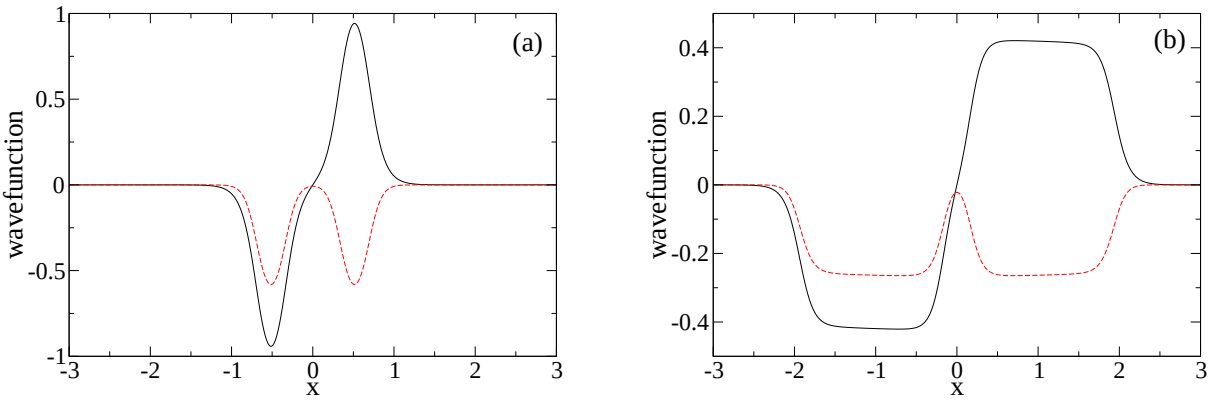

Figure 2: Double bright soliton solutions in a trapped interacting system for $N = 100$ (a) and $N = 1000$ (b), $\varepsilon = 0$. In both panels ϕ_a are represented by black solid lines and ϕ_m by red dashed ones.

valid for $q \gg l$, where

$$l = \left(\frac{36}{\alpha^2 N}\right)^{1/3}, \quad A = \frac{3}{\sqrt{2N}\alpha l^2}, \tag{15}$$

and $\mu = -2/l^2$, $\varepsilon = -6/l^2$. Due to symmetry of Eqs. (6) the atomic wavefunctions can be even or odd, whereas the molecular ones must be even (because of the ϕ_a^2 term).

Using the first excited state of the harmonic potential as an initial state for imaginary time evolution makes it possible to numerically find stationary states of the form (14). We have found double solitonic states also in the interacting system (8) in the trap, and for unequal atom and molecule numbers, see Fig. 2. Note that the widths of the states in panel (a) are much smaller than the first excited state width of the harmonic oscillator, which indicates that also here it is the nonlinearities that determine the shapes of the states.

With an increasing number of particles the healing length defined as

$$\xi = \frac{1}{\sqrt{\lambda_a N \left(|\phi_a|^2 + |\phi_m|^2\right)}}, \tag{16}$$

becomes much smaller than the spatial extent of the two-solitonic state. This, in addition to the phase flip along the atomic wavefunction makes density profiles resemble those of dark solitons known for condensates with repulsive interactions [41, 42]. Applying in (6) the Thomas Fermi approximation and using dark soliton profiles, an exact eigenstate can be approximated by the wavefunctions

$$\phi_a(x) \approx \phi_a^{\mathrm{TF}}(x) \tanh\left(\frac{x}{\xi}\right),$$

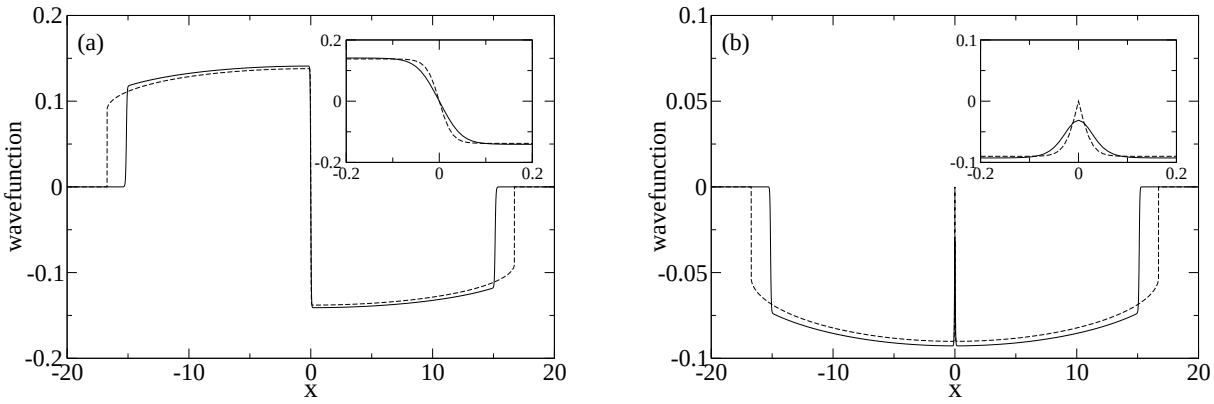

Figure 3: Dark soliton approximation (dashed lines) to eigenstates of (6) (solid lines) for $N = 10^5$. Panel (a) shows the atomic whereas panel (b) the molecular wavefunctions. The insets show a central region of the order of the healing length.

$$\phi_m(x) \approx \phi_m^{\mathrm{TF}}(x) \left| \tanh\left(\frac{x}{\xi}\right) \right|, \tag{17}$$

where

$$\begin{aligned} \phi_m^{\mathrm{TF}}(x) &= \frac{\gamma}{2} - \sqrt{\frac{\gamma^2}{4} + \frac{2\mu - x^2}{6\lambda_a N}}, \\ \phi_a^{\mathrm{TF}}(x) &= \sqrt{\frac{2\mu - x^2}{2\lambda_a N} - \frac{\sqrt{2}\alpha}{\lambda_a\sqrt{N}}\phi_m^{\mathrm{TF}}(x) - [\phi_m^{\mathrm{TF}}(x)]^2}, \\ \gamma &= \frac{\sqrt{2}}{3\alpha\sqrt{N}}\left(\frac{x^2 - 2\mu}{2} - \frac{\alpha^2}{\lambda_a}\right). \end{aligned} \tag{18}$$

The corresponding chemical potential can be found from the normalization condition (7) (see Figure 3).

2.3 Center of mass oscillations in a trap

In the case of a harmonic trap (with equal trapping frequencies for atoms and molecules), having any solutions $\phi_{a0}(x)$ and $\phi_{m0}(x)$ of the time-independent problem (6), corresponding to the chemical potential μ, one can find harmonic oscillations of the center of mass of the particle cloud described by translated functions $\phi_{a0}(x-q)$ and $\phi_{m0}(x-q)$. The time evolution is given by

$$\phi_a(x,t) = \phi_{a0}(x-q)e^{-i\mu t}e^{i[\dot{q}x - S(q)]},$$

$$\phi_m(x,t) \;=\; \phi_{m0}(x-q)e^{-i2\mu t}e^{2i[\dot{q}x-S(q)]}, \tag{19}$$

where

$$S(q) = \frac{1}{2}\int_{t_0}^{t} \mathrm{d}t' \left[\dot{q}^2(t') - q^2(t')\right], \tag{20}$$

and

$$\frac{\mathrm{d}^2 q}{\mathrm{d}t^2} + q = 0. \tag{21}$$

The proof can be done by direct substitution of (19) into (9).

This indicates that, similarly as in the case of the Gross-Pitaevskii equation for a single condensate in a harmonic trap, time evolution of the translated stationary solutions reveals harmonic oscillations of the center of mass of the particle cloud.

3 Simulations of an experimental production

Molecule observation in magnetically tunable Feshbach resonances can be achieved using two experimental schemes. If we start with a pure atomic condensate, a rapid change of the magnetic field towards its resonant value and back produces a quantum superposition state of atoms and molecules, i.e. an atom - molecule coherent state. Consequently a number of atoms in the atomic fraction oscillates with a frequency corresponding to the molecular binding energy [29, 50, 59]. In the other technique the magnetic field is slowly varied in the direction from negative to positive scattering lengths so that an initial state adiabatically follows ground states close to a resonance [30, 31, 50, 60]. For the Feshbach resonance under study this requires a magnetic field to be rapidly changed to an above resonance value (where $a < 0$) before an actual molecule production.

3.1 Production of soliton-like ground states

We assume that the condensate has already been prepared in its ground state far above the resonance, i.e. $B \gg B_0$, where the amount of molecules is very small. The timescale of a molecule production has to be carefully chosen. It should be long enough to preserve the adiabaticity so that we would end up in a solitonic ground state, but also short enough in order not to make loss processes dominant.

We consider a ^{87}Rb condensate around the Feshbach resonance at $B_r = 685.43$ G and of the width $\Delta B = 0.017$ G. We have studied production of soliton-like states for N in the range between 100 and 10000. As initial states we took ground states of the model (6) for $\varepsilon = 3331$ and performed time integration of equations (9) assuming different ramp speeds of linear magnetic field changes. The final detuning value was $\varepsilon_{end} = 0$ (so the total change in the magnetic field value was $B = \Delta B = 0.017$ G), which was motivated by smaller expected losses for the magnetic

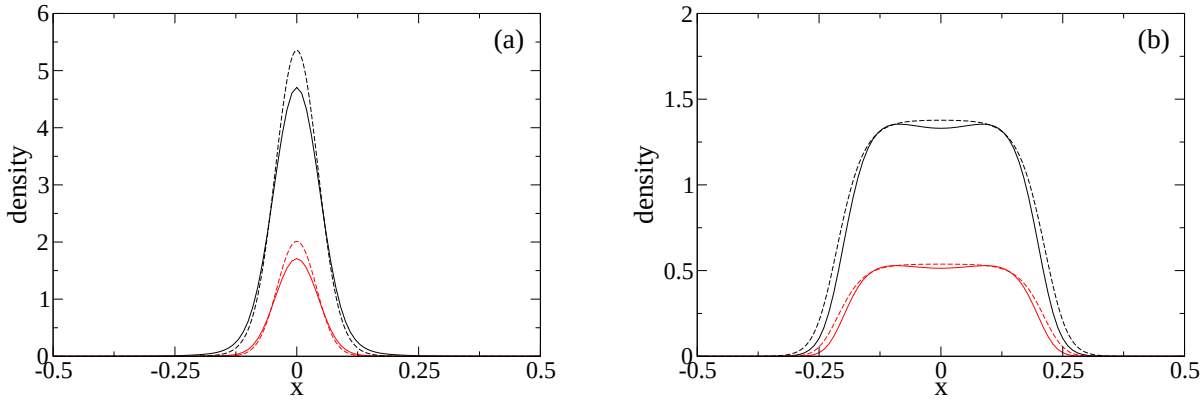

Figure 4: Density profiles of solitons produced after 95.5 ms of the magnetic field sweeping for $N = 100$ (a) and after 93.8 ms for $N = 1000$ (b) – solid lines. Dashed lines show exact ground states corresponding to the magnetic field at the end of the sweeping. In each panel, the black curves represent atoms and the red ones molecules. The norm in the time evolution is preserved on the level of 10^{-5}. The simulated state contains tiny excitations outside the center, not shown in the Figure.

field off the resonance center (i.e. $B_{final} > B_r$) and the fact that ground states for $\varepsilon = 0$ already reveal soliton-like behaviour. The fraction of atoms in the initial states, $\int |\phi_a|^2$, was 99% and 93% for $N = 100$ and $N = 10000$, respectively.

The square overlap between final states from the time evolution and the corresponding ground states in the trap depends nonlinearly on the evolution time. We have found that it approaches unity for evolution times longer than 90 ms, which should be an experimentally accessible timescale [31]. Figure 4 shows simulated soliton-like states that reveal square overlaps 0.94 and 0.92 with exact ground states for the final detuning value, for $N = 100$, $t_{evol} = 95.5$ ms and $N = 1000$, $t_{evol} = 93.8$ ms, respectively. For $N = 10000$ the shortest evolution time that results in a reasonably high squared overlap (i.e. 0.83) is 90.7 ms.

Evolution times shorter than the ones mentioned above might also prove useful. Final states after such nonadiabatic evolution reveal a soliton train structure similar to soliton trains observed in an attractive ^7Li [40]. Figure 5 shows a state produced during 25.5 ms in a system of $N = 1000$ atoms. Actually stationary multi-peak soliton solutions should exist for an arbitrary number of peaks. Unfortunately it is not possible to obtain them by means of the imaginary time evolution method. The symmetry properties of the set (6) make an initial state collapse to the ground or the first excited state having the number of peaks equal to 1 and 2, respectively. The state in Fig. 5 contains one or several excited soliton-like states in the 1D trapping potential.

Solitons created in a quasi-1D trap can be experimentally verified when an axial trap is turned off and the measured wavepackets propagate without spreading [39, 40]. We have confirmed that

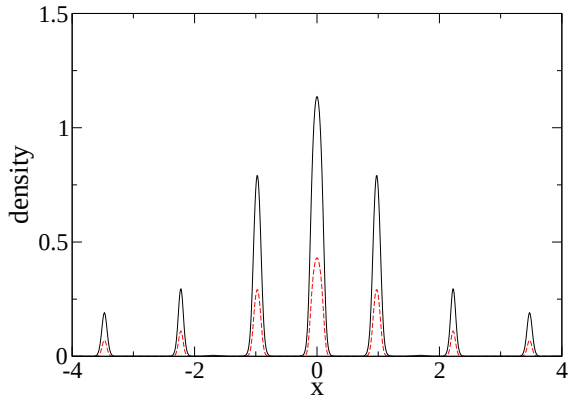

Figure 5: Soliton train obtained for $N = 1000$ after 25.5 ms magnetic field sweeping. Solid black line represents the atomic while the dashed red one the molecular density.

soliton-like states produced in the simulations (such as those presented in Fig. 4) preserve their shapes without axial trapping within the time 100 ms that was chosen in the simulations.

3.2 Atom losses

One of the signatures of a Feshbach resonance is an enhanced loss rate of atoms when approaching a resonance value [17]. Atom loss processes can be due to two or three body collisions. Two body inelastic collisions which are significant in a ^{85}Rb Feshbach resonance [61] are absent in Feshbach resonances of ^{87}Rb atoms in the $|1,1\rangle$ ground state, which is the case here. Three atoms can scatter to form a molecule and an atom carrying away the excess energy. Both can escape from the trap if their kinetic energy is high enough [62]. Molecules produced by means of a Feshbach resonance are often produced in high vibrational states, which makes them prone to deexcitation or dissociation to noncondensed atoms and possibly a trap escape [63, 64].

Experimental analysis of atom losses is often not straightforward since usually only atoms can be detected. Conversion of atoms into molecules at the broadest resonance in ^{87}Rb, subsequent separation of the two species by means of a Stern-Gerlach field (i.e. a magnetic field gradient) and conversion back, reveals a 63% atom loss due to inelastic collisions [31]. In the systematic studies [52] the fraction of atoms lost during a 50 ms hold time at the center of $B_r = 685.43$ G resonance is 78%. There, however, the detection scheme is different. After the 50 ms hold time the magnetic field is rapidly switched off, the condensate is released from a trap and after another 14 ms the atomic fraction is detected. Most probably not all molecules formed in the experiment are dissociated back to atoms, therefore the estimated loss rate is *an upper limit* to an actual inelastic loss rate. We estimate central densities of particles at resonance in [52] and in our simulations to be of the same order of magnitude, 10^{15} cm^{-3}. This is because on one hand we

have taken much smaller particle numbers (maximum of 10^4 compared to $N = 4 \times 10^6$ in [52]), but the strong transverse confinement necessary to achieve solitons increases the density with respect to the 3D situation in [52]. A possible way to reduce the peak density could be to reduce the transverse confinement as much as possible. We have checked that even in a transverse trap with a frequency $2\pi \times 200$ Hz the condition for a quasi-1D configuration is fulfilled. The crucial idea of how to reduce the losses is to finish the time evolution off-resonance, at a magnetic field already supporting soliton-like states.

Actually, if atoms escaping from a trap do not excite the trapped mixture, solitons can exist even in the presence of losses. This is because the attractive "solitonic" coupling comes from the transfer term scaling as $\sqrt{N}$ whereas interactions scale as N with the total particle number. The focusing effect of the former should in fact be enhanced by losses.

In conclusion to this section, inelastic losses although significant close to the Feshbach resonance that we are studying, should not prohibit the opportunity of observing atom-molecule solitons. More experimental data and precise theoretical models would be necessary to study the losses near the Feshbach resonance that we have chosen.

4 Time evolution in an inhomogeneous magnetic field

As already mentioned in the previous section, a magnetic field gradient is often used to separate atoms and molecules, such as it was done in a 3D setup [31]. We will show that the separation effect resulting from different magnetic moment values can be suppressed by the strong coupling in (6) that is responsible for the solitonic states. In the present section we will assume a more general version of the time evolution equations (9). The magnetic field is now given by two parameters, B, that tells us how far from the resonance we are, and B_{grad} which is responsible for the magnetic field gradient. Using the units (5) we have

$$\begin{aligned} i\frac{\partial \phi_a}{\partial t} &= \left[-\frac{1}{2}\frac{\partial^2}{\partial x^2} + \frac{1}{2}x^2 + \frac{\tilde{\mu}_a}{E_0}(B_{grad}x_0 x + B) + \lambda_a N|\phi_a|^2 + \lambda_{am}N|\phi_m|^2\right]\phi_a + \alpha\sqrt{2N}\phi_m\phi_a^* \\ i\frac{\partial \phi_m}{\partial t} &= \left[-\frac{1}{4}\frac{\partial^2}{\partial x^2} + x^2 + \frac{\tilde{\mu}_m}{E_0}(B_{grad}x_0 x + B) + \lambda_m N|\phi_m|^2 + \lambda_{am}N|\phi_a|^2\right]\phi_m + \alpha\sqrt{\frac{N}{2}}\phi_a^2. \end{aligned} \quad (22)$$

Note that equations (9) correspond to the situation where $B_{grad} = 0$. It is possible to transform these equations so that the magnetic field is present only in one of them. First, a coordinate transformation $x \to x + \beta_a$ can be applied. Then, phases of the wavefunctions are adjusted according to

$$\phi_a \to \phi_a \exp\left(\frac{i}{2}\left(\beta_a^2 - \frac{\tilde{\mu}_a B}{E_0}\right)t\right), \quad \phi_m \to \phi_m \exp\left(i\left(\beta_a^2 - \frac{\tilde{\mu}_a B}{E_0}\right)t\right), \quad (23)$$

where $\beta_a = x_0\tilde{\mu}_a B_{\rm grad}/E_0$, and the equations (22) take finally the form

$$i\frac{\partial \phi_a}{\partial t} = \left[-\frac{1}{2}\frac{\partial^2}{\partial x^2} + \frac{1}{2}x^2 + \lambda_a N|\phi_a|^2 + \lambda_{am}N|\phi_m|^2\right]\phi_a + \alpha\sqrt{2N}\phi_m\phi_a^*$$

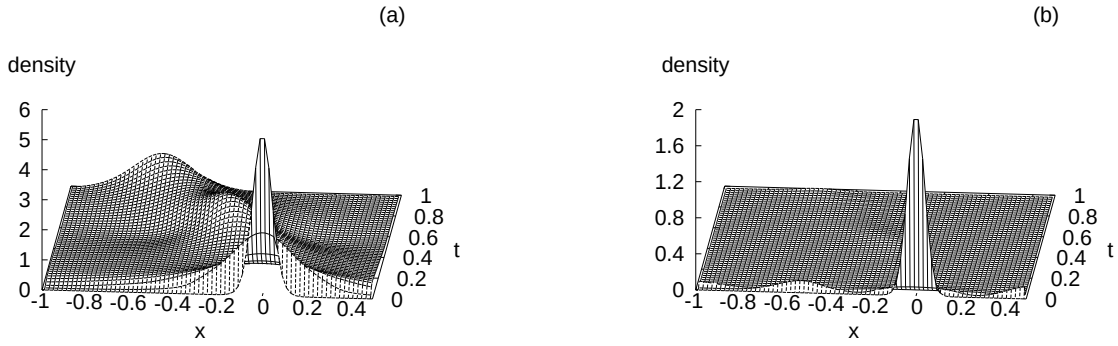

Figure 6: Time evolution of an initial soliton-like state for $N = 100$ in a magnetic field gradient $B_{\rm grad} = 1$ G/cm, for the detuning $\varepsilon_{\rm grad} = 2216$ (Eq. (26)). Panel (a) shows the atomic wavepacket, whereas panel (b) the molecular one. The time $t = 1$ corresponds to 15.9 ms.

$$i\frac{\partial\phi_m}{\partial t} = \left[-\frac{1}{4}\frac{\partial^2}{\partial x^2} + x^2 + \beta x + \varepsilon_{grad} + \lambda_m N|\phi_m|^2 + \lambda_{am} N|\phi_a|^2\right]\phi_m + \alpha\sqrt{\frac{N}{2}}\phi_a^2, \qquad (24)$$

where

$$\beta = \frac{x_0\Delta\tilde{\mu}}{E_0}B_{\rm grad}, \qquad (25)$$

and the parameter

$$\varepsilon_{\rm grad} = \varepsilon - \left(\frac{x_0}{E_0}B_{\rm grad}\right)^2 \tilde{\mu}_a\Delta\tilde{\mu}, \qquad (26)$$

can be regarded as an effective detuning, modified with respect to the case without gradient (given by ε). As initial states for the time evolution without the axial trapping but with the transverse traps present we have taken ground states of the system (6) for $\varepsilon = 0$ and particle numbers $N = 100$ and $N = 1000$. As we can see from (26) a sudden turn-on of a 1 G/cm magnetic field gradient modifies the detuning to $\varepsilon_{grad} = 2216$. We have studied the time evolution with that value, but checked also what happens for a magnetic field such that $\varepsilon_{grad} = 0$.

In the former case molecules are generally converted back to atoms, see Fig. 6 and 7, which is not surprising because of the positive value of the effective detuning. On the evolution timescale $t_{evol} = 15.9$ ms, almost all of the initial $N = 100$ particles end up as individual atoms, the attractive coupling provided by the atom-molecule transfer term practically disappears, and consequently the atomic wavefunction ϕ_a begins to spread. For $N = 1000$ during the same evolution time the coupling term is effectively stronger and its competition against the gradient results in the wavefunction splitting and soliton train production (see Fig. 7). Similar splitting

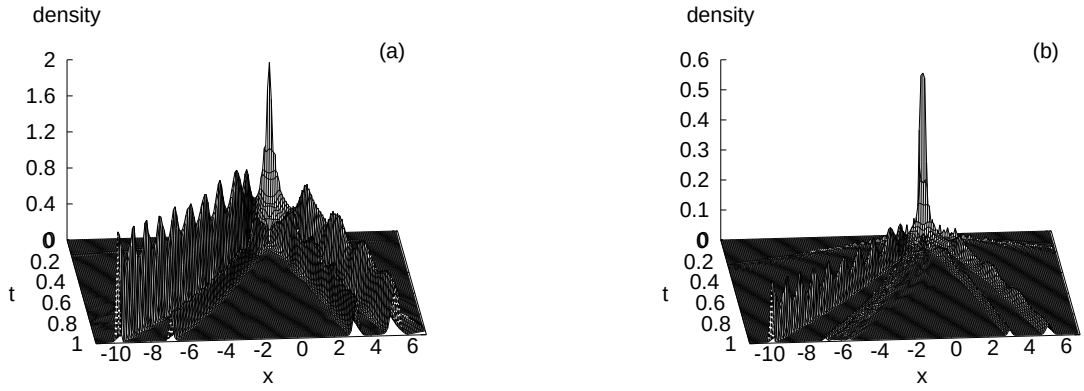

Figure 7: Time evolution of an initial soliton-like state for $N = 1000$ in an inhomogeneous magnetic field $B_{\rm grad} = 1$ G/cm, for the detuning $\varepsilon_{\rm grad} = 2216$ (see Eq. (26)). Panel (a) shows the atomic wave-packet, whereas panel (b) the molecular one. The time $t = 1$ corresponds to 15.9 ms.

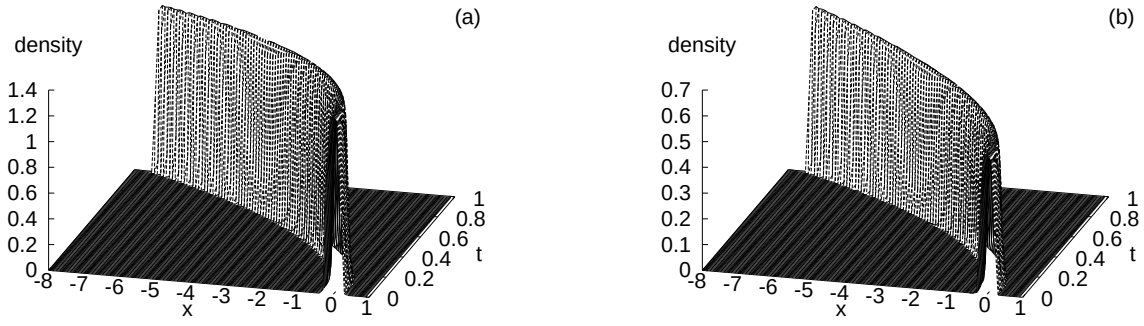

Figure 8: Time evolution of an initial soliton-like state for $N = 1000$ in a magnetic field gradient $B_{\rm grad} = 1$ G/cm, for the detuning $\varepsilon_{\rm grad} = 0$ (see Eq. (26)). Panel (a) shows the atomic wave-packet, whereas panel (b) the molecular one. The time $t = 1$ corresponds to 15.9 ms.

of solitonic wavepackets has been analyzed in the case of a single component BEC in the presence of the gravitational field [65].

In the case with $\varepsilon_{grad} = 0$ we are effectively on the molecular side of the resonance, the transfer (coupling) term dominates over the splitting effect caused by the gradient, and as can be seen in Figure 8, the soliton-like state propagates without loosing its shape or splitting to smaller wavepackets. A closer look on the Figure 8 reveals a slow conversion of atoms into molecules.

For a higher field gradient than the value chosen in the simulations shown in figures 6-8 or for slightly different values of the elastic interaction coupling constants λ_a, λ_m, λ_{am}, we have observed qualitatively similar behaviour, i.e. no separation to atomic and molecular clouds, as well as the relevance of the ε_{grad} value. We attribute this behaviour to the strongly confined quasi-1D geometry.

Part III
Density fluctuations and phase separation in a two component BEC

Soon after first experiments that produced a Bose Einstein condensate [66, 67, 68] atoms in two different hyperfine states were simultaneously trapped in a magnetooptical trap and subsequent cooling produced a double condensate [69]. Application of optical traps made it possible to investigate spinor condensates where spin changing collisions do not lead to atom escape from a trap [70]. With the additional degree of freedom spin domains could be observed [70, 71] and various magnetic phases in optical lattice potentials were studied theoretically [72]. Collective oscillatory modes were studied in a condensate composed of two different atomic species produced by means of sympathetic cooling [73]. Quantum phase transitions in Bose-Fermi mixtures were observed [74, 75].

In a double condensate system atom interferometry experiments were performed [76] where dynamics of the relative phase was investigated [76, 77]. It was shown that two condensates can repel each other and spatially separate, one forming a shell around the other [78]. The binary atomic condensate systems and phase separation were discussed within the mean field theory [79, 80, 81] and dynamical instabilities leading to phase separation were identified from linearized equations of motion [82]. Phase separated configurations breaking the symmetry of a trap were also found [83, 84, 85, 86].

Ideal condensates are sufficiently well described within the mean field theory and a corresponding Gross-Pitaevskii equation [4]. The Bogoliubov theory [87] is usually applied (i) to test for the dynamical stability of mean field solutions; (ii) to find collective excitations such as dipole oscillations in a trap [4]; (iii) to study a quasiparticle excitation spectrum; (iv) and finally to check the initial assumption of all particles occupying the same single particle mode.

In the Bogoliubov theory small quantum corrections to a mean field solution are introduced. A key idea of the original Bogoliubov theory [87] is a $U(1)$ symmetry breaking assumption that an atomic field operator has a nonzero expectation value. Such a *coherent* state involves superposition of states with different numbers of atoms, which is in principle far from the experimental reality. Moreover, a careful analysis shows that it involves an eigenvalue problem of an operator which is not diagonalizable. Consequently the theory must break down in finite time [51, 88].

A number conserving version of the Bogoliubov theory overcomes the above problems [89, 90, 91]. It should give the same results for large particle numbers. There are, however, examples where the N-conserving theory works in a regime of the standard approach breakdown [92].

Generalization of the Bogoliubov theory to homogeneous double condensate systems was done in [93, 94] and for the number conserving version in [95].

In the present chapter we will study a homogeneous two component condensate using the number conserving Bogoliubov theory. We will derive the system ground state in the particle

representation in the presence of intra- and intercomponent interactions. Based upon the Bogoliubov vacuum state we will show that in a finite system the phase separation is followed by significant long wavelength density fluctuations.

5 Two component Bose Einstein condensate

We consider a two component Bose-Einstein condensate formed by a mixture of two kinds of atoms (or the same atoms in two different internal states), i.e. N_a atoms of type a and N_b atoms of type b [96]. The Hamiltonian of the system reads

$$\begin{aligned}\hat{H} &= \int d^3r \left(\hat{\psi}_a^\dagger \left[-\frac{\hbar^2}{2m_a}\nabla^2 + V_a(\vec{r}) + \frac{g_a}{2}\hat{\psi}_a^\dagger\hat{\psi}_a \right] \hat{\psi}_a \right. \\ &+\hat{\psi}_b^\dagger \left[-\frac{\hbar^2}{2m_b}\nabla^2 + V_b(\vec{r}) + \frac{g_b}{2}\hat{\psi}_b^\dagger\hat{\psi}_b \right] \hat{\psi}_b \\ &\left. +g\hat{\psi}_a^\dagger\hat{\psi}_b^\dagger\hat{\psi}_a\hat{\psi}_b \right), \end{aligned} \tag{27}$$

where m_a, m_b are the particle masses, $V_a(\vec{r})$, $V_b(\vec{r})$ stand for trapping potentials and

$$g_a = \frac{4\pi\hbar^2 a_a}{m_a}, \quad g_b = \frac{4\pi\hbar^2 a_b}{m_b}, \quad g = 2\pi\hbar^2 a_{ab}\left(\frac{1}{m_a}+\frac{1}{m_b}\right), \tag{28}$$

where a_a, a_b, a_{ab} are the scattering lengths. Similarly as in the previous chapter we assume that interparticle interactions are given by the contact potential [51].

The number conserving Bogoliubov theory [51, 89, 95] assumes the following decomposition of the bosonic field operators

$$\hat{\psi}_a(\vec{r}) = \phi_{a0}(\vec{r})\hat{a}_0 + \delta\hat{\psi}_a(\vec{r}), \quad \hat{\psi}_b(\vec{r}) = \phi_{b0}(\vec{r})\hat{b}_0 + \delta\hat{\psi}_b(\vec{r}), \tag{29}$$

where we separate the operators $\hat{a}_0$ and $\hat{b}_0$ that annihilate atoms in modes ϕ_{a0} and ϕ_{b0}, respectively, from *quantum corrections* $\delta\hat{\psi}_a(\vec{r})$, $\delta\hat{\psi}_b(\vec{r})$ that are assumed small. Consequently the modes ϕ_{a0} and ϕ_{b0} are macroscopically occupied by atoms

$$\langle\hat{a}_0^\dagger\hat{a}_0\rangle \approx N_a, \qquad \langle\hat{b}_0^\dagger\hat{b}_0\rangle \approx N_b. \tag{30}$$

The perturbation expansion of the Hamiltonian in powers of $\delta\hat{\psi}_a$ and $\delta\hat{\psi}_b$ [95] leads to the following results. Minimizing the system energy in the zero order we obtain coupled Gross-Pitaevskii equations [96]

$$H_{GP}^a\phi_{a0} = 0, \qquad H_{GP}^b\phi_{b0} = 0, \tag{31}$$

where

$$H_{GP}^a = -\frac{\hbar^2}{2m_a}\nabla^2 + V_a + g_a N_a|\phi_{a0}|^2 + gN_b|\phi_{b0}|^2 - \mu_a,$$

$$H^b_{GP} = -\frac{\hbar^2}{2m_b}\nabla^2 + V_b + g_b N_b|\phi_{b0}|^2 + gN_b|\phi_{b0}|^2 - \mu_b. \tag{32}$$

It is possible then to find the single particle modes macroscopically occupied by atoms together with the corresponding chemical potentials μ_a and μ_b. The first order terms disappear and the second order terms of the expansion, the actual Bogoliubov theory, will be discussed in the following section.

5.1 Number conserving Bogoliubov theory

Following [89, 95] we can write an effective second order Hamiltonian as

$$\hat{H}_{\text{eff}} \approx \frac{1}{2}\int d^3r \left(\hat{\Lambda}^\dagger_a, -\hat{\Lambda}_a, \hat{\Lambda}^\dagger_b, -\hat{\Lambda}_b\right)\mathcal{L}\begin{pmatrix}\hat{\Lambda}_a\\ \hat{\Lambda}^\dagger_a\\ \hat{\Lambda}_b\\ \hat{\Lambda}^\dagger_b\end{pmatrix}, \tag{33}$$

where

$$\mathcal{L} = \begin{pmatrix} H^a_{GP} + g_a N_a \hat{Q}_a|\phi_{a0}|^2\hat{Q}_a & g_a N_a \hat{Q}_a\phi^2_{a0}\hat{Q}^*_a & g\sqrt{N_aN_b}Q_a\phi_{a0}\phi^*_{b0}Q_b & g\sqrt{N_aN_b}Q_a\phi_{a0}\phi_{b0}Q^*_b \\ -g_a N_a \hat{Q}^*_a\phi^{*2}_{a0}\hat{Q}_a & -H^a_{GP} - g_a N_a \hat{Q}^*_a|\phi_{a0}|^2\hat{Q}^*_a & -g\sqrt{N_aN_b}Q^*_a\phi^*_{a0}\phi^*_{b0}Q_b & -g\sqrt{N_aN_b}Q^*_a\phi^*_{a0}\phi_{b0}Q^*_b \\ g\sqrt{N_aN_b}Q_b\phi^*_{a0}\phi_{b0}Q_a & g\sqrt{N_aN_b}Q_b\phi_{a0}\phi_{b0}Q^*_a & H^b_{GP} + g_b N_b \hat{Q}_b|\phi_{b0}|^2\hat{Q}_b & g_b N_b \hat{Q}_b\phi^2_{b0}\hat{Q}^*_b \\ -g\sqrt{N_aN_b}Q^*_b\phi^*_{a0}\phi^*_{b0}Q_a & -g\sqrt{N_aN_b}Q^*_b\phi_{a0}\phi^*_{b0}Q^*_a & -g_b N_b \hat{Q}^*_b\phi^{*2}_{b0}\hat{Q}_b & -H^b_{GP} - g_b N_b \hat{Q}^*_b|\phi_{b0}|^2\hat{Q}^*_b \end{pmatrix}, \tag{34}$$

and

$$\hat{Q}_a = 1 - |\phi_{a0}\rangle\langle\phi_{a0}|, \quad \hat{Q}_b = 1 - |\phi_{b0}\rangle\langle\phi_{b0}| \tag{35}$$

are projection operators to "non-condensate" subspaces. Diagonalization of the effective Hamiltonian (33) amounts to solving an eigenproblem of the non-hermitian operator $\mathcal{L}$, so-called Bogoliubov-de Gennes equations [51]. The single particle excitation operators creating an atom out of a condensate mode are given by

$$\hat{\Lambda}^\dagger_a(\vec{r}) = \frac{\hat{a}_0}{\sqrt{N_a}}\delta\hat{\psi}^\dagger_a(\vec{r}), \quad \hat{\Lambda}^\dagger_b(\vec{r}) = \frac{\hat{b}_0}{\sqrt{N_b}}\delta\hat{\psi}^\dagger_b(\vec{r}), \tag{36}$$

and fulfil the following commutation relations

$$[\hat{\Lambda}_a(\vec{r}), \hat{\Lambda}^\dagger_a(\vec{r}\,')] \approx \langle\vec{r}|\hat{Q}_a|\vec{r}\,'\rangle, \quad [\hat{\Lambda}_b(\vec{r}), \hat{\Lambda}^\dagger_b(\vec{r}\,')] \approx \langle\vec{r}|\hat{Q}_b|\vec{r}\,'\rangle. \tag{37}$$

In order to define the Bogoliubov transformation we will take advantage of two symmetry properties of the operator $\mathcal{L}$, analogous to a single condensate case [51, 89]

$$u_1\mathcal{L}u_1 = -\mathcal{L}^*, \quad u_3\mathcal{L}u_3 = \mathcal{L}^\dagger, \tag{38}$$

where

$$u_1 = \left(\begin{array}{c|c} \sigma_1 & 0 \\ \hline 0 & \sigma_1 \end{array}\right), \qquad u_3 = \left(\begin{array}{c|c} \sigma_3 & 0 \\ \hline 0 & \sigma_3 \end{array}\right), \tag{39}$$

and

$$\sigma_1 = \begin{pmatrix} 0 & 1 \\ 1 & 0 \end{pmatrix}, \qquad \sigma_3 = \begin{pmatrix} 1 & 0 \\ 0 & -1 \end{pmatrix}, \tag{40}$$

are the Pauli matrices. Now suppose that all eigenvalues of the $\mathcal{L}$ operator are real. This is in fact an important assumption of dynamical stability [51] that should be verified for a given system. The symmetries (38) imply that if

$$|\Psi_n^{\mathrm{R}}\rangle = \begin{pmatrix} |u_n^a\rangle \\ |v_n^a\rangle \\ |u_n^b\rangle \\ |v_n^b\rangle \end{pmatrix}, \tag{41}$$

is a right eigenvector of $\mathcal{L}$ to an eigenvalue E_n, then $|\Psi_n^{\mathrm{L}}\rangle = u_3|\Psi_n^{\mathrm{R}}\rangle$ is a left eigenvector to the same eigenvalue E_n. Simultaneously $u_1|\Psi_n^{R*}\rangle$ is a right eigenvector to an eigenvalue $-E_n$.

There are four eigenvectors of $\mathcal{L}$ corresponding to a zero eigenvalue,

$$\begin{pmatrix} |\phi_a\rangle \\ 0 \\ 0 \\ 0 \end{pmatrix}, \begin{pmatrix} 0 \\ |\phi_a^*\rangle \\ 0 \\ 0 \end{pmatrix}, \begin{pmatrix} 0 \\ 0 \\ |\phi_b\rangle \\ 0 \end{pmatrix}, \begin{pmatrix} 0 \\ 0 \\ 0 \\ |\phi_b^*\rangle \end{pmatrix}. \tag{42}$$

The other eigenstates of $\mathcal{L}$ can be divided into two families "+" and "−", according to the sign of a norm defined as

$$\langle\Psi_n^{\mathrm{R}}|u_3|\Psi_{n'}^{\mathrm{R}}\rangle = \pm\delta_{n,n'}. \tag{43}$$

Having a complete set of eigenvectors of $\mathcal{L}$ we obtain an important completeness relation

$$\begin{aligned} \hat{1} \;=\; & \sum_{n\in\text{"+"}} \begin{pmatrix} |u_n^a\rangle \\ |v_n^a\rangle \\ |u_n^b\rangle \\ |v_n^b\rangle \end{pmatrix} \Big(\langle u_n^a|, -\langle v_n^a|, \langle u_n^b|, -\langle v_n^b|\Big) + \sum_{n\in\text{"+"}} \begin{pmatrix} |v_n^{a*}\rangle \\ |u_n^{a*}\rangle \\ |v_n^{b*}\rangle \\ |u_n^{b*}\rangle \end{pmatrix} \Big(-\langle v_n^{a*}|, \langle u_n^{a*}|, -\langle v_n^{b*}|, \langle u_n^{b*}|\Big) \\ & + \begin{pmatrix} |\phi_{a0}\rangle\langle\phi_{a0}| & 0 & 0 & 0 \\ 0 & |\phi_{a0}^*\rangle\langle\phi_{a0}^*| & 0 & 0 \\ 0 & 0 & |\phi_{b0}\rangle\langle\phi_{b0}| & 0 \\ 0 & 0 & 0 & |\phi_{b0}^*\rangle\langle\phi_{b0}^*| \end{pmatrix}. \end{aligned} \tag{44}$$

The eigenvectors of the $\mathcal{L}$ operator define the Bogoliubov transformation

$$\begin{pmatrix} \hat{\Lambda}_a \\ \hat{\Lambda}_a^\dagger \\ \hat{\Lambda}_b \\ \hat{\Lambda}_b^\dagger \end{pmatrix} = \sum_{n\in"+"} \begin{pmatrix} u_n^a \\ v_n^a \\ u_n^b \\ v_n^b \end{pmatrix} \hat{c}_n + \sum_{n\in"+"} \begin{pmatrix} v_n^{a*} \\ u_n^{a*} \\ v_n^{b*} \\ u_n^{b*} \end{pmatrix} \hat{c}_n^\dagger, \tag{45}$$

where quasi-particle excitations are described by operators that approximately fulfill the bosonic commutation relation $[\hat{c}_n, \hat{c}_{n'}^\dagger] \approx \delta_{n,n'}$. Employing the Bogoliubov transformation (45) we can diagonalize the effective Hamiltonian (33) to a simple form

$$\hat{H}_{\text{eff}} \approx \sum_{n\in"+"} E_n \hat{c}_n^\dagger \hat{c}_n, \tag{46}$$

where E_n are energies of the "+" family solutions to the Bogoliubov-de Gennes equations, $\{u_n^a, v_n^a, u_n^b, v_n^b\}$. The quasi-particle excitation operators can be written as

$$\hat{c}_n^\dagger \;=\; \langle u_n^a|\hat{\Lambda}_a^\dagger\rangle - \langle v_n^a|\hat{\Lambda}_a\rangle + \langle u_n^b|\hat{\Lambda}_b^\dagger\rangle - \langle v_n^b|\hat{\Lambda}_b\rangle, \tag{47}$$

and their application, due to (36), does not change the particle number, contrary to the standard Bogoliubov theory.

5.2 Bogoliubov ground state in a particle representation

Ground state of the Hamiltonian up to the second order of the perturbative expansion (46) reveals no quasi-particle excitations

$$\hat{c}_n|0_B\rangle = 0, \tag{48}$$

for all $n \in "+"$. Excited states can be generated acting with quasi-particle creation operators $\hat{c}_n^\dagger$ on the Bogoliubov vacuum state $|0_B\rangle$. The quasi-particle representation (46) is natural to represent system eigenstates within the Bogoliubov theory. It is also suitable to find low order correlation functions. The original particle representation is, however, much more convenient if we need predictions for density measurements. Simulations of atomic positions in a cloud can provide us with information about possible density fluctuations.

The Bogoliubov ground state is a certain particle state so we assume that it can be obtained acting with some particle creation operators $\hat{d}_a^\dagger$ and $\hat{d}_b^\dagger$ on the particle vacuum

$$|0_B\rangle \sim \left(\hat{d}_a^\dagger\right)^{M_a} \left(\hat{d}_b^\dagger\right)^{M_b} |0\rangle. \tag{49}$$

If we require that $\hat{d}_a^\dagger$ and $\hat{d}_b^\dagger$ commute with all quasi-particle annihilation operators [92],

$$[\hat{c}_n, \hat{d}_a^\dagger] = 0, \quad [\hat{c}_n, \hat{d}_b^\dagger] = 0, \tag{50}$$

then the Bogoliubov ground state is indeed annihilated by all quasi-particle annihilation operators,

$$\hat{c}_n \left(\hat{d}_a^\dagger\right)^{M_a} \left(\hat{d}_b^\dagger\right)^{M_b} |0\rangle = \left(\hat{d}_a^\dagger\right)^{M_a} \left(\hat{d}_b^\dagger\right)^{M_b} \hat{c}_n |0\rangle = 0. \tag{51}$$

In the following we will show that the set of equations (50) is solved by particle creation operators of the form

$$\hat{d}_a^\dagger = \hat{a}_0^\dagger \hat{a}_0^\dagger + \sum_{\alpha,\beta=1}^{\infty} Z_{\alpha\beta}^a \hat{a}_\alpha^\dagger \hat{a}_\beta^\dagger, \quad \hat{d}_b^\dagger = \hat{b}_0^\dagger \hat{b}_0^\dagger + \sum_{\alpha,\beta=1}^{\infty} Z_{\alpha\beta}^b \hat{b}_\alpha^\dagger \hat{b}_\beta^\dagger, \tag{52}$$

where $\hat{a}_\alpha^\dagger$ ($\hat{b}_\alpha^\dagger$) are bosonic particle creation operators that create atoms in modes $\phi_{a\alpha}$ ($\phi_{b\alpha}$) orthogonal to the condensate wavefunction ϕ_{a0} (ϕ_{b0}). $Z_{\alpha\beta}^a$ and $Z_{\alpha\beta}^b$ are symmetric matrices to be found.

The operator $\hat{d}_a^\dagger$ that accounts for creating pairs of atoms in the Bogoliubov vacuum was introduced in a single condensate case in a variational approximation [96]. Later it was proved to produce an exact Bogoliubov vacuum both in homogeneous and inhomogeneous condensates [92, 97]. In a two component condensate the Bogoliubov state (49) was used in a system of two independent (i.e. noninteracting) condensates [98]. We will show that it can be applied also to a system with nonzero intercomponent interactions.

Substituting the ansatz (52) into (50) we obtain equations (see also (47))

$$\langle v_n^a | \phi_{a\alpha}^* \rangle = \sum_{\beta=1}^{\infty} \langle u_n^a | \phi_{a\beta} \rangle Z_{\beta\alpha}^a, \quad \langle v_n^b | \phi_{b\alpha}^* \rangle = \sum_{\beta=1}^{\infty} \langle u_n^b | \phi_{b\beta} \rangle Z_{\beta\alpha}^b, \tag{53}$$

which, when multiplied by $\langle \phi_{a\gamma} | u_n^a \rangle$ and $\langle \phi_{b\gamma} | u_n^b \rangle$, respectively, and summed over n, are transformed to

$$\begin{aligned} \langle \phi_{a\gamma} | \hat{\Gamma}_a | \phi_{a\alpha}^* \rangle &= \sum_{\beta=1}^{\infty} \langle \phi_{a\gamma} | \hat{U}_a | \phi_{a\beta} \rangle Z_{\beta\alpha}^a \\ \langle \phi_{b\gamma} | \hat{\Gamma}_b | \phi_{b\alpha}^* \rangle &= \sum_{\beta=1}^{\infty} \langle \phi_{b\gamma} | \hat{U}_b | \phi_{b\beta} \rangle Z_{\beta\alpha}^b, \end{aligned} \tag{54}$$

where $\hat{\Gamma}_a$, $\hat{\Gamma}_b$, $\hat{U}_a$ and $\hat{U}_b$ are built with quasiparticle modes

$$\begin{aligned} \hat{\Gamma}_a &= \sum_{n\in\text{"+"}} |u_n^a\rangle\langle v_n^a|, \quad \hat{\Gamma}_b = \sum_{n\in\text{"+"}} |u_n^b\rangle\langle v_n^b|, \\ \hat{U}_a &= \sum_{n\in\text{"+"}} |u_n^a\rangle\langle u_n^a|, \quad \hat{U}_b = \sum_{n\in\text{"+"}} |u_n^b\rangle\langle u_n^b|. \end{aligned} \tag{55}$$

The completeness relation (44) implies that the $\hat{\Gamma}_a$ and $\hat{\Gamma}_b$ operators are symmetric and that

$$\hat{U}_a = \sum_{n\in\text{"+"}} |v_n^{a*}\rangle\langle v_n^{a*}| + \hat{1}_\perp^a, \quad \hat{U}_b = \sum_{n\in\text{"+"}} |v_n^{b*}\rangle\langle v_n^{b*}| + \hat{1}_\perp^b, \tag{56}$$

where $\hat{1}^a_\perp$ and $\hat{1}^b_\perp$ are identity operators in subspaces orthogonal to condensate wavefunctions ϕ_{a0} and ϕ_{b0}, respectively. We can write a reduced single particle density matrix for the component a (and b analogously)

$$\langle 0_B|\hat{\psi}^\dagger_a(\vec{r})\hat{\psi}_a(\vec{r}\,')|0_B\rangle = N_a\phi^*_{a0}(\vec{r})\phi_{a0}(\vec{r}\,') + \sum_{n\in"+"} v^a_n(\vec{r})v^{a*}_n(\vec{r}\,'). \tag{57}$$

Comparing the first of the equations (56) with (57) we can see that $\hat{U}_a$ is diagonal in a basis of single particle density matrix eigenstates $\phi_{a\alpha}$. Similarly $\hat{U}_b$ in a basis built with $\phi_{b\alpha}$. Then one immediately obtains solutions for the $Z^{a,b}_{\alpha\beta}$ matrices

$$Z^a_{\alpha\beta} = \frac{\langle\phi_{a\alpha}|\hat{\Gamma}_a|\phi^*_{a\beta}\rangle}{dN^a_\alpha + 1}, \quad Z^b_{\alpha\beta} = \frac{\langle\phi_{b\alpha}|\hat{\Gamma}_b|\phi^*_{b\beta}\rangle}{dN^b_\alpha + 1}, \tag{58}$$

where $dN^{a,b}_\alpha$ are eigenvalues of the single particle density matrices, that is numbers of atoms depleted from the condensate wavefunctions. For the component a we have

$$\langle 0_B|\hat{\psi}^\dagger_a(\vec{r})\hat{\psi}_a(\vec{r}\,')|0_B\rangle \approx N_a\phi^*_{a0}(\vec{r})\phi_{a0}(\vec{r}\,') + \sum_{\alpha=1}^{\infty} dN^a_\alpha\phi^*_{a\alpha}(\vec{r})\phi_{a\alpha}(\vec{r}\,'). \tag{59}$$

Note that the matrices $Z^a_{\alpha\beta}$, $Z^b_{\alpha\beta}$, $\langle\phi_{a\alpha}|\hat{\Gamma}_a|\phi^*_{a\beta}\rangle$ and $\langle\phi_{b\alpha}|\hat{\Gamma}_b|\phi^*_{b\beta}\rangle$ are symmetric. The ansatz (52) is therefore self-consistent if the operators $\hat{\Gamma}_{a,b}$ are also diagonal in a basis built with single particle density matrix eigenvectors. We have proved analytically that this is the case in a homogeneous system, as well as for a two component BEC in a double well trapping potential. We have also confirmed that numerically for a system trapped in a spherically symmetric trap.

The final form of the solution for the Bogoliubov vacuum state in the particle representation is

$$|0_B\rangle \sim \left[\left(\hat{a}^\dagger_0\right)^2 + \sum_{\alpha=1}^{\infty}\lambda^a_\alpha\left(\hat{a}^\dagger_\alpha\right)^2\right]^{N_a/2} \times \left[\left(\hat{b}^\dagger_0\right)^2 + \sum_{\alpha=1}^{\infty}\lambda^b_\alpha\left(\hat{b}^\dagger_\alpha\right)^2\right]^{N_b/2}|0\rangle \tag{60}$$

where

$$\lambda^a_\alpha = \frac{\langle\phi_{a\alpha}|\hat{\Gamma}_a|\phi^*_{a\alpha}\rangle}{dN^a_\alpha + 1}, \quad \lambda^b_\alpha = \frac{\langle\phi_{b\alpha}|\hat{\Gamma}_b|\phi^*_{b\alpha}\rangle}{dN^b_\alpha + 1}. \tag{61}$$

6 Density fluctuations close to a phase separation transition

6.1 Density measurement

A single particle density (i.e. the first order correlation function) can give quite unexpected results if we ask about an atomic density measured in an experiment. In a numerical simulation

[99] it was shown that two condensates prepared in an initial Fock state acquire a relative phase during a density measurement process. A single experiment reveals interference fringes located at random positions, whereas the single particle density being an average over many measurements, remains flat. This Fock state interference has been proved experimentally [100, 101] showing interference fringes between independent condensates. In a theoretical analysis the build-up of a relative phase was studied [102] and in an exact analytical work interference effects in second- and higher-order correlation functions were confirmed [103]. Situations when a single photo of a system may be significantly different from the averaged picture involve also collisions of two non-ideal condensates [104] a and condensate with a dark soliton [97, 105].

In order to perform a simulation of the density measurement we generally need the full many body probability density. As the number of particles grows, however, using that function to find atomic positions quickly becomes a very formidable task. Instead one could use a sequential method from [99]. Having found successive atoms at certain positions one builds there a conditional probability density for finding an additional one. Using this method within the Bogoliubov theory is however not so straightforward, since it would require inversion of the nonlinear transformation (47), unless we have written the Bogoliubov vacuum in the particle representation. We will however apply yet another method, which will clearly show us how density profiles are acquired as we perform the measurement on the Bogoliubov vacuum state. The approximate method was introduced for a single condensate [97] but since the two component ground state has a similar structure, we can use it also in the present case.

First, we can adjust phases of the eigenmodes of the single particle density matrices (see (59) and (61))

$$\varphi_{a\alpha}(\vec{r}) = \phi_{a\alpha}(\vec{r})\, e^{-i\mathrm{Arg}(\lambda^a_\alpha)/2}, \quad \varphi_{b\alpha}(\vec{r}) = \phi_{b\alpha}(\vec{r})\, e^{-i\mathrm{Arg}(\lambda^b_\alpha)/2}, \tag{62}$$

sa that the coefficients $\lambda^{a,b}$ are real and positive. Then, we can restrict to only those modes that have the largest values of the Bogoliubov vacuum coefficients (61)

$$\Lambda^{a,b}_\alpha \equiv \frac{\lambda^{a,b}_\alpha}{1-\lambda^{a,b}_\alpha} \gg 1. \tag{63}$$

The above adjustment of the phases makes it possible to rewrite the Bogoliubov vacuum state as a gaussian superposition over perfect condensate states [97]

$$|0_b\rangle \sim \int dq_a dq_b \exp\left(-\sum_{\alpha=1}^{M_a} \frac{q^2_{a\alpha}}{2\Lambda^a_\alpha}\right) \exp\left(-\sum_{\alpha=1}^{M_b} \frac{q^2_{b\alpha}}{2\Lambda^b_\alpha}\right) |N_a : \phi_{qa}\rangle |N_b : \phi_{qb}\rangle, \tag{64}$$

where $|N_a : \phi_{qa}\rangle$ and $|N_b : \phi_{qb}\rangle$ are many body states where, respectively, N_a and N_b atoms occupy single particle wavefunctions

$$\phi_{qa}(\vec{r}) = \frac{\phi_{0a}(\vec{r}) + \frac{1}{\sqrt{N_a}} \sum_{\alpha=1}^{M_a} q_{a\alpha}\varphi_{a\alpha}(\vec{r})}{\sqrt{1+\frac{1}{\sqrt{N_a}}\sum_{\alpha=1}^{M_a} q_{a\alpha}}}, \quad \phi_{qb}(\vec{r}) = \frac{\phi_{0b}(\vec{r}) + \frac{1}{\sqrt{N_b}} \sum_{\alpha=1}^{M_b} q_{b\alpha}\varphi_{b\alpha}(\vec{r})}{\sqrt{1+\frac{1}{\sqrt{N_b}}\sum_{\alpha=1}^{M_b} q_{b\alpha}}}. \tag{65}$$

Consequently, results of a single measurement to a system in the state (60) can be approximated by the densities

$$\begin{aligned} \sigma_a(\vec{r}) &\sim \left| \phi_{a0}(\vec{r}) + \frac{1}{\sqrt{N_a}} \sum_{\alpha=1}^{M_a} q_{a\alpha}\, \varphi_{a\alpha}(\vec{r}) \right|^2 , \\ \sigma_b(\vec{r}) &\sim \left| \phi_{b0}(\vec{r}) + \frac{1}{\sqrt{N_b}} \sum_{\alpha=1}^{M_b} q_{b\alpha}\, \varphi_{b\alpha}(\vec{r}) \right|^2 , \end{aligned} \tag{66}$$

where real parameters $q_{a\alpha}$ and $q_{b\alpha}$ have to be chosen randomly, for each experimental realization, from the Gaussian probability density

$$P(q_a, q_b) \sim \prod_{\alpha=1}^{M_a} \exp\left(-\frac{q_{a\alpha}^2}{\Lambda_\alpha^a} \right) \prod_{\beta=1}^{M_b} \exp\left(-\frac{q_{b\beta}^2}{\Lambda_\beta^b} \right) . \tag{67}$$

6.2 Density fluctuations in a finite box

A two component homogeneous condensate is an example of a Bose system where the Bogoliubov theory gives analytical results even in the presence of a process which transfers atoms between the two components. For such a Josephson-like coupled system a linear stability analysis was performed to study the dispersion relation for the excitation spectra [106, 107], and a Bogoliubov transformation was derived with subsequent stability analysis with respect to fluctuations of the relative number of atoms [108]. In the system preserving numbers of atoms in its components a dynamical instability leading to a phase separation was inferred from the quasi-particle excitation spectrum [106, 107, 109]. In the phase-segregated regime, the linearization of Gross-Pitaevskii equations revealed no quasi-particle excitations localized near the phase boundary [110].

In the following we will study the Bogoliubov vacuum state in the particle representation for a system approaching the phase separation transition. We will assume fixed particle numbers in both components and repulsive interactions, i.e. g_a, g_b, $g > 0$. The condensates are confined in a box of $L \times L \times L$ size with periodic boundary conditions. The ground state solution of the Gross-Pitaevskii equations (31) is

$$\phi_{a0} = \frac{1}{\sqrt{L^3}}, \quad \phi_{b0} = \frac{1}{\sqrt{L^3}}, \tag{68}$$

and the chemical potentials

$$\mu_a = g_a \rho_a + g\rho_b, \quad \mu_b = g_b \rho_b + g\rho_a, \tag{69}$$

where $\rho_{a,b} = N_{a,b}/L^3$ are densities of the a and b components. In a homogeneous system it is convenient to switch to the momentum space and look for solutions of the Bogoliubov-de Gennes

equations of the form

$$\begin{pmatrix} u_k^a \\ v_k^a \\ u_k^b \\ v_k^b \end{pmatrix} \frac{e^{i\vec{k}\cdot\vec{r}}}{\sqrt{L^3}}. \tag{70}$$

We obtain two quasi-particle excitation branches [109]

$$E_{k,\pm} = \left[\frac{\omega_{ak}^2 + \omega_{bk}^2}{2} \pm \sqrt{\frac{\left(\omega_{ak}^2 - \omega_{bk}^2\right)^2}{4} + \frac{\hbar^2 k^4}{m_a m_b} g^2 \rho_a \rho_b} \right]^{1/2}, \tag{71}$$

where

$$\begin{aligned} \omega_{ak}^2 &= \frac{\hbar^2 k^2}{2m_a}\left(\frac{\hbar^2 k^2}{2m_a} + 2g_a\rho_a\right), \\ \omega_{bk}^2 &= \frac{\hbar^2 k^2}{2m_b}\left(\frac{\hbar^2 k^2}{2m_b} + 2g_b\rho_b\right). \end{aligned} \tag{72}$$

are the usual single condensate Bogoliubov dispersions. In the long wavelength limit $k \to 0$ we have $\omega_{i,k} \approx \hbar c_i k$ where $c_i = \sqrt{g_i \rho_i}$ is the sound velocity of the $i = a, b$ condensate. The double condensate dispersions are phonon-like in this limit,

$$E_{k,\pm} \approx \hbar c_\pm k, \tag{73}$$

with sound velocities

$$c_\pm^2 = \frac{1}{2}\left(c_a^2 + c_b^2 \pm \sqrt{\left(c_a^2 - c_b^2\right)^2 + 4\frac{g^2}{g_a g_b} c_a^2 c_b^2}\right). \tag{74}$$

The quasiparticle modes (solutions to the Bogoliubov-de Gennes equations) are given by

$$\begin{pmatrix} u_{k,\pm}^a \\ v_{k,\pm}^a \\ u_{k,\pm}^b \\ v_{k,\pm}^b \end{pmatrix} = \begin{pmatrix} 2g\mathcal{E}_{kb}\left(\mathcal{E}_{ka} + E_{k,\pm}\right)\sqrt{\rho_a\rho_b} \\ 2g\mathcal{E}_{kb}\left(\mathcal{E}_{ka} - E_{k,\pm}\right)\sqrt{\rho_a\rho_b} \\ \left(E_{k,\pm}^2 - \omega_{ak}^2\right)\left(\mathcal{E}_{kb} + E_{k,\pm}\right) \\ \left(E_{k,\pm}^2 - \omega_{ak}^2\right)\left(\mathcal{E}_{kb} - E_{k,\pm}\right) \end{pmatrix} \chi_\pm, \tag{75}$$

where

$$\mathcal{E}_{ka} = \frac{\hbar^2 k^2}{2m_a}, \quad \mathcal{E}_{kb} = \frac{\hbar^2 k^2}{2m_b}, \tag{76}$$

and the normalization factor

$$\chi_\pm = \left\{ 4\mathcal{E}_{kb}\left[4\mathcal{E}_{ka}\mathcal{E}_{kb} g^2 \rho_a \rho_b + \left(E_{k,\pm}^2 - \omega_{ak}^2\right)^2 \right] E_{k,\pm} \right\}^{-1/2}.$$

(77)

The reduced single particle density matrices (57) are diagonal in the $e^{i\vec{k}\cdot\vec{r}}/\sqrt{L^3}$ basis. However, in order to have the $\hat{\Gamma}_{a,b}$ operators (55) also diagonal we have to switch to the basis

$$\phi_{a\vec{k}s} = \phi_{b\vec{k}s} = \sqrt{\frac{2}{L^3}} \sin\left(\vec{k}\cdot\vec{r}\right), \quad \phi_{a\vec{k}c} = \phi_{b\vec{k}c} = \sqrt{\frac{2}{L^3}} \cos\left(\vec{k}\cdot\vec{r}\right). \tag{78}$$

The Bogoliubov vacuum state in the particle representation reads then

$$|0_B\rangle \sim \left[\hat{a}_0^\dagger \hat{a}_0^\dagger + \sum_{\vec{k}} \lambda_k^a \left(\hat{a}_{\vec{k}s}^\dagger \hat{a}_{\vec{k}s}^\dagger + \hat{a}_{\vec{k}c}^\dagger \hat{a}_{\vec{k}c}^\dagger\right)\right]^{N_a/2} \times \left[\hat{b}_0^\dagger \hat{b}_0^\dagger + \sum_{\vec{k}} \lambda_k^b \left(\hat{b}_{\vec{k}s}^\dagger \hat{b}_{\vec{k}s}^\dagger + \hat{b}_{\vec{k}c}^\dagger \hat{b}_{\vec{k}c}^\dagger\right)\right]^{N_b/2} |0\rangle, \tag{79}$$

where

$$\lambda_k^a = \frac{u_{k,+}^a v_{k,+}^a + u_{k,-}^a v_{k,-}^a}{\left(v_{k,+}^a\right)^2 + \left(v_{k,-}^a\right)^2 + 1}, \quad \lambda_k^b = \frac{u_{k,+}^b v_{k,+}^b + u_{k,-}^b v_{k,-}^b}{\left(v_{k,+}^b\right)^2 + \left(v_{k,-}^b\right)^2 + 1}, \tag{80}$$

and the operators $\hat{a}_{\vec{k}s}^\dagger$, $\hat{a}_{\vec{k}c}^\dagger$ $\hat{b}_{\vec{k}s}^\dagger$ and $\hat{b}_{\vec{k}c}^\dagger$ create atoms in the modes (78).

If the intercomponent interactions g are strong enough it is no longer energetically favorable to mix the condensates, the uniform solutions (68) to the Gross-Pitaevskii equations become unstable, and the two components spatially separate. In an infinite box ($L \to \infty$ and $N_{a,b} \to \infty$ but $\rho_{a,b} = const$) an imaginary eigenvalue in the Bogoliubov spectrum (71) appears for

$$g^2 > g_a g_b. \tag{81}$$

In a finite box with periodic boundary conditions, however, the momentum of a quasiparticle can have only discrete values

$$\vec{k} = \frac{2\pi}{L}\left(n_x\vec{e}_x + n_y\vec{e}_y + n_z\vec{e}_z\right), \tag{82}$$

where n_x, n_y, n_z are non-zero integers. The minimal momentum value of a quasiparticle is $2\pi/L$ and consequently the phase separation condition is modified

$$g^2 > \left(\frac{\hbar^2\pi^2}{m_a L^2}\frac{1}{\rho_a} + g_a\right)\left(\frac{\hbar^2\pi^2}{m_b L^2}\frac{1}{\rho_b} + g_b\right). \tag{83}$$

This shows that for the finite system the minimal value of the interactions g leading to the phase separation has to be higher than the corresponding value for $L \to \infty$. We will show that approaching the condition (83) one can observe density fluctuations on a scale of the order of L.

We consider a two component condensate of ^{87}Rb atoms in two different internal states. We have taken $N_a = 5000$ and $N_b = 20000$ atoms, the intra-component scattering lengths

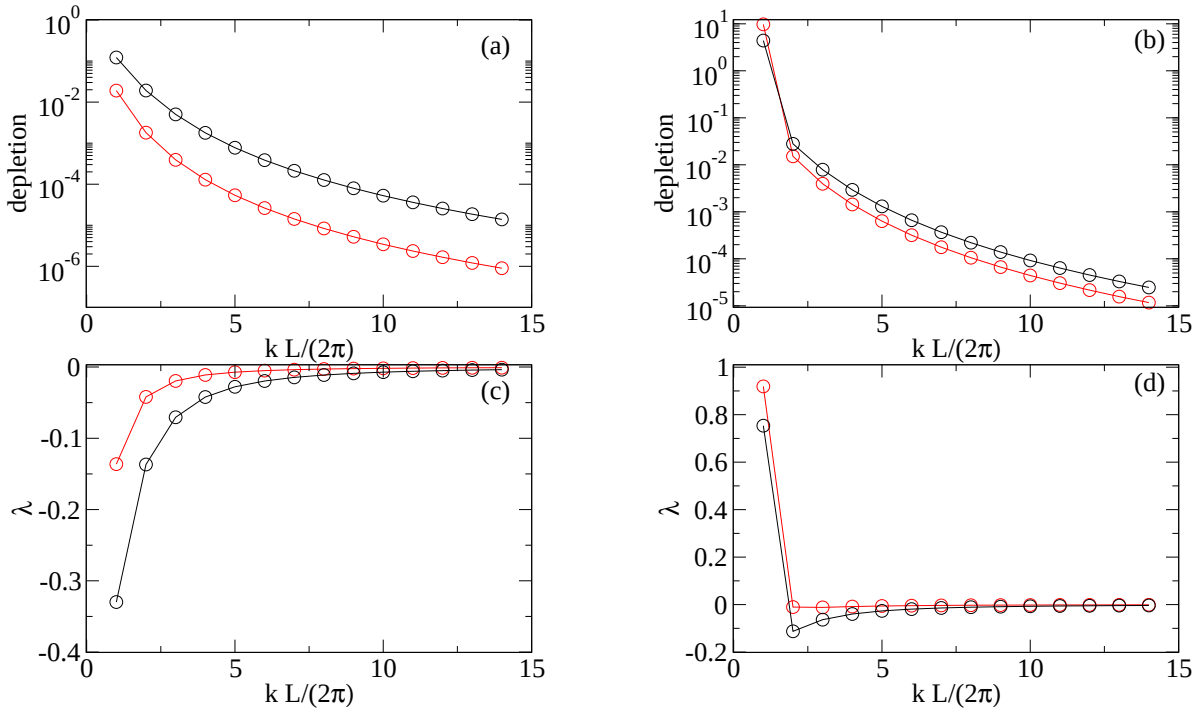

Figure 9: Condensate depletion far (panel (a)) and close (panel (b)) to the phase separation transition point. Panels (c) and (d) show corresponding coefficients $\lambda_k^{a,b}$ of the Bogoliubov vacuum state (60). Red circles represent modes of the smaller condensate ($N_a = 5000$) whereas black circles of the larger one ($N_b = 20000$). The far-from phase separation scattering length is $a_{ab} = 10.0a_0$ and close to the transition it is equal to $a_{ab} = 193.9a_0$.

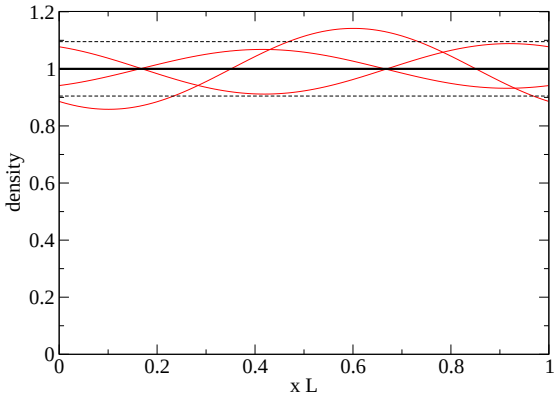

Figure 10: Density measurement simulations for the component a — densities integrated over y and z directions, i.e. $L\int \sigma_a(\vec{r})\, dydz$, are shown. Red lines correspond to densities found in a single measurement whereas the black solid line is the reduced single particle density matrix prediction, i.e. density averaged over many experimental runs. Dashed lines indicate the average density plus/minus the standard deviation equal to $2\sqrt{\Lambda^a_k/N_a} \approx 0.1$.

$a_a = 108.8a_0$, $a_b = 109.1a_0$ (a_0 is the Bohr radius) [80] and the intercomponent scattering length a_{ab} varied e.g. by means of a Feshbach resonance. The box size is $L = 50$ μm.

In Fig. 9 we show average numbers of atoms depleted to the modes (78) as well as the corresponding $\lambda^{a,b}_k$ values for the Bogoliubov ground state. Far from the phase separation we have taken $a_{ab} = 10a_0$, and for $a_{ab} = 193.9a_0$ we are very close to the condition (83).

In order to obtain predictions for density measurements one has to change phases of the modes, see (62), which far from the phase separation (all $\lambda^{a,b}_k$ are then negative) leads to

$$\varphi_{a\vec{k}s} = \phi_{a\vec{k}s} e^{-i\mathrm{Arg}(\lambda^a_\alpha)/2} = i\phi_{a\vec{k}s}, \quad \varphi_{b\vec{k}s} = \phi_{b\vec{k}s} e^{-i\mathrm{Arg}(\lambda^b_\alpha)/2} = i\phi_{b\vec{k}s}, \tag{84}$$

and similarly for $\varphi_{a\vec{k}c}$ and $\varphi_{b\vec{k}c}$. Since ϕ_{a0} and ϕ_{b0} are real and all the φ modes are purely imaginary we obtain, see (66),

$$\sigma_a(\vec{r}) \sim \phi^2_{a0}(\vec{r}) + \frac{1}{N_a}\left|\sum_{\alpha=1}^{M_a} q_{a\alpha}\, \varphi_{a\alpha}(\vec{r})\right|^2, \quad \sigma_b(\vec{r}) \sim \phi^2_{b0}(\vec{r}) + \frac{1}{N_b}\left|\sum_{\alpha=1}^{M_b} q_{b\alpha}\, \varphi_{b\alpha}(\vec{r})\right|^2. \tag{85}$$

Because $q^2_{a\alpha} \sim \Lambda^a_\alpha/2$, $q^2_{b\alpha} \sim \Lambda^b_\alpha/2$ and $\Lambda^{a,b}_\alpha \ll N_{a,b}$ the density fluctuations turn out to be negligible and the density remains almost perfectly flat.

We can see in panels (b) and (d) of Fig. 9 that the numbers of depleted atoms are not dramatically higher close to phase separation but the lowest quasiparticle modes acquire positive $\lambda^{a,b}_k$ values. The latter has dramatic consequences for density fluctuations because modes φ

corresponding to the positive $\lambda_k^{a,b}$ are real and their contributions to the atomic density are of the order of $\sqrt{\Lambda_\alpha^{a,b}/N_{a,b}}$. Neglecting contributions of the order of $\Lambda_\alpha^{a,b}/N_{a,b}$ we can make predictions for atomic density measurements based upon

$$\begin{aligned}\sigma_a(\vec{r}) &\sim \phi_{a0}^2(\vec{r}) + \frac{2\phi_{a0}(\vec{r})}{\sqrt{N_a}}{\sum_{\vec{k}}}' \left[q_{a\vec{k}s}\varphi_{a\vec{k}s}(\vec{r}) + q_{a\vec{k}c}\varphi_{a\vec{k}c}(\vec{r})\right], \\ \sigma_b(\vec{r}) &\sim \phi_{b0}^2(\vec{r}) + \frac{2\phi_{b0}(\vec{r})}{\sqrt{N_b}}{\sum_{\vec{k}}}' \left[q_{b\vec{k}s}\varphi_{b\vec{k}s}(\vec{r}) + q_{b\vec{k}c}\varphi_{b\vec{k}c}(\vec{r})\right], \end{aligned} \tag{86}$$

where $\sum_{\vec{k}}'$ runs over modes corresponding to positive $\lambda_k^{a,b}$ only. In a single realization of the density measurement one has to choose $q_{a\vec{k}s}$, $q_{a\vec{k}c}$, $q_{b\vec{k}s}$ and $q_{b\vec{k}c}$ randomly according to the probability density (67).

In Fig. 10 we show densities simulated close to the phase separation, $a_{ab} = 193.9a_0$. "Single shot" results (red lines) reveal density fluctuations on the length scale of L, whereas density obtained from the single particle density matrix remains flat. Despite the small number of atoms depleted to the lowest momentum mode ($\sim 0.3\%$) the density changes by 10% from shot to shot. The standard deviation of the fluctuations behaves as

$$\sqrt{\frac{\Lambda_k^{a,b}}{N_{a,b}}} \sim \frac{1}{\left(a_{ab}^{\mathrm{c}} - a_{ab}\right)^{1/4}}. \tag{87}$$

Note that the largest density fluctuations correspond to quasi-particles with the momentum $k = 2\pi/L$ so in a real experiment one may use low resolution so that shot noise fluctuations should be practically eliminated.

In the example considered, the range of a_{ab} where one deals with positive $\lambda_k^{a,b}$ is about 10×Bohr radius, which should be wide enough with present possibilities of the scattering length tuning.

7 Bogoliubov vacuum state in a trapped system

Present section is intended to be a complementary to the derivation of the Bogoliubov vacuum in the particle representation. The Bogoliubov vacuum (60) can be used if operators $\hat{\Gamma}_a$, $\hat{\Gamma}_b$ (55) are diagonal in a basis built with single particle density matrix eigenvectors. This can be shown analytically for a homogeneous condensate and for a condensate in a double well potential (see chapter VI). Now we will consider a two component condensate trapped in a spherically symmetric harmonic trap and perform a numerical test of the state (60). We assume in (27) the following trapping potentials

$$V_a(\vec{r}) = \frac{1}{2}m\omega_a^2(x^2+y^2+z^2), \quad V_b(\vec{r}) = \frac{1}{2}m\omega_b^2(x^2+y^2+z^2). \tag{88}$$

First, we will solve the Gross-Pitaevskii equations written in the spherical coordinates, assuming the following form of solutions

$$\phi_{a0}(\vec{r}) = R^{(a)}(r)Y_{l,m}(\theta,\varphi), \quad \phi_{b0}(\vec{r}) = R^{(b)}(r)Y_{l,m}(\theta,\varphi), \tag{89}$$

where $Y_{l,m}(\theta,\varphi)$ are spherical harmonic functions. Upon defining $R^{(i)} = \psi_i(\vec{r})/r$ and using $\sqrt{\hbar/m_b\omega_b}$ and $\hbar\omega_b$ as the length and energy units, respectively, we end up with stationary mean field equations that depend only on the radial variable. For a ground state we can take the angular momentum $l = 0$,

$$\begin{aligned}
\mu_a\psi_a(r) &= \left(-\frac{1}{2}\frac{d^2}{dr^2} + \frac{1}{2}\frac{\omega_a^2}{\omega_b^2}r^2 + 4\pi N_a a_a \frac{\psi_a^2(r)}{r^2} + 4\pi N_a a_{ab}\frac{\psi_b^2(r)}{r^2}\right)\psi_a(r) \\
\mu_b\psi_b(r) &= \left(-\frac{1}{2}\frac{d^2}{dr^2} + \frac{1}{2}r^2 + 4\pi N_b a_b \frac{\psi_b^2(r)}{r^2} + 4\pi N_b a_{ab}\frac{\psi_a^2(r)}{r^2}\right)\psi_b(r),
\end{aligned} \tag{90}$$

where a_a, a_b, a_{ab} are the scattering lengths. If the scattering lengths fulfill $a_{ab}^2 > a_a a_b$, we have the phase separation. With the assumption of the spherical symmetry this means that one of the condensates will occupy the center of the trap, and the other one will form a shell around. In the following we assumed a double ^{87}Rb condensate with the scattering lengths $a_a = 108.8a_0$ and $a_b = 109.1a_0$ (a_0 is the Bohr length), and particle numbers $N_a = N_b = 10^6$. Figure 11 shows radial densities found in the mean field ground states on both sides of the phase separation condition. In the phase segregated case we had to increase the trapping frequency of one of the condensates because otherwise a quasi-particle mode for $l = 1$ would be unstable.

The matrix $\mathcal{L}$ factorizes into blocks of different angular momenta which can be diagonalized separately. We have found the quasi-particle excitation spectra corresponding to the mean field states shown in Fig. 11. Taking the quasiparticle functions, eigenstates of $\mathcal{L}$, for both components we have built the operators (55) and density matrices (see (57)). Having diagonalized the density matrices we have checked whether the operators $\hat{\Gamma}_a$ and $\hat{\Gamma}_b$ are diagonal in a basis built with their respective eigenvectors. In order to do that, in each of the density matrix eigenmodes we have calculated the variance

$$var(\hat{\Gamma}_a) = \langle\hat{\Gamma}_a^2\rangle_a - \langle\hat{\Gamma}_a\rangle_a^2, \quad var(\hat{\Gamma}_b) = \langle\hat{\Gamma}_b^2\rangle_b - \langle\hat{\Gamma}_b\rangle_b^2. \tag{91}$$

The results are summarized in Fig. 12 which plots the values of $\sqrt{var(\hat{\Gamma})}/\langle\hat{\Gamma}\rangle$ for both condensates, calculated in the bases of the respective density matrices. In the miscible regime the above quantity is below 1% whereas in the case of the phase separation it approaches 25%. These are the estimates of whether the assumption about the form of the Bogoliubov state in the particle representation is correct. The latter case suggests that strong intercomponent interactions have significant impact and in general the state (60) might not be valid.

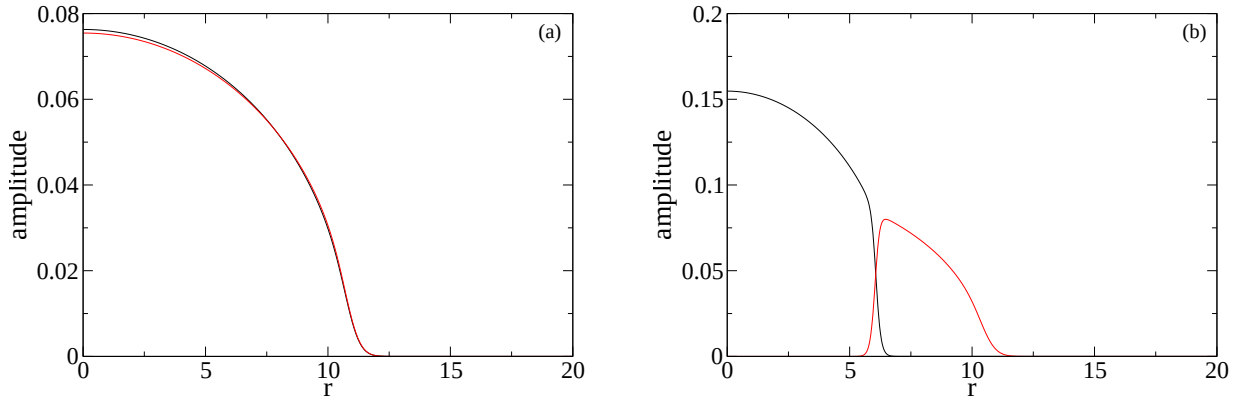

Figure 11: Radial profiles of the mean field ground states of the two component trapped condensate for $a_{ab} = 100a_0$ (panel (a)) and $a_{ab} = 200a_0$ (panel (b)). Black lines represent the condensate (a). The scattering lengths $a_a = 108.8a_0$, $a_b = 109.1a_0$. The trapping potentials are $(\frac{\omega_a}{\omega_b})^2 = 1$ in panel (a) $(\frac{\omega_a}{\omega_b})^2 = 5$ in panel (b).

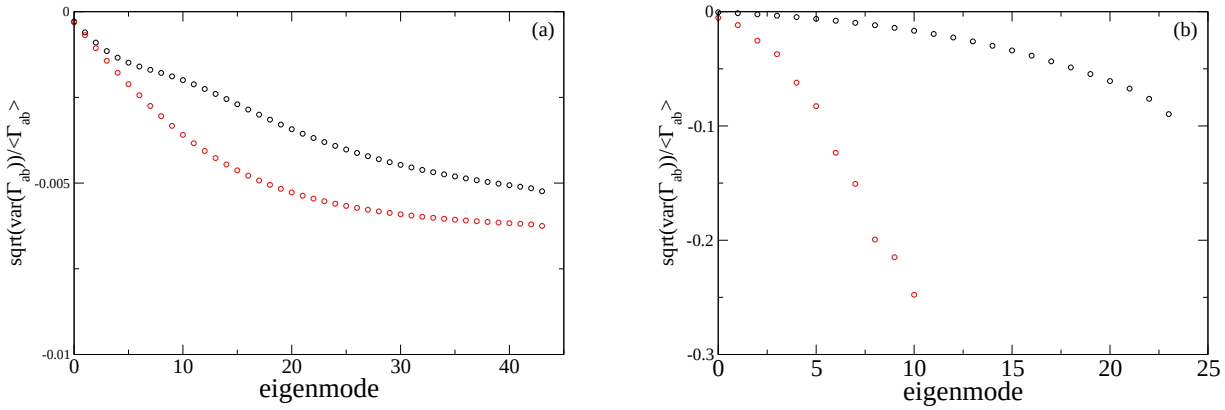

Figure 12: Standard deviation divided by respective mean values of the operators $\hat{\Gamma}_a$ (black circles) and $\hat{\Gamma}_b$ (red) in subsequent eigenmodes of the a and b density matrices, for Bogoliubov ground states built upon the mean field solutions shown in Figure 11. The modes are ordered according to a decreasing depletion. Plotted are only those whose depletion is higher than 0.013 (panel (a) and the inner condensate in panel (b)) or 0.04 in the case of the outer condensate in panel (b). The scattering lengths and trapping potentials are $a_{ab} = 100$, $(\frac{\omega_a}{\omega_b})^2 = 1$ (panel (a)) and $a_{ab} = 200$, $(\frac{\omega_a}{\omega_b})^2 = 5$ (panel (b)).

Part IV
Critical fluctuations of an attractive Bose gas in a double-well potential

Bose Einstein condensates prepared in an effectively one-dimensional symmetric double well potential offer an opportunity of a remarkable simplification of the theoretical description [111]. Due to properties of the energy spectrum the Hilbert space can be reduced to two modes. The resulting two mode model provides description of a bosonic Josephson junction where two localized matter wave packets in the two wells are weakly coupled via tunnelling of particles through the potential barrier. The dynamics of oscillations between the wells was described by means of the mean field theory [112, 113] and a quantum model adopting the Matthieu equation [114].

As it was shown in a numerical simulation, a condensate prepared in a Fock state reveals interference fringes due to the build-up of a relative phase during a measurement process [99]. Interference between two initially separated condensates was indeed measured experimentally [100, 115].

For a repulsive BEC with a growing barrier height or interactions there is a transition from a coherent regime where a constant relative phase can be defined to a fragmented condensate where the position of the interference fringes will vary randomly from one run to another [99, 116]. The coherence of the system was discussed in terms of the visibility of interference fringes. A relative importance of the quantum and the thermal fluctuations in driving the transition between the coherent and the incoherent regimes was studied [117]. Thermal fluctuations of the relative phase arising from the interaction of the BEC with its thermal environment were investigated experimentally [118] and proved dominant even at very low temperatures.

Atom interferometry measurements were performed to probe atom number statistics in the transition from coherent to number squeezed states [119]. With increasing interactions or barrier the atom number fluctuations turn from poissonian to sub-poissonian [120]. Experiments applying an adiabatic splitting of a condensate revealed enhanced coherence times [121, 122].

Both for repulsive and attractive condensates when the interactions exceed a critical value, the nonlinearity in the mean field theory produces self-trapped states with asymmetric distributions of atoms over the two wells [113]. Coherent oscillations due to tunneling are then suppressed [123]. Such symmetry breaking states were found analytically for a double square well potential [124, 125]. In the case of attractive interactions it is the mean field ground states that break the symmetry beyond the bifurcation [126]. Since the full many body state must preserve the symmetry of the potential, real eigenstates are macroscopic quantum superposition states [124]. In a two mode model with a Josephson-like laser coupling the ground state becomes a Schrödinger cat and the system can be prepared in such a state by adiabatically changing the strength of the coupling [127]. The macroscopic superposition can be produced also by the dynamic evolution of

the system due to the Josephson coupling on/off switching [128]. Detection, or loss, of one atom would be, however, enough to destroy the superposition, since such a detection would allow us to distinguish between the two macroscopic states that were populated before the measurement. A decoherence rate for the Schrödinger cat was calculated and shown to be indeed a significant threat [129].

We will study the vicinity of the bifurcation in the case of an attractive BEC in the double well potential [9]. The main purpose of the analysis is to show that the bifurcation is in fact a critical point known from the Landau-Ginzburg theory of the second-order phase transitions. The mean field approach has made it possible to identify the symmetry breaking states and define the order parameter. We have found breakdown of the Bogoliubov theory very close to the critical point. In a region where it works reasonably well we have estimated density fluctuations of symmetric ground states.

An introduced continuum model based upon quantization of the mean field Hamiltonian has been verified by an exact solution of the two mode model. Fluctuations of the order parameter are maximal at the critical point.

8 Two mode model and mean field results

We consider N atoms trapped in a double well potential and assume that one may restrict the single-particle Hilbert space to two modes only [96, 111, 120, 130]. Choosing states $\psi_{1,2}$, localized in each of the potential wells as these modes, we obtain the Hamiltonian

$$\hat{H} = -\frac{J}{2}\left(\hat{a}_1^\dagger \hat{a}_2 + \hat{a}_2^\dagger \hat{a}_1\right) + \frac{U}{2}\left(\hat{a}_1^\dagger \hat{a}_1^\dagger \hat{a}_1 \hat{a}_1 + \hat{a}_2^\dagger \hat{a}_2^\dagger \hat{a}_2 \hat{a}_2\right), \tag{92}$$

where the $\hat{a}_1$ ($\hat{a}_2$) operator annihilates an atom in the left (right) well, J stands for the tunneling rate between the wells and U is the on-site interaction strength (here we consider attractive interactions so U is negative). Note that the total number of particles N remains a conserved quantity, hence we can extract a constant part from the Hamiltonian (92)

$$\hat{H} = -\frac{J}{2}\left(\hat{a}_1^\dagger \hat{a}_2 + \hat{a}_2^\dagger \hat{a}_1\right) + \frac{U}{4}\left(\hat{a}_1^\dagger \hat{a}_1 - \hat{a}_2^\dagger \hat{a}_2\right)^2 + \frac{U}{4}\left(\hat{N}^2 - 2\hat{N}\right), \tag{93}$$

which will be neglected in the further considerations.

A foundation of the mean field approach is an assumption that all the atoms are in the same quantum state. The most general form of such a state is

$$\frac{1}{\sqrt{N!}}\left(\sqrt{\frac{1+z}{2}}e^{i\varphi/2}\hat{a}_1^\dagger + \sqrt{\frac{1-z}{2}}e^{-i\varphi/2}\hat{a}_2^\dagger\right)^N |\mathrm{vac}\rangle. \tag{94}$$

Here, z is the relative population difference between the wells, φ is the relative phase and $|\mathrm{vac}\rangle$ denotes the vacuum state. Within the mean-field method we can calculate an expectation value

of the Hamiltonian (93) in the state (94). It reads

$$\langle \hat{H} \rangle = \frac{JN}{2} \left(\frac{\gamma}{2} z^2 - \sqrt{1 - z^2} \cos \varphi \right), \tag{95}$$

where the dimensionless parameter

$$\gamma = \frac{UN}{J}, \tag{96}$$

is a ratio of the on-site interaction to the tunneling rate[2]. Note that the minimum of the expectation value (95) occurs for $\varphi = 0$. In case of $\gamma \geq -1$ the minimum appears for $z = 0$ and for $\gamma < -1$ it is shifted to the point $\pm z_0$, where

$$z_0 = \sqrt{1 - \frac{1}{\gamma^2}}. \tag{97}$$

The non-zero value of z_0 indicates, that the solution of the mean field approximation breaks the symmetry of the trapping potential. We can introduce an order parameter which measures the population imbalance between the wells. If we choose $N|z|$ we can use it to distinguish two "phases"; symmetric with the wavefunction

$$\phi_0 = \frac{1}{\sqrt{2}} \left(\psi_1 + \psi_2 \right), \tag{98}$$

and an asymmetric one

$$\phi_{0,\pm} = \sqrt{\frac{1 \pm z_0}{2}} \psi_1 + \sqrt{\frac{1 \mp z_0}{2}} \psi_2. \tag{99}$$

In order to associate the bifurcation mentioned above with the phenomenon of the phase transition we have to introduce the thermodynamic limit. In our case it will be $N \to \infty$ with γ remaining constant. With this limit in mind we can see that the mean field approximation predicts a second order phase transition in our system.

9 Number conserving Bogoliubov theory

Similarly as in the previous chapter we will write a Bogoliubov ground state of the system in the particle representation and use it to estimate density fluctuations as we approach the critical point. In the case of repulsive condensates in a double well potential the Bogoliubov vacuum state provides a perfect approximation to an exact ground state for arbitrary interactions and

[2]Strictly speaking, the term $z^2\gamma/2$ should be multiplied by $(N-1)/N$. However, as we are in the large-N limit, we set this prefactor to unity.

tunnelling [92]. We will show that here the Bogoliubov approximation works very well except for a close vicinity of the critical point. Density fluctuations are enhanced near the critical point but quantitative predictions based upon the Bogoliubov theory should be treated carefully.

In the two-mode model (92) there is only one mode orthogonal to a condensate wavefunction. The many body ground state in the N-conserving Bogoliubov theory can be written in the following form [92, 96]

$$|0_b\rangle \;\sim\; \left(\hat{c}_0^\dagger \hat{c}_0^\dagger + \lambda \hat{c}_1^\dagger \hat{c}_1^\dagger\right)^{N/2} \;|0\rangle \;, \tag{100}$$

where the operators $\hat{c}_0^\dagger$ and $\hat{c}_1^\dagger$ create atoms in the condensate ϕ_0 and in a mode ϕ_1 orthogonal to ϕ_0, respectively. The coefficient λ is given by

$$\lambda = \frac{\langle \phi_1 | \hat{\Gamma} | \phi_1^* \rangle}{dN + 1}, \tag{101}$$

where the operator $\hat{\Gamma} = |u\rangle\langle v|$ is built with modes u and v that are solutions to the Bogoliubov-de Gennes equations [51, 92]. Quantum depletion (average number of particles occupying the mode orthogonal to the condensate wavefunction) is equal to $dN = \langle v|v\rangle$.

9.1 Bogoliubov vacuum for symmetric mean field solutions

For $\gamma > -1$ we have $\hat{c}_0^\dagger = (\hat{a}_1^\dagger + \hat{a}_2^\dagger)/\sqrt{2}$, so $\hat{c}_0^\dagger$ creates atoms in a symmetric superposition over the two wells. The non-condensate mode is given by $\hat{c}_1^\dagger = (\hat{a}_1^\dagger - \hat{a}_2^\dagger)/\sqrt{2}$. The quasi-particle excitation energy is $E = J\sqrt{\gamma + 1}$ and the corresponding quasi-particle modes are

$$\begin{pmatrix} u \\ v \end{pmatrix} = \begin{pmatrix} 1 + \sqrt{\gamma+1} \\ 1 - \sqrt{\gamma+1} \end{pmatrix} \frac{\phi_1}{2(\gamma+1)^{1/4}}, \tag{102}$$

where $\phi_1 = (\psi_1 - \psi_2)/\sqrt{2}$. Depletion of atoms from the condensate is

$$dN = \frac{(1 - \sqrt{\gamma+1})^2}{4\sqrt{\gamma+1}}, \tag{103}$$

and the coefficient λ of the particle representation of the Bogoliubov vacuum (100) reads

$$\lambda = \frac{1 - \sqrt{1+\gamma}}{1 + \sqrt{1+\gamma}}. \tag{104}$$

Note that at the critical point ($\gamma = -1$) depletion estimated by means of equation (103) diverges. This suggests that the Bogoliubov vacuum for $\gamma = -1$ is far from an exact ground state of the system.

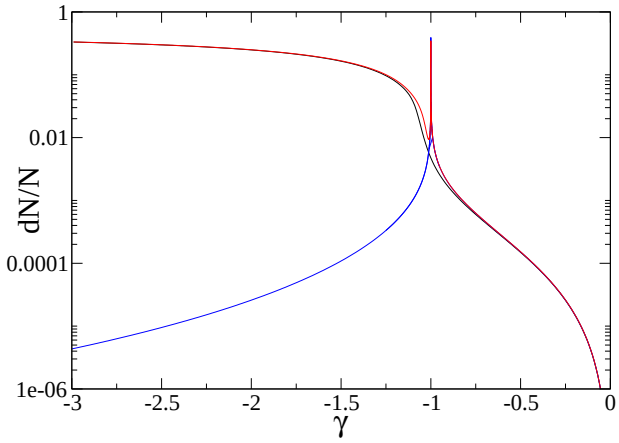

Figure 13: Depletion from the condensate for $N = 200$. Black line corresponds to exact results, blue line to depletion calculated from eqs. (103), (109), and the red one to depletion found in the superposition state (107). The formula (109) is not sufficient because for large negative values of γ the system reveals fragmentation, i.e. the single particle density matrix has two macroscopic eigenvalues, we have $dN \to N/2$ for $\gamma \to -\infty$.

9.2 Bogoliubov vacuum for asymmetric states

For $\gamma < -1$ the condensate mode corresponds to one of the stationary points ($z = \pm z_0, \varphi = 0$), where z_0 is given in (97), and describes an unequal population of atoms in the wells, see (99). Consequently one can build Bogoliubov vacuum states around either of the fixed points, $z = +z_0$ or $z = -z_0$. The two states are degenerate and a proper ground state of the system (which for the symmetric double well potential must be parity symmetric) is a symmetric superposition of the two Bogoliubov vacuum states.

The non-condensate mode is now

$$\phi_{1,\pm} = \sqrt{\frac{1 \mp z_0}{2}}\psi_1 - \sqrt{\frac{1 \pm z_0}{2}}\psi_2. \tag{105}$$

so operators $\hat{c}^\dagger_{0,\pm}$ and $\hat{c}^\dagger_{1,\pm}$ create atoms in the modes (99) and (105), respectively. The Bogoliubov quasi-partice modes

$$\begin{pmatrix} u \\ v \end{pmatrix} = \begin{pmatrix} 1 + z_0 \\ 1 - z_0 \end{pmatrix} \frac{\phi_{1,\pm}}{2\sqrt{z_0}}. \tag{106}$$

The ground state in the Bogoliubov approximation is now

$$|\Psi\rangle \quad = \quad |0_b\rangle_+ + |0_b\rangle_-, \tag{107}$$

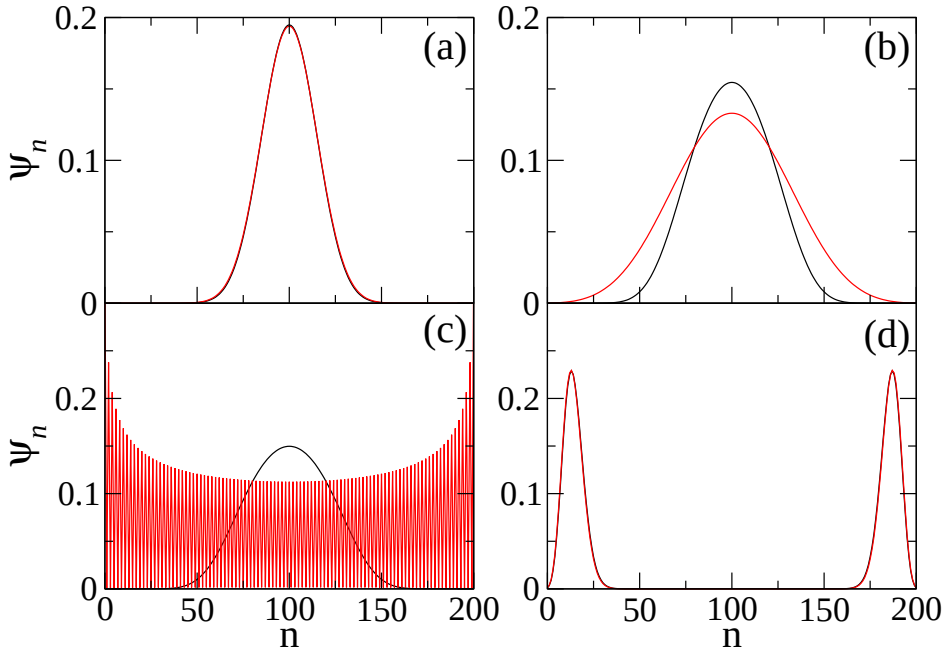

Figure 14: Amplitudes ψ_n of ground states of the double well system in the basis of Fock states $|N-n,n\rangle$, where n denotes the number of particles in the right well. The total number of atoms $N = 200$ and $\gamma = -0.8$ (a), $\gamma = -0.99$ (b), $\gamma = -1$ (c) and $\gamma = -2$ (d). Black lines correspond to exact results while the red ones to the Bogoliubov predictions.

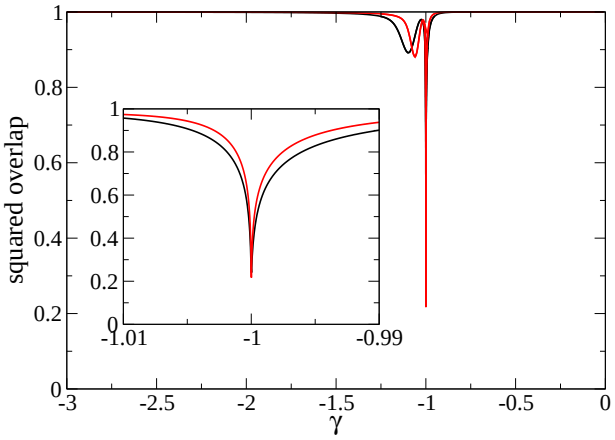

Figure 15: Squared overlap between an exact ground state and the Bogoliubov prediction. Black lines correspond to $N = 100$ whereas the red ones to $N = 200$. The inset shows the enlarged region around $\gamma = -1$.

where

$$|0_b\rangle_\pm \sim \left[\left(\hat{c}^\dagger_{0,\pm}\right)^2 + \lambda\left(\hat{c}^\dagger_{1,\pm}\right)^2\right]^{N/2}|0\rangle, \tag{108}$$

are the Bogoliubov vacuum states built upon the condensate wavefunctions $\phi_{0,+}$ and $\phi_{0,-}$.

For either choice of $\pm z_0$ the quasi-particle excitation energy is $E = J\sqrt{\gamma^2 - 1}$, depletion $dN_\pm$ and the coefficient λ are, respectively

$$dN_\pm = \frac{(1 - z_0)^2}{4z_0}, \quad \lambda = \frac{1}{\gamma^2 (1 + z_0)^2}. \tag{109}$$

As we can see in Figure 13, the above formula is not sufficient to find the number of non-condensed particles. In order to find the depletion, we need to perform the expansion in the superposition state (107).

The Bogoliubov ground states of the double well system can be compared with corresponding exact ground states found numerically. In Fig. 14 we show exact ground states for $N = 200$ and different values of γ. Figure 15 presents squared overlap between the Bogoliubov and exact states for $N = 100$ and $N = 200$. We can see that as long as γ is sufficiently far from -1 the agreement is very good and at the critical point, i.e. $\gamma = -1$, the Bogoliubov theory is not able to describe the system. The reason for that is that for the critical point $\gamma = -1$ the second order terms in the Hamiltonian disappear while the Bogoliubov theory truncates the perturbative expansion in terms of quantum corrections precisely at the second order. In the

next section we will present a theory that includes higher order contributions. Apart from the drop at $\gamma = -1$ we can see a local minimum in the overlap slightly below the critical point. It is a region where the Bogoliubov wavefunction splits into two maxima faster than an exact state. As the total particle number N grows, the range of γ where there is discrepancy between the Bogoliubov predictions and the exact results is smaller.

Note that for $\gamma \to -\infty$ the Bogoliubov prediction (107) tends to

$$|\Psi\rangle \quad \sim \quad \left(\hat{a}_1^\dagger\right)^N |0\rangle + \left(\hat{a}_2^\dagger\right)^N |0\rangle, \tag{110}$$

which corresponds to an exact ground state of the system, a *Schrödinger cat* -like superposition of all atoms over the two wells.

10 Continuous description

The vicinity of the critical point is correctly described within a continuous description introduced by Paweł Ziń [9], see also [116, 120]. The Schrödinger equation obtained from the Hamiltonian (92) reduces to a one-dimensional Schrödinger-like equation of a fictitious particle in an effective potential. In the evolution of the shape of this potential from a parabolic, through quartic, to double well as we vary the interaction strength, one can recognize a second order phase transition. It also shows a clear picture of the increase of fluctuations in the vicinity of the critical point. We will outline derivation and the main results of the model, for details see [9].

Making a substitution

$$\hat{a}_1 \to \sqrt{N}\sqrt{\frac{1+z}{2}}e^{i\varphi_1}, \quad \hat{a}_2 \to \sqrt{N}\sqrt{\frac{1-z}{2}}e^{i\varphi_2}. \tag{111}$$

one can write the mean field Hamiltonian in an alternative form (up to a constant term proportional to N^2)

$$H = \frac{JN}{2}\left(\frac{1}{2}\sqrt{1-z^2}(1-\cos\varphi) + \frac{1}{2}(1-\cos\varphi)\sqrt{1-z^2} + V(z)\right), \tag{112}$$

where $\varphi = \varphi_1 - \varphi_2$ and the effective potential

$$V(z) = -\sqrt{1-z^2} + \frac{\gamma}{2}z^2. \tag{113}$$

Now we can perform quantization by replacing the conjugate variables z and φ with operators $\hat{z}$ and $\hat{\varphi}$ obeying the commutation relation $[\hat{\varphi}, \hat{z}] = \frac{2i}{N}$ [96, 117].

- In the case of repulsive interactions, the phase fluctuations are dominant over fluctuations of the population imbalance z. In that case it is convenient to choose the phase representation, i.e. replace $\hat{z}$ with $\frac{2i}{N}\frac{\mathrm{d}}{\mathrm{d}\varphi}$ [117].

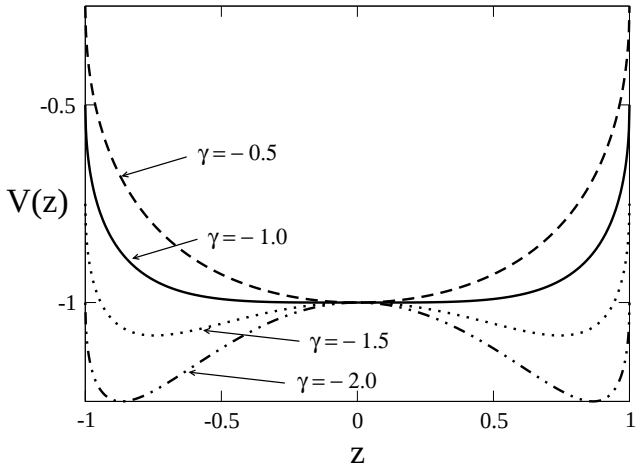

Figure 16: Effective potential (113) for different values of γ.

- On the other hand, in the case of attractive interactions the phase fluctuations are small, $\cos\hat{\varphi} \approx 1 - \frac{1}{2}\hat{\varphi}^2$, and it is more convenient to choose the z representation; $\hat{\varphi} = \frac{2i}{N}\frac{\mathrm{d}}{\mathrm{d}z}$.

In the case of attractive interactions, we obtain

$$\hat{H} = \frac{JN}{2}\left(-\frac{1}{N^2}\sqrt{1-z^2}\frac{\mathrm{d}^2}{\mathrm{d}z^2} - \frac{1}{N^2}\frac{\mathrm{d}^2}{\mathrm{d}z^2}\sqrt{1-z^2} + V(z)\right). \tag{114}$$

The effective one-dimensional Schrödinger equation takes the form

$$-\frac{1}{N^2}\left(\sqrt{1-z^2}\frac{\mathrm{d}^2}{\mathrm{d}z^2} + \frac{\mathrm{d}^2}{\mathrm{d}z^2}\sqrt{1-z^2}\right)\psi(z) + V(z)\psi(z) = \frac{2E}{NJ}\psi(z). \tag{115}$$

Note that the coefficient $2/N$ plays the role of $\hbar$. Looking at the shape of the effective potential $V(z)$ (see Figure 16) we can see in which regions of our space the wavefunction should localize.

Equation (115) generates accurate results even for a relatively low number of atoms. In order to evaluate the quality of the continuum approximation, we have diagonalized the Hamiltonian (92) numerically and compared the eigenstates (Fig. 17) as well as the energy spectrum (Fig. 18) with those obtained from (115). Already at the level of a few hundred particles ($N = 200$ in the calculations), the results obtained within the continuum approximation seem to be indiscernible from the exact ones. It is worth noticing that a similar effective one-dimensional Schrödinger equation was derived in [131] but a continuous variable used there does not possess a clear interpretation of the relative population difference.

Note that the continuum approximation makes it possible to predict properties of a system simply by analyzing a form of the effective potential. Figure 16 presents the shape of the potential for the three relevant regions: before ($\gamma > -1$), at ($\gamma = -1$), and beyond ($\gamma < -1$) the critical point. In the first region the potential has typically a quadratic form, while at $\gamma = -1$

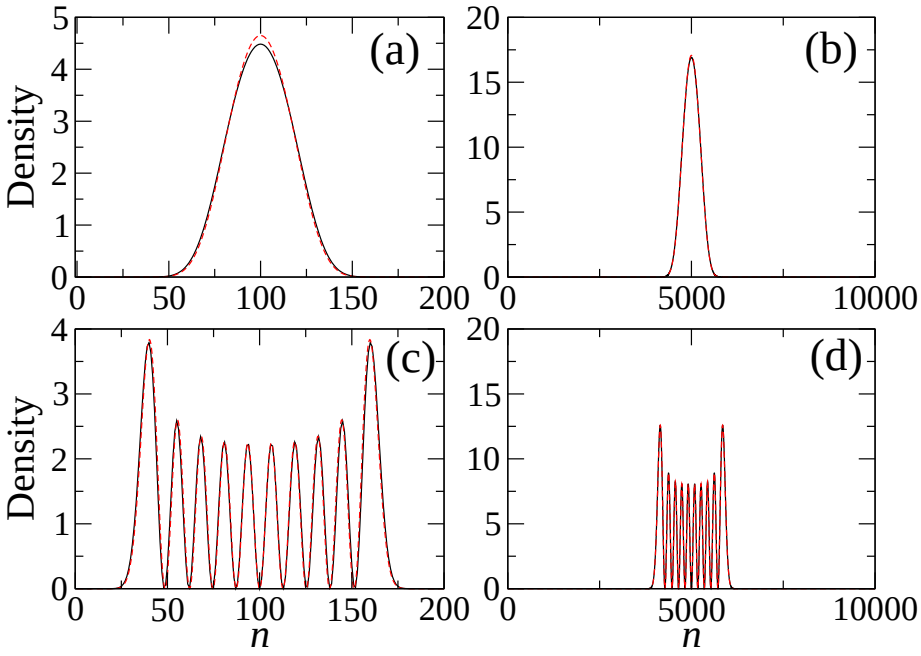

Figure 17: Comparison of the probability density $|\psi(z_n)|^2$ obtained by diagonalization of the exact Hamiltonian (93) (solid black lines) and by solution of Eq.(115) (dashed red lines) at the critical point, i.e. for $\gamma = -1$. Panels (a) and (b) correspond to ground states while (c) and (d) to the ninth excited states. Results for $N = 200$ are presented in (a) and (c) and for $N = 10^4$ in (b) and (d).

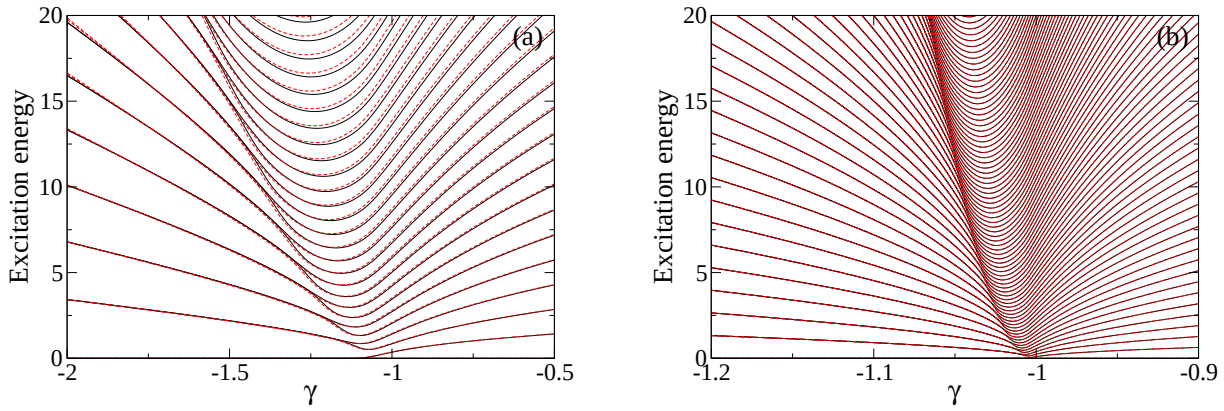

Figure 18: Energy levels (i.e. $2(E - E_0)/J$ where E_0 is the ground state energy) obtained by diagonalization of the exact Hamiltonian (93) (solid black lines) and by solution of Eq.(115) (dashed red lines) versus γ for $N = 200$ (a) and $N = 10^4$ (b).

it broadens substantially and becomes quartic. In the last region it has a form of a double well with the minima at $z = \pm z_0$. This analysis paints a picture of the second-order quantum phase transition, with the critical point at $\gamma = -1$.

We have chosen the order parameter to be $N|z|$ already upon discussing the mean field approximation. Within the mean field approach we are dealing with the average value of $N|z|$. The same variable can be defined in the quantum model (93). The order parameter can be expressed in terms of creation and annihilation operators

$$\hat{\mathcal{B}} = \left| \hat{a}_1^\dagger \hat{a}_1 - \hat{a}_2^\dagger \hat{a}_2 \right| . \tag{116}$$

With an increasing N the quantum average $\langle \hat{\mathcal{B}} \rangle / N$ tends towards the mean field value of $|z|$, which can be seen in Figure 19. The Bogoliubov prediction follows the exact result for $\gamma > -1$ and the mean field theory for $\gamma < -1$. The shape of the potential determines the shape of the ground state wave-function, which is always symmetric. For $\gamma \geq -1$ it is bell shaped and centered around $z = 0$, and when $\gamma < -1$ the wave-function has a double hump structure, centered around $\pm z_0$. Since the effective $\hbar$ is $2/N$, the width of the wave-function decreases with an increasing N. The wave-function will be centered around the minima of the potential $V(z)$, which, as we mentioned above, is given by the mean field approximation. This shows that the mean value of $\langle \hat{\mathcal{B}} \rangle / N$ indeed will approach the mean field value. This fact was noticed in Ref. [132].

Employing the modulus in the mean field approach makes the order parameter the same regardless of whether we choose a solution at the fixed point $z = z_0$ or $z = -z_0$. In the quantum case the ground state is a superposition of wave-packets localized in the two wells of the

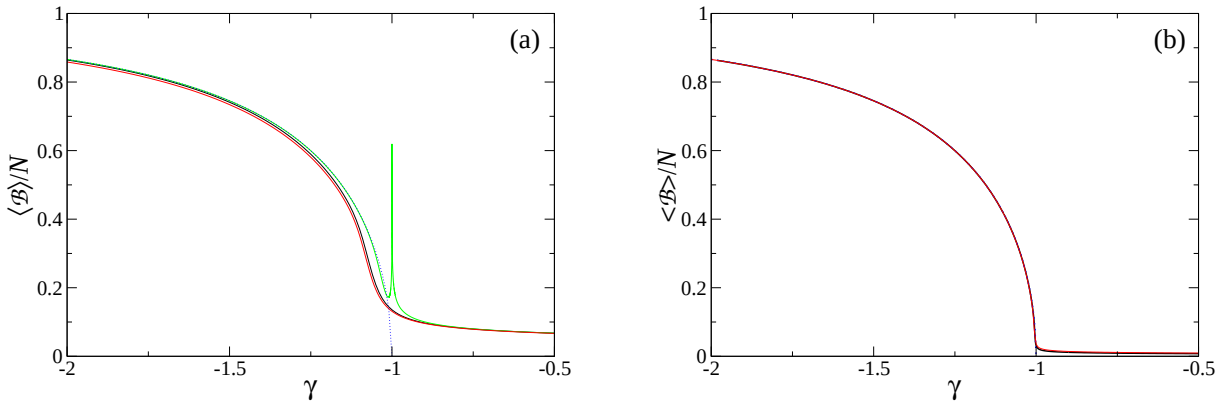

Figure 19: The order parameter, i.e. average value of the operator $\hat{\mathcal{B}}$ (116), obtained from an exact diagonalization of the Hamiltonian (92) (black lines), from the continuum model (115) (red lines), compared to the Bogoliubov theory (100), (107) (green lines) and mean field results (blue dotted lines), for $N = 200$ (a) and $N = 10^4$ (b). The Bogoliubov prediction is plotted only in panel (a).

potential $V(z)$. Here the order parameter with the modulus is insensitive to the superposition and examines only the width of the wave-function. This motivates our choice of the order parameter.

In the remainder of this chapter we will discuss density and particle number fluctuations near the critical point. An extension of the continuum model to an effectively two-dimensional system will be discussed in the next chapter.

11 Critical fluctuations

In Bose-Einstein condensate systems quantum density fluctuations (i.e. the fluctuations not induced by thermal effects) are usually negligible. When the parameter γ approaches the critical point, however, we may expect an increase in the density fluctuations [6]. For $\gamma < -1$ the fluctuations will grow even more, due to condensate fragmentation, as can be seen in Fig. 13. In the first part of this section we will show that although the number of depleted atoms on the "symmetric side" of the critical point remains negligible, the density fluctuations are of the order of a few percent of the total density, for γ close to -1. In the last part critical fluctuations of the order parameter will be distinguished from the fluctuations resulting from the quantum superposition.

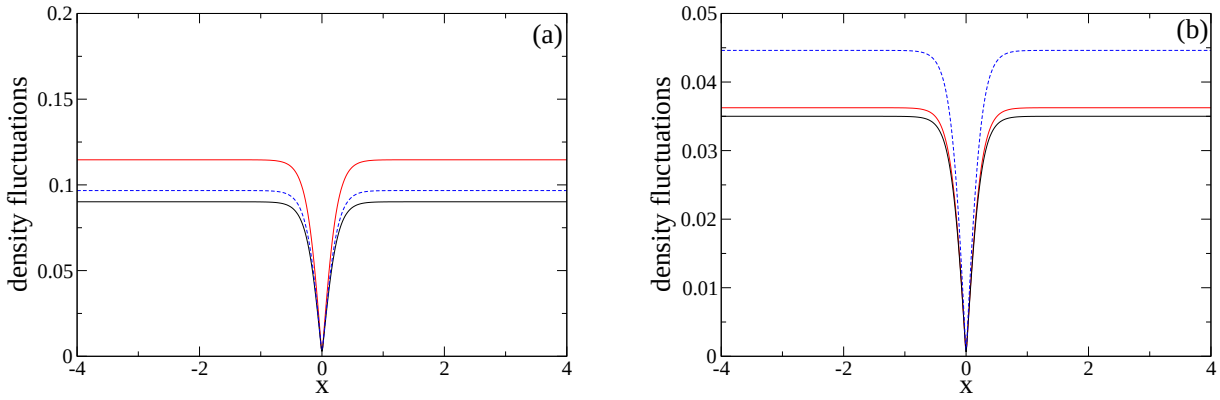

Figure 20: Standard deviation of the density fluctuations divided by the average density for $N = 1000$ (a) and $N = 10000$ (b). Solid lines correspond to results for $\gamma = -0.995$ (black lines - exact; red lines - Bogoliubov estimates (122)). Dashed blue lines depict exact results for $\gamma = -1$.

11.1 Density fluctuations

To estimate quantum density fluctuations for $\gamma > -1$ we can rewrite the Bogoliubov vacuum state as a gaussian superposition over perfect condensate states [92]

$$|0_b\rangle \sim \int dq \exp\left(-\frac{q^2}{2\Lambda}\right)|N:\phi_q\rangle, \tag{117}$$

where $|N:\phi_q\rangle$ is an N-body state where all N particles occupy a single particle wavefunction

$$\phi_q = \frac{\phi_0 + \frac{q}{\sqrt{N}}\phi_1}{\sqrt{1+\frac{q}{N}}}, \tag{118}$$

and

$$\Lambda = \frac{\lambda}{1-\lambda}. \tag{119}$$

The parameter λ and the modes ϕ_0 and ϕ_1 were defined in sections 8 and 9.1 (see Eqs. (98), (102)). Results of single measurements of the system density can be simulated using an approximate density [92], see also chapter III,

$$\rho_q = |\phi_q|^2 \sim \phi_0^2 + 2\frac{q}{\sqrt{N}}\phi_0\phi_1 + \frac{q^2}{N}\phi_1^2, \tag{120}$$

where, for each experimental realization, the real parameter q has to be chosen randomly from the gaussian probability density [97]

$$P(q) \sim \exp\left(-\frac{q^2}{\Lambda}\right). \tag{121}$$

The last term in Eq. (120) can be skipped because for small depletion we have $q^2/N \sim \Lambda/N \approx dN/N$. The middle term $q/\sqrt{N}$ is, however, of the order of $\sqrt{dN/N}$ and for a moderate particle number may lead to noticeable density fluctuations. The estimated variance of the density fluctuations reads

$$\mathrm{var}(\rho_q) = \frac{1-\sqrt{1+\gamma}}{N\sqrt{1+\gamma}}\phi_0^2\phi_1^2. \tag{122}$$

In order to compare these predictions with exact results we have chosen the localized modes as

$$\psi_{1,2}(x) = \left(\frac{2}{\pi}\right)^{1/4} \exp\left[-(x \pm 2)^2\right]. \tag{123}$$

The standard deviation of the fluctuations divided by the average density, i.e. $\sqrt{\mathrm{var}(\rho_q)}/\langle\rho_q\rangle$ is plotted in Fig. (20). If we set the critical parameter e.g. to $\gamma = -0.995$, we can see that for $N = 1000$ we have density fluctuations of the order of 10%, but the Bogoliubov approximation is biased with a significant error and overestimates the effect. For larger particle numbers, such as $N = 10^4$, the agreement between the Bogoliubov and the exact result is perfect, but the fluctuations drop to below 4% of the density. To realize the magnitude of fluctuations for different particle numbers see the exact results for $\gamma = -1$.

11.2 Fluctuations of the order parameter

As already mentioned, for $\gamma < -1$ and decreasing, the condensate fragmentation induces growing density fluctuations. Intuitively one can see that realizing the growing distance between the two peaks in the ground state, see Fig. 14 (d). These fluctuations are extremely sensitive to experimental imperfections and consequently are difficult to test.

On the other hand, since the potential is of the Landau-Ginzburg type, it is clear that the fluctuations of the order parameter will be maximal at the critical point. The quantitative analysis of this issue can be made using the continuum approximation and the exact diagonalization of the quantum model. The variance of $\hat{\mathcal{B}}$ in the ground state of the double well system versus γ is shown in Fig. 21 for two different numbers of particles. Indeed, the fluctuations are maximal around the critical point. With the increasing value of N the width of the peak of the variance decreases and its position tends to $\gamma = -1$.

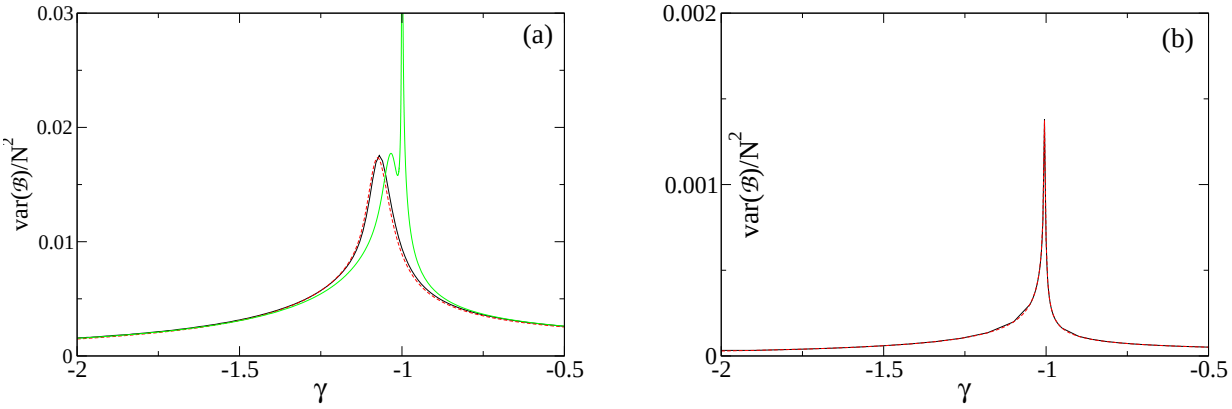

Figure 21: Variance of the $\hat{\mathcal{B}}$ operator, Eq.(116), in a ground state obtained from exact diagonalization of the Hamiltonian (93) (black lines), by solving Eq.(115) (red lines) and from the Bogoliubov theory (green lines) for $N = 200$ (a) and $N = 10^4$ (b).

Part V
Second order quantum phase transition of a homogeneous Bose gas with attractive interactions

Motivated by the studies of a homogeneous two component condensate close to the phase separation transition (see chapter III) we will consider a single attractive condensate trapped in an elongated 3D box with periodic boundary conditions. We expect that similarly as in the former case there is a range of interaction values for which the finite size of the system ensures the stability. We will focus our attention on quantum fluctuations close to the instability point.

An attractive homogeneous Bose gas in a large volume ($V \to \infty$) reveals no condensation [133, 134]. A hand-waving argument based upon the uncertainty principle is that particles attracting one another in the position space will act repulsively in the momentum space. The energy is therefore minimized when many plane wave states are occupied. Indeed, a many body ground state of such system is a fragmented condensate, i.e. there are many macroscopic eigenvalues of the single particle density matrix.

For a finite one-dimensional system the mean field theory (Gross-Pitaevskii equation [1, 2, 3]) predicts a spontaneous symmetry breaking, i.e. breaking of the translational invariance [135]. When the strength of the attractive interaction reaches a critical value a solution becomes localized. On the other hand the one-particle density has to be uniform in a ground state of the full quantum Hamiltonian, due to the translational invariance of the system. The connection between the mean field spontaneous symmetry breaking, Bogoliubov, and the full quantum many body theory symmetry restoring was analyzed by a few authors [137]. It was shown that for a 1D Bose gas in a box, when the interaction strength exceeds a critical value, even weak external symmetry breaking perturbation leads to a localized state. A translation of the soliton costs no energy (this is a zero-mode of the Bogoliubov theory) and the corresponding quantum fluctuations (in the position and momentum) of the center of mass of the soliton were analyzed [138].

We will show that in the vicinity of the critical point the Hilbert space can be divided into a subspace, which can be described by the Bogoliubov theory, and a subspace where two modes unstable in the Bogoliubov description can be conveniently treated with the aid of a continuous description. Only the latter contains relevant information about critical behaviour of the system. We obtain a Schrödinger equation of a fictitious particle moving in an effective two-dimensional potential and a transition of the potential from a parabolic to a Mexican hat shape reflects the second order quantum phase transition. In the effective Hilbert space numerical studies of fluctuations in the vicinity of the critical point have become possible.

12 Bogoliubov theory

We consider a gas of Bose particles with contact attractive interaction in a 3D box with periodic boundary conditions. The Hamiltonian of the system reads

$$\hat{H} = \int d^3r \hat{\psi}^\dagger(\mathbf{r}) \left[-\frac{\hbar^2}{2m}\nabla^2 + \frac{g}{2}\hat{\psi}^\dagger(\mathbf{r})\hat{\psi}(\mathbf{r}) \right] \hat{\psi}(\mathbf{r}), \tag{124}$$

where $\hat{\psi}(\mathbf{r})$ is the bosonic field operator, and $g = 4\pi\hbar^2 a/m$, is the coupling constant that characterizes the particle interaction (a is the s-wave scattering length which for the attractive interaction is negative). In the case of a homogeneous system it is convenient to switch to a momentum basis,

$$\hat{\psi}(\mathbf{r}) = \sum_{\mathbf{k}} \frac{e^{i\mathbf{k}\cdot\mathbf{r}}}{\sqrt{V}} \hat{a}_{\mathbf{k}}, \tag{125}$$

where $V = L_x L_y L_z$ is the volume of the box and the sum runs over discrete momenta,

$$\mathbf{k} = 2\pi \left(\frac{n_x}{L_x}, \frac{n_y}{L_y}, \frac{n_z}{L_z} \right), \tag{126}$$

with integer n_x, n_y, n_z. Then, the Hamiltonian reads

$$\hat{H} = \sum_{\mathbf{k}} \frac{\hbar^2 k^2}{2m} \hat{a}^\dagger_{\mathbf{k}} \hat{a}_{\mathbf{k}} + \frac{g}{2V} \sum_{\mathbf{k},\mathbf{k}',\mathbf{q}} \hat{a}^\dagger_{\mathbf{k}+\mathbf{k}'-\mathbf{q}} \hat{a}^\dagger_{\mathbf{q}} \hat{a}_{\mathbf{k}'} \hat{a}_{\mathbf{k}}. \tag{127}$$

Exact diagonalization is impossible because of an enormous size of the Hilbert space of the system. However, we are interested in a ground state of the system in the case of weak particle interactions. Then, one can expect that only one mode macroscopically occupied by atoms and, in the first approximation, we may use a mean field approach which relies on substitution of the bosonic operator $\hat{\psi}(\mathbf{r})$ with a classical field $\phi_0(\mathbf{r})$. This assumption is valid only for a finite and small system. As it was shown in [133, 134] attractive bosons confined in a large volume reveal fragmentation, i.e. the energy is minimized by a configuration where many momentum modes are macroscopically occupied. The resulting in our case Gross-Pitaevskii equation reveals a homogeneous stationary solution (i.e. the condensate wavefunction)

$$\phi_0(\mathbf{r}) = \frac{1}{\sqrt{V}}, \tag{128}$$

and a chemical potential $\mu = gN/V$. Quantum fluctuations around the mean field solution can be described within the Bogoliubov theory [87]. We employ its number conserving version [89, 90, 91] where a part of the Hamiltonian (127), minus a constant term $\mu\hat{N}$, with contributions of the second order in $\hat{a}_{\mathbf{k}}$ (where $\mathbf{k} \neq 0$),

$$\hat{H}_B = \sum_{\mathbf{k}\neq 0} \left[\left(\frac{\hbar^2 k^2}{2m} + \frac{2g}{V}\hat{a}^\dagger_0 \hat{a}_0 - \frac{gN}{V} \right) \hat{a}^\dagger_{\mathbf{k}} \hat{a}_{\mathbf{k}} + \frac{g}{2V} \left(\hat{a}^\dagger_0 \hat{a}^\dagger_0 \hat{a}_{-\mathbf{k}} \hat{a}_{\mathbf{k}} + \hat{a}_0 \hat{a}_0 \hat{a}^\dagger_{-\mathbf{k}} \hat{a}^\dagger_{\mathbf{k}} \right) \right], \tag{129}$$

is substituted with

$$\hat{H}_B = \sum_{\mathbf{k}\neq 0}\left[\left(\frac{\hbar^2 k^2}{2m}+\frac{gN}{V}\right)\hat{\Lambda}^\dagger_{\mathbf{k}}\hat{\Lambda}_{\mathbf{k}}+\frac{gN}{2V}\left(\hat{\Lambda}^\dagger_{\mathbf{k}}\hat{\Lambda}^\dagger_{-\mathbf{k}}+\hat{\Lambda}_{\mathbf{k}}\hat{\Lambda}_{-\mathbf{k}}\right)\right], \tag{130}$$

where

$$\hat{\Lambda}_{\mathbf{k}} = \frac{\hat{a}^\dagger_0}{\sqrt{N}}\hat{a}_{\mathbf{k}}. \tag{131}$$

The Bogoliubov transformation $\hat{b}_{\mathbf{k}} = \langle u_k|\hat{\Lambda}_{\mathbf{k}}\rangle - \langle v_k|\hat{\Lambda}^\dagger_{-\mathbf{k}}\rangle$, with

$$u_k + v_k = \left(\frac{\frac{\hbar^2 k^2}{2m}}{\frac{\hbar^2 k^2}{2m}+\frac{2gN}{V}}\right)^{1/4}, \quad u_k - v_k = (u_k+v_k)^{-1}, \tag{132}$$

allows one to write the Hamiltonian (130) in a diagonal form, $\hat{H}_B = \sum_{\mathbf{k}\neq 0} E_k \hat{b}^\dagger_{\mathbf{k}}\hat{b}_{\mathbf{k}}$, where the Bogoliubov spectrum reads

$$E_k = \sqrt{\frac{\hbar^2 k^2}{2m}\left(\frac{\hbar^2 k^2}{2m}+\frac{2gN}{V}\right)}. \tag{133}$$

Within the N-conserving Bogoliubov theory we can obtain an N-body ground state in the particle representation in a simple form [92, 96, 97], see also chapter III,

$$|0_b\rangle \sim \left[\hat{a}^\dagger_0\hat{a}^\dagger_0 + \sum_{\mathbf{k}\neq 0}\lambda_k\left(\hat{a}^\dagger_{c,\mathbf{k}}\hat{a}^\dagger_{c,\mathbf{k}}+\hat{a}^\dagger_{s,\mathbf{k}}\hat{a}^\dagger_{s,\mathbf{k}}\right)\right]^{N/2}|0\rangle, \tag{134}$$

where

$$\hat{a}_{c,\mathbf{k}} = \frac{\hat{a}_{\mathbf{k}}+\hat{a}_{-\mathbf{k}}}{\sqrt{2}}, \quad \hat{a}_{s,\mathbf{k}} = \frac{\hat{a}_{\mathbf{k}}-\hat{a}_{-\mathbf{k}}}{i\sqrt{2}}, \tag{135}$$

and

$$\lambda_k = \sqrt{\frac{dN_k}{1+dN_k}}. \tag{136}$$

Here

$$dN_k = \langle v_k|v_k\rangle, \tag{137}$$

are eigenvalues of the reduced single particle density matrix. The total number of atoms depleted from the condensate mode reads

$$dN = \sum_{\mathbf{k}\neq 0} dN_k. \tag{138}$$

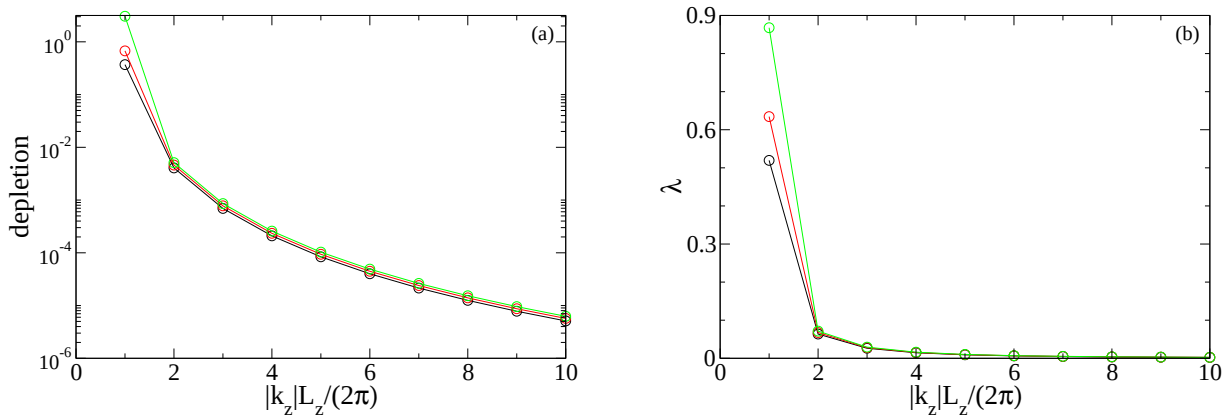

Figure 22: Panel (a) shows depletion to non-condensate modes (in the direction of the lowest excitation) calculated for three different values of the parameter α within the Bogoliubov theory. Black circles correspond to $\alpha = -0.9$, red circles to $\alpha = -0.95$ and the green ones to $\alpha = -0.995$. Here we have taken $L_z = 100$ μm, $L_x = L_y = 40$ μm, so for $N = 500$ the scattering length is within the range between $a = -1450 a_B$ and $a = -1603 a_B$ whereas for $N = 10^5$ it is between $a = -7.25 a_B$ and $a = -8.02 a_B$ (a_B is the Bohr length), see (140). Panel (b) shows the coefficients λ_k from the Bogoliubov vacuum state (134). The lines are guides to eyes.

In the following we will consider the system in a box where $L_x, L_y \leq L_z/2$. Then, the lowest Bogoliubov excitation energy corresponds to momenta

$$\mathbf{k}_\pm = \pm \frac{2\pi}{L_z} (0, 0, 1) , \tag{139}$$

and it is real provided a parameter[3]

$$\alpha = \frac{2gN}{\epsilon_0 V} = \frac{4NaL_z}{L_x L_y}, \tag{140}$$

where

$$\epsilon_0 = \frac{\hbar^2}{2m} \left(\frac{2\pi}{L_z} \right)^2 , \tag{141}$$

is greater than -1. For $\alpha = -1$ the energy gap between the ground state and the first excited state disappears, the homogeneous mean field solution (128) looses its stability and the quantum depletion dN diverges because $dN_{k_\pm}$ diverge. More precisely, for $\alpha < -1$ the mean field solution

[3]Note that for a given box geometry and particle number we can always adjust the scattering length a so that values of α are close to -1.

spontaneously breaks the translational symmetry of the system. In the next section we show that this point can be regarded as a critical point.

We conclude that the Bogoliubov approximation breaks down at the critical point. As can be seen in Fig. 22 the population of $\mathbf{k}_\pm$ grows significantly as we approach the instability, but populations of higher momentum modes are within this approximation still negligible. The average number of particles in these modes for α around -1 can be estimated as follows:

$$\sum_{\mathbf{k}\neq 0,\mathbf{k}_\pm} dN_k = \sum_{\mathbf{k}\neq 0,\mathbf{k}_\pm} \langle v_k|v_k\rangle \approx \frac{V}{2\pi^2}\int_{4\pi/L_z}^{\infty} dk\; k^2\; \langle v_k|v_k\rangle, \tag{142}$$

and it is not greater than 0.2 in a vicinity of the critical point for our box geometry. Note that the coefficients in the Bogoliubov vacuum state (134) depicted in panel (b) of Fig. 22 for a few lowest momentum modes are all positive. In the case of the two-component homogeneous BEC an occurrence of a mode with the positive λ_k was a signature that we have entered a regime where an infinite system would be unstable while a finite one was still stable against phase separation. Here, as soon as the interactions become attractive, an infinite system loses its stability against fragmentation, and consequently for all modes we have $\lambda_k > 0$. Density fluctuations should be significant as we approach the instability and can be estimated in a completely analogous way as those in a two-component condensate.

13 Effective Hamiltonian in a continuous description

The Bogoliubov theory provides us with information about the modes requiring a special treatment. In the present section we will present derivation of a model introduced by P. Ziń [10] and describing the critical point in terms of the most populated modes only. Then we will use the model to analyze the vicinity of the critical point. The Hamiltonian restricted to the condensate and $\mathbf{k}_\pm$ modes reads

$$\begin{aligned}\hat{H} \approx\; & \epsilon_0\left(\hat{a}_+^\dagger\hat{a}_+ + \hat{a}_-^\dagger\hat{a}_-\right) + \frac{g}{V}\left(\hat{a}_0^\dagger\hat{a}_0^\dagger\hat{a}_+\hat{a}_- + \hat{a}_+^\dagger\hat{a}_-^\dagger\hat{a}_0\hat{a}_0\right)\\ & + \frac{g}{2V}\left(\hat{a}_0^\dagger\hat{a}_0^\dagger\hat{a}_0\hat{a}_0 + \hat{a}_+^\dagger\hat{a}_+^\dagger\hat{a}_+\hat{a}_+ + \hat{a}_-^\dagger\hat{a}_-^\dagger\hat{a}_-\hat{a}_-\right)\\ & + \frac{2g}{V}\left(\hat{a}_0^\dagger\hat{a}_0\left(\hat{a}_+^\dagger\hat{a}_+ + \hat{a}_-^\dagger\hat{a}_-\right) + \hat{a}_+^\dagger\hat{a}_+\hat{a}_-^\dagger\hat{a}_-\right),\end{aligned} \tag{143}$$

where we introduced the notation $\hat{a}_{\mathbf{k}_\pm} \equiv \hat{a}_\pm$. Since the total number of particles is conserved and equal to N we can eliminate one of the modes from the above Hamiltonian. Here we choose to eliminate the $k = 0$ mode. In order to do so we substitute operators $\hat{a}_0$ and $\hat{a}_0^\dagger$ by an operator $\sqrt{N - \left(\hat{a}_+^\dagger\hat{a}_+ + \hat{a}_-^\dagger\hat{a}_-\right)}$ (see [139]). Now our Hamiltonian can be written as

$$\hat{H} = \frac{g}{2V}(N^2 - N) + \hat{H}', \tag{144}$$

where

$$\hat{H}' = (\epsilon_0 + gn)\left(\hat{a}_+^\dagger \hat{a}_+ + \hat{a}_-^\dagger \hat{a}_-\right) + gn\left(\hat{a}_+\hat{a}_- + \hat{a}_+^\dagger \hat{a}_-^\dagger\right)$$
$$-\frac{g}{V}\left(\hat{a}_+^\dagger \hat{a}_+ \hat{a}_+^\dagger \hat{a}_+ + \hat{a}_-^\dagger \hat{a}_- \hat{a}_-^\dagger \hat{a}_- + \hat{a}_+^\dagger \hat{a}_+ \hat{a}_-^\dagger \hat{a}_-\right)$$
$$-\frac{g}{V}\left(\left(\hat{a}_+^\dagger \hat{a}_+ + \hat{a}_-^\dagger \hat{a}_-\right)\hat{a}_+\hat{a}_- + \hat{a}_+^\dagger \hat{a}_-^\dagger \left(\hat{a}_+^\dagger \hat{a}_+ + \hat{a}_-^\dagger \hat{a}_-\right)\right). \tag{145}$$

Note, that the above Hamiltonian commutes with the total momentum operator which in this case is equal to

$$\hat{P} = \frac{2\pi\hbar}{L_z}\left(\hat{a}_+^\dagger \hat{a}_+ - \hat{a}_-^\dagger \hat{a}_-\right). \tag{146}$$

Next we introduce symmetric and antisymmetric combinations of $\hat{a}_\pm$, see Eq. (135), and describe dynamics of these modes using the position-momentum representation

$$\hat{a}_c = \frac{\hat{x}_c + i\hat{p}_c}{\sqrt{2}}, \quad \hat{a}_s = \frac{\hat{x}_s + i\hat{p}_s}{\sqrt{2}}. \tag{147}$$

In this representation the Hamiltonian $\hat{H}'$ can be split into several parts

$$\frac{\hat{H}'}{\epsilon_0} = -1 - \frac{\alpha}{2} - \frac{3\alpha}{8N} + \frac{\hat{H}_F}{\epsilon_0} + \frac{\delta\hat{H}}{\epsilon_0}, \tag{148}$$

where

$$\frac{\hat{H}_F}{\epsilon_0} = \frac{1}{2}\left(\hat{p}_c^2 + \hat{p}_s^2\right) + \frac{1+\alpha}{2}\left(\hat{x}_c^2 + \hat{x}_s^2\right) - \frac{7\alpha}{32N}\left(\hat{x}_c^2 + \hat{x}_s^2\right)^2 \tag{149}$$

and

$$\frac{\delta\hat{H}}{\epsilon_0} = -\frac{\alpha}{8N}\left(\hat{p}_c^2 + \hat{p}_s^2\right) + \frac{7\alpha}{8N}\left(\hat{x}_c^2 + \hat{x}_s^2\right) - \frac{3\alpha}{32N}\left((\hat{p}_c^2 + \hat{p}_s^2)(\hat{x}_c^2 + \hat{x}_s^2) + (\hat{x}_c^2 + \hat{x}_s^2)(\hat{p}_c^2 + \hat{p}_s^2)\right)$$
$$-\frac{\alpha}{32N}\left(4\left(\hat{p}_c\hat{x}_s - \hat{p}_s\hat{x}_c\right)^2 - \left(\hat{p}_c^2 + \hat{p}_s^2\right)^2\right). \tag{150}$$

The total momentum operator (146) is in this representation proportional to $\hat{p}_c\hat{x}_s - \hat{p}_s\hat{x}_c$ and it commutes both with $\hat{H}_F$ and $\delta\hat{H}$. Hence any excitation caused by the latter can not change the value of the total momentum, which is equal to zero in the ground state.

Up to now we have divided our Hamiltonian into two parts and in what follows we will show that for large N (strictly speaking in the limit of N tending to infinity while α is kept constant) the dominating contribution arises from the effective Hamiltonian $\hat{H}_F$. This is a Hamiltonian of a fictitious particle moving in a two-dimensional effective potential. Indeed, upon defining $\hat{r}^2 = \hat{x}_c^2 + \hat{x}_s^2$ we can derive a Schrödinger equation

$$E\psi(r) = -\frac{1}{2}\triangle\psi(r) + V_{eff}(r)\psi(r), \tag{151}$$

where the 2D effective potential is equal to

$$V_{eff}(r) = \frac{1+\alpha}{2} r^2 - \frac{7\alpha}{32N} r^4. \tag{152}$$

This potential evolves, when we pass through the critical point, from a parabolic ($\alpha > -1$), through quartic well ($\alpha = -1$) to a Mexican hat shape ($\alpha < -1$), which is a signature of the second order quantum phase transition.

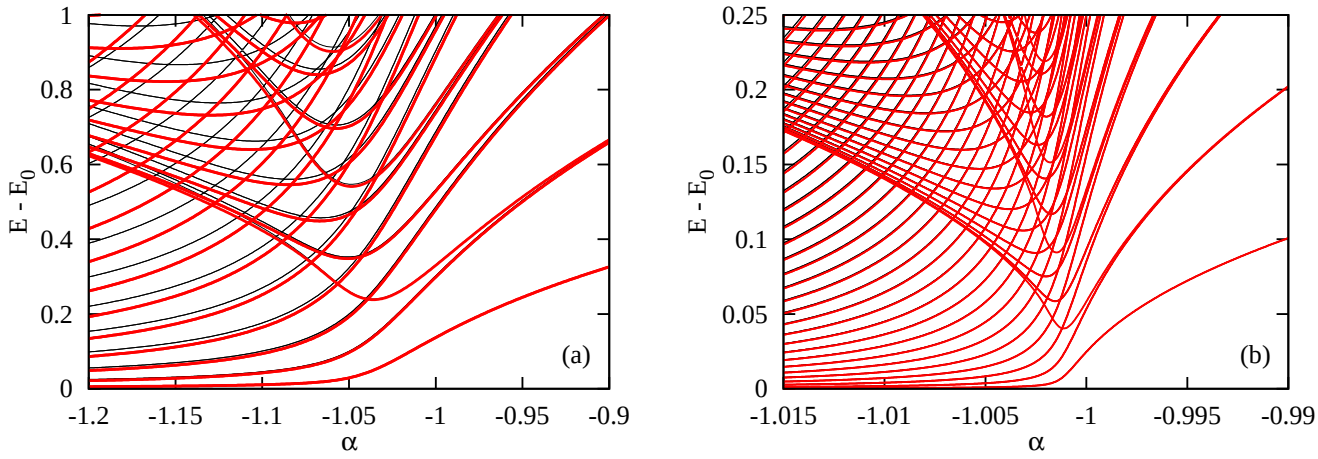

Figure 23: Energy levels with respect to the ground state energy of the Hamiltonian H' (black lines) and H_F (red lines). Panel (a) shows results for $N = 500$ while panel (b) for $N = 10^5$.

In [10] there are P. Ziń's analytic approximations to the solution of this Schrödinger equation as well as estimates of the contribution from the Hamiltonian $\delta\hat{H}$ in all the three regions mentioned above. In the most interesting situation, $\alpha = -1$, the Schrödinger equation (151) takes the form

$$-\frac{1}{2}\triangle\psi(r) + \frac{7}{32N} r^4 \psi(r) = E\psi(r). \tag{153}$$

We can switch to a new variable $\tilde{r} = r/N^{1/6}$ and obtain

$$-\frac{1}{2}\triangle\psi(\tilde{r}) + \frac{7}{32}\tilde{r}^4\psi(\tilde{r}) = N^{1/3}E\psi(\tilde{r}). \tag{154}$$

From dimensional analysis we estimate ΔE, the energy difference between the ground and the first excited state with the total momentum equal to zero, to be of the order of $N^{-1/3}$. On the other hand the dominant contribution to the Hamiltonian $\delta\hat{H}$ comes from the terms $\hat{x}^2/N$ and is of the order of $N^{-2/3}$. So in the limit of a large N it can be neglected. Notice that as we mentioned above the total momentum operator (146) commutes with both $\hat{H}_F$ and $\delta\hat{H}$. Hence, any excitation caused by the latter can not change the value of the total momentum, which is

equal to zero in the ground state. If we use the continuous description and express the total momentum operator in the polar coordinates, it turns out that it is proportional to $\partial/\partial\phi$. Hence any state with the total momentum equal to zero does not depend on ϕ. This is why estimating ΔE we have neglected the ϕ dependence.

To prove that the contribution from $\delta\hat{H}$ is indeed negligible we have diagonalized the Hamiltonian $\hat{H}'$ and $\hat{H}_F$ numerically. In Fig. 23 we show energy levels obtained in each case. One can see that already for a moderate particle number ($N = 500$) the low-lying energy levels of the two sets coincide and for the greater N ($N = 10^5$) even the higher excited states are properly reproduced. In conclusion even for a moderate number of particles the Hamiltonian $\hat{H}_F$ is a very good approximation to $\hat{H}'$ apart from the constant term $-1 - \frac{\alpha}{2} - \frac{3\alpha}{8N}$.

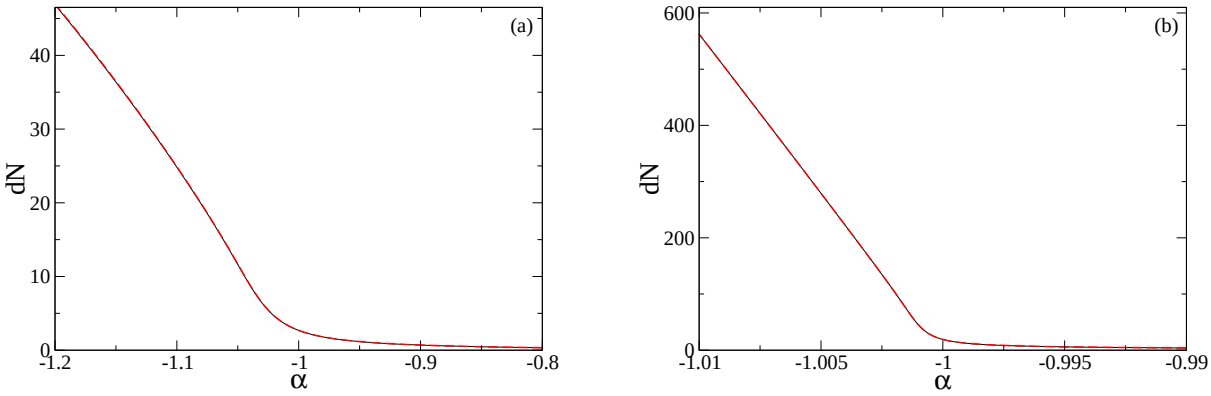

Figure 24: Mean depletion from the condensate as a function of α for $N = 500$ (a) and $N = 10^5$ (b). Black solid lines correspond to the Hamiltonian $\hat{H}'$ while red dashed lines to $\hat{H}_F$.

14 Critical fluctuations

When we use the concept of the effective potential (152), description of an attractive homogeneous Bose gas around the critical point becomes particularly simple. One could study the dynamical transition of the system when the scattering length is changed in time, especially for a system entering the critical region. Here, however, we restrict our considerations to the static (ground state) properties of the system around the critical point. Since the effective potential undergoes the transition from quadratic through quartic to a Mexican hat shape, which is a typical signature of the second order phase transition, we expect critical fluctuations to show up. Hence we search for an observable that will show clear evidence of the critical behaviour (will have maximal fluctuations at the critical point). Analogously as in the double well case,

we have to distinguish the critical fluctuations from fluctuations occurring due to superpositions of symmetry breaking states, studied in [138].

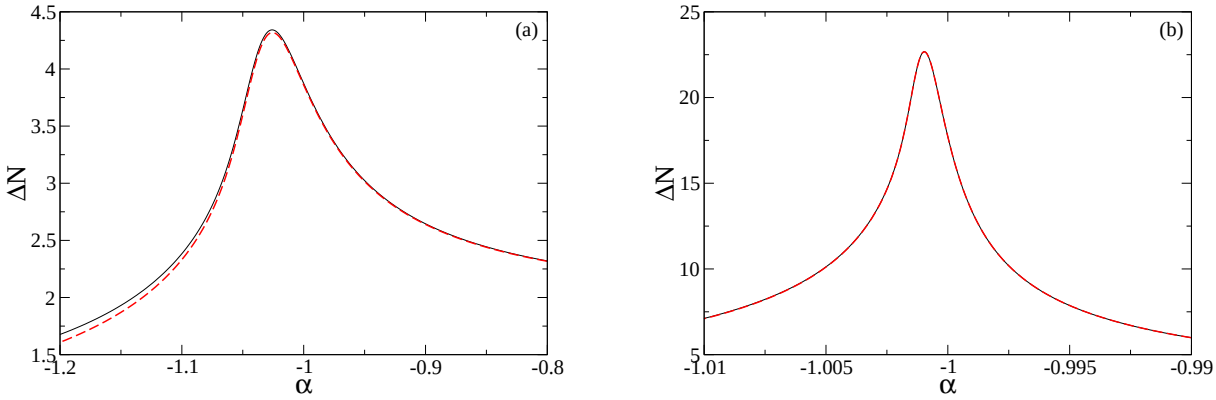

Figure 25: Fluctuations of the condensate depletion (157) for $N = 500$ (a) and $N = 10^5$ (b) as a function of α. Black solid lines correspond to the Hamiltonian $\hat{H}'$ and red dashed lines to $\hat{H}_F$.

Let us consider the operator $d\hat{N}$ representing the number of atoms depleted from a condensate. The contribution (142) from the modes described by the Bogoliubov Hamiltonian is very small and can be neglected, therefore

$$d\hat{N} \approx \hat{n}_c + \hat{n}_s, \tag{155}$$

where

$$\hat{n}_c = \frac{1}{2}\left(\hat{p}_c^2 + \hat{x}_c^2 - 1\right), \quad \hat{n}_s = \frac{1}{2}\left(\hat{p}_s^2 + \hat{x}_s^2 - 1\right). \tag{156}$$

The depletion, $dN = \langle d\hat{N}\rangle$, increases as we approach and pass through the critical point, see Fig. 24. We compare in that figure the mean value of atoms depleted from the condensate as a function of the parameter α for two different total number of atoms. Each panel represents two curves that practically sit on top of each other; one obtained from the Hamiltonian $\hat{H}'$ and the other from $\hat{H}_F$. The linear behaviour for $\alpha < -1$ is due to the linear dependence of the square of the position of the minimum in the Mexican hat — r_0^2 on the interaction strength α. For large N we can estimate that $\langle \hat{n}_c + \hat{n}_s\rangle \simeq \langle \hat{x}_c^2 + \hat{x}_s^2\rangle/2 \simeq r_0^2/2 = N\frac{4(\alpha+1)}{7\alpha}$.

The variance of $d\hat{N}$ increases as we cross the critical point but if we calculate the variance relative to the average depletion it turns out that the critical point region is clearly indicated by the maximum of such fluctuations. In Fig. 24 we present the variable

$$\Delta N = \frac{\langle (d\hat{N} - \langle d\hat{N}\rangle)^2\rangle}{\langle d\hat{N}\rangle}, \tag{157}$$

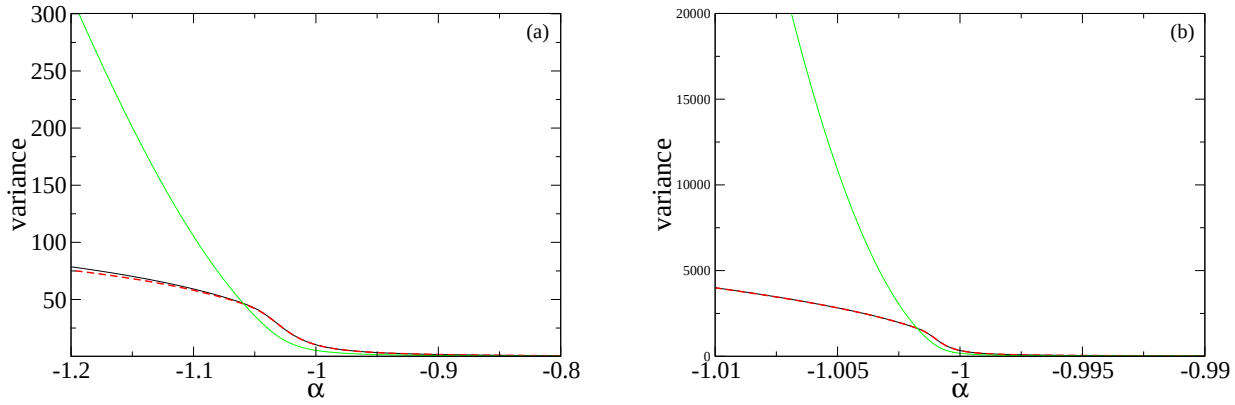

Figure 26: Variance of the operator $d\hat{N}$ found from the Hamiltonian $\hat{H}'$ (black solid lines) and from $\hat{H}_F$ (red dashed lines) compared to the variance of depletion to the single non-condensate mode ($var(\hat{n}_c)$ found from $\hat{H}'$) – green lines. Panel (a) shows results for $N = 500$ whereas panel (b) for $N = 10^5$.

as a function of α around the critical point. We compare again two curves obtained using Hamiltonians $\hat{H}'$ and $\hat{H}_F$ for two different numbers of particles. The agreement is already satisfactory for 500 particles and it is excellent in the case of 10^5 particles. We observe that the maximum is shifted from the point $\alpha = -1$ and this shift tends to zero with the increasing number of particles.

It is interesting to note that for $\alpha < -1$ the fluctuations of $d\hat{N}$ are much smaller than the fluctuations of $\hat{n}_c$ and $\hat{n}_s$ separately, see Fig. 26. Indeed, for $\alpha < -1$, the ground state solution corresponds to the wavefunction concentrated around a circle with a radius r_0, and because $d\hat{N}$ is a function of the distance from the origin its fluctuations are small. The operators $\hat{n}_c$ and $\hat{n}_s$ are related to distances from the axes, and their fluctuations are larger than the fluctuations of $d\hat{N}$ if the wavefunction is localized around the circle. While the number of depleted atoms is expected to be roughly the same in each experiment, these atoms may differently occupy the two orthogonal modes (139) or any other orthogonal combination of them. This is the origin of the spontaneous symmetry breaking predicted by the mean field theory, or condensate fragmentation predicted by the many body theory. Atoms depleted from a condensate in different experiments may differently occupy the modes (139) and resulting density profiles of atomic clouds reveal bright solitons localized at different positions.

Part VI
Phase separation in a two-component condensate in a double well potential

As already discussed, a system of two condensates made of different atomic species or atoms of the same specie in different hyperfine states can reveal phase separation. With varying interspecies interactions we pass a critical point beyond which mean field ground states break symmetry of a Hamiltonian. We will study a two component condensate trapped in the double well potential. In such a system solution for the two-component Bogoliubov vacuum state in the particle representation is available by analytical means. Exact diagonalization of the two mode Hamiltonian is possible for a moderate particle number in each of the components. Preliminary results that we have obtained for the system suggest that for weak intercomponent interactions the phase separation transition has the same origins as the transitions in single attractive condensates. Experimental observation of critical fluctuations should be easier than in the latter system.

Previous studies of two component condensates in the double well potential have concentrated on intercomponent correlations. It was predicted that atoms of two condensates that were initially prepared in different wells can tunnel as pairs through the potential barrier in opposite directions [140]. Such a correlated motion of tunneling atoms leads to the generation of quantum entanglement between the two macroscopically coherent systems [141]. A substantial increase of entanglement can be achieved for tunnelling rates and interactions in the vicinity of the stability limit [142], as well as large interaction values with respect to tunnelling [143]. The initial state in the above dynamical simulations was a ground state of the two specie system without interactions.

The aim of the present chapter is to find ground states of the two component condensate in the vicinity of the critical point and study its signatures such as critical fluctuations. Applicability of the Bogoliubov theory will be verified, since it predicts quite a drastic reduction of possible correlations. Indeed, especially a strongly interacting limit reveals significant entanglement and breakdown of the mean field theory.

15 Phase transition in a mixture of two condensates

15.1 Mean field critical parameter

We will study a two component Bose-Einstein condensate in the double well potential treated within the two mode approximation. If we choose ψ_1, ψ_2 as the two states localized in the wells

of the potential, then the Hamiltonian reads:

$$\begin{aligned}\hat{H} &= -\frac{J}{2}\left(\hat{a}_1^\dagger\hat{a}_2+\hat{a}_2^\dagger\hat{a}_1+\hat{b}_1^\dagger\hat{b}_2+\hat{b}_2^\dagger\hat{b}_1\right)+\frac{U}{2}\left(\hat{a}_1^\dagger\hat{a}_1^\dagger\hat{a}_1\hat{a}_1+\hat{a}_2^\dagger\hat{a}_2^\dagger\hat{a}_2\hat{a}_2+\hat{b}_1^\dagger\hat{b}_1^\dagger\hat{b}_1\hat{b}_1+\hat{b}_2^\dagger\hat{b}_2^\dagger\hat{b}_2\hat{b}_2\right)\\ &+ U_{ab}\left(\hat{a}_1^\dagger\hat{a}_1\hat{b}_1^\dagger\hat{b}_1+\hat{a}_2^\dagger\hat{a}_2\hat{b}_2^\dagger\hat{b}_2\right),\end{aligned} \tag{158}$$

where $\hat{a}_1$ ($\hat{b}_1$) annihilates an atom belonging to the component a (b) in the first well and $\hat{a}_2$ ($\hat{b}_2$) annihilates an atom of the a (b) component in the other well. The parameter J stands for the tunnelling frequency of atoms between the two wells and U and U_{ab} describe intra- and inter-condensate interactions. For simplicity we have assumed equal intra-component interactions and particle numbers for both components ($U \equiv U_a = U_b$ and $N \equiv N_a = N_b$). Such condition is a good approximation to ^{87}Rb condensate of atoms in hyperfine spin states $|F=2, m_f=1\rangle$ and $|F=1, m_f=-1\rangle$ [78]. The following calculations can be performed in a general case as well.

We will study ground states of the system for varying values of a parameter

$$\gamma = \frac{N(U_{ab}-U)}{J}. \tag{159}$$

The mean field theory predicts that if $\gamma < 1$ the ground state of both condensates is a symmetric superposition over the two wells

$$\phi_{a0} = \phi_{b0} = \frac{1}{\sqrt{2}}\left(\psi_1+\psi_2\right), \tag{160}$$

For a critical value $\gamma_c = 1$ the above solution is unstable and for $\gamma > 1$ we have symmetry breaking mean field solutions

$$\phi_{a0,\pm} = \sqrt{\frac{1\pm z_0}{2}}\psi_1 + \sqrt{\frac{1\mp z_0}{2}}\psi_2, \quad \phi_{b0,\pm} = \sqrt{\frac{1\mp z_0}{2}}\psi_1 + \sqrt{\frac{1\pm z_0}{2}}\psi_2 \tag{161}$$

where z_0 is now defined as

$$z_0 = \sqrt{1-\frac{1}{\gamma^2}}. \tag{162}$$

Note that the form of the solutions (161) is the same as in the single condensate case (99), except for the different definition of the critical parameter (159).

15.2 Bogoliubov ground state for symmetric solutions

Solution of the Bogoliubov-de Gennes equations reveals two quasi-particles corresponding to excitation energies:

$$E_\pm = \sqrt{J\left(J+NU\pm NU_{ab}\right)}, \tag{163}$$

and modes:

$$\begin{pmatrix} u^a_\pm \\ v^a_\pm \\ u^b_\pm \\ v^b_\pm \end{pmatrix} = \begin{pmatrix} (J+2E_\pm)\phi_{a1} \\ (2E_\pm - J)\phi_{a1} \\ (J+2E_\pm)\phi_{b1} \\ (2E_\pm - J)\phi_{b1} \end{pmatrix} \chi_\pm, \tag{164}$$

where

$$\phi_{a1} = \phi_{b1} = \frac{1}{\sqrt{2}}(\psi_1 - \psi_2) \tag{165}$$

is the non-condensate mode and

$$\chi_\pm = \frac{1}{4\sqrt{JE_\pm}}, \tag{166}$$

is the normalization factor.

The Bogoliubov vacuum state can be written in the particle representation as

$$|0_B\rangle \sim \left(\hat{c}^\dagger_{a0}\hat{c}^\dagger_{a0} + \lambda_a \hat{c}^\dagger_{a1}\hat{c}^\dagger_{a1}\right)^{N/2} \times \left(\hat{c}^\dagger_{b0}\hat{c}^\dagger_{b0} + \lambda_b \hat{c}^\dagger_{b1}\hat{c}^\dagger_{b1}\right)^{N/2} |0\rangle, \tag{167}$$

where the operators $\hat{c}^\dagger_{a0}$ ($\hat{c}^\dagger_{b0}$) create atoms of the a (b) component in the condensate mode (160) and $\hat{c}^\dagger_{a1}$ ($\hat{c}^\dagger_{b1}$) create respective atoms in the non-condensate mode (165). The coefficients

$$\lambda_a = \lambda_b = \frac{\left(4E_+^2 - J^2\right)\chi_+^2 + \left(4E_-^2 - J^2\right)\chi_-^2}{1 + (2E_+ - J)^2\chi_+^2 + (2E_- - J)^2\chi_-^2}. \tag{168}$$

15.3 Bogoliubov vacuum for phase separated condensates

For $\gamma > 1$ the condensate wavefunctions are given by (161), now the quasi-particle excitation energies are

$$E_\pm = \sqrt{J\left(J\gamma^2 + \frac{2(U \pm U_{ab})}{\gamma}\right)} \tag{169}$$

and the quasi-particle functions are proportional to non-condensate modes

$$\phi_{a1,\pm} = \sqrt{\frac{1 \mp z_0}{2}}\psi_1 - \sqrt{\frac{1 \pm z_0}{2}}\psi_2, \quad \phi_{b1,\pm} = \sqrt{\frac{1 \pm z_0}{2}}\psi_1 - \sqrt{\frac{1 \mp z_0}{2}}\psi_2. \tag{170}$$

Similarly as in the case of an attractive condensate in the double well we can use the Bogoliubov vacuum state to recover the symmetry of the system (see (107)). The ground state in that approximation is

$$|\Psi\rangle \;\; = \;\; |0_b\rangle_+ + |0_b\rangle_-, \tag{171}$$

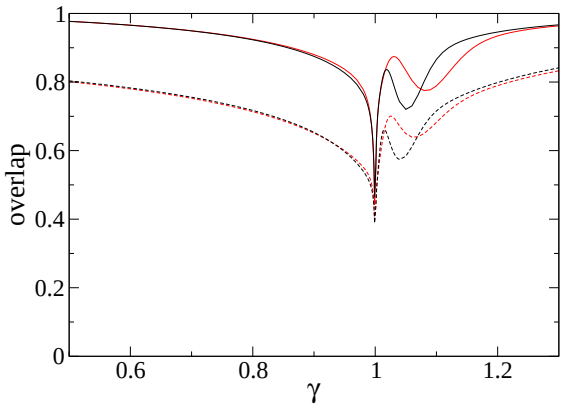

Figure 27: Squared overlap between an exact ground state and the Bogoliubov prediction for $J = 1$, $N = 100$ (black lines) and $N = 50$ (red lines) in each of the condensates. Solid lines correspond to the weakly interacting regime, i.e. the interaction is equal to $U = 0.001$ for $N = 100$ and $U = 0.002$ for $N = 50$. Dashed lines present results for $U = 0.1$ ($N = 100$) and $U = 0.2$ ($N = 50$). The parameter γ is varied by means of U_{ab} changes (see (159)).

where

$$|0_b\rangle_\pm \sim \left(\left(\hat{c}^\dagger_{a0,\pm}\right)^2 + \lambda\left(\hat{c}^\dagger_{a1,\pm}\right)^2\right)^{N/2}\left(\left(\hat{c}^\dagger_{b0,\pm}\right)^2 + \lambda\left(\hat{c}^\dagger_{b1,\pm}\right)^2\right)^{N/2}|0\rangle, \tag{172}$$

is the Bogoliubov vacuum states built upon the condensate wavefunctions $\phi_{a0,\pm}$ and $\phi_{b0,\pm}$.

The state (172) is a good approximation for the ground state of the system provided the states $|0_b\rangle_+$ and $|0_b\rangle_-$ are orthogonal. As γ is increased with the fixed N their overlap falls to zero the faster, the higher N we choose. Note that even in the regime of these states being orthogonal, the corresponding single particle states $\phi_{a0,+}$ and $\phi_{a0,-}$ need not be orthogonal. If we are, however, far from the critical point, also the Gross-Pitaevskii solutions have zero overlap, i.e. $\langle\phi_{a0,+}|\phi_{a0,-}\rangle \approx 0$. For $\gamma \to \infty$ the state (171) is a a Schrödinger cat state.

15.4 Exact diagonalization of the two mode model

In order to verify the Bogoliubov prediction and study the critical point we have diagonalized the Hamiltonian (158) numerically. Most of the calculations were done for $J = 1$, $N = 100$ in each of the two condensates and the interaction U set in the range between $U = 0.001$ and $U = 1000$. The mean field parameter was varied in each case in the vicinity of the critical point, $\gamma = 0 \ldots 2$, by means of the interaction U_{ab} variations (see (159)).

Apart from the known fact about the Bogoliubov theory breakdown for $\gamma = \gamma_c$ we can distinguish three regimes with respect to the interaction strength relative to the tunnelling (see

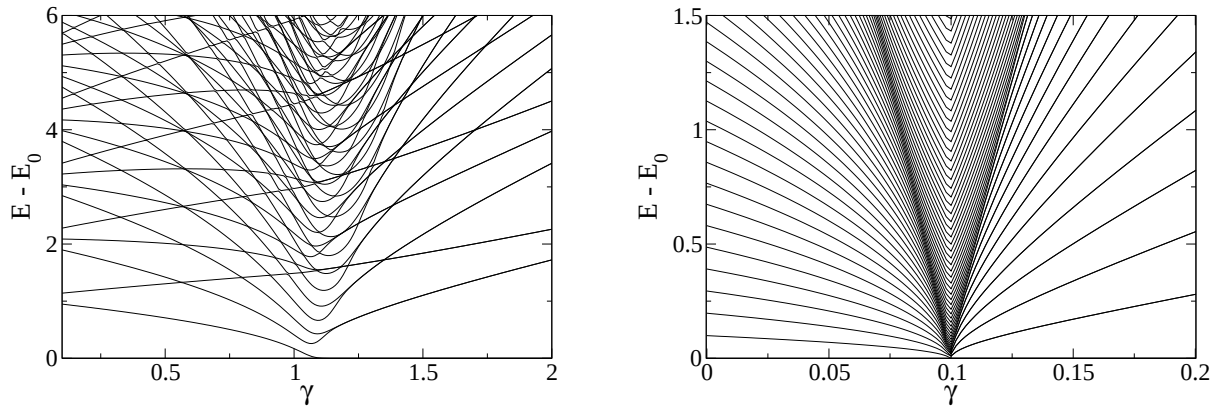

Figure 28: Energy levels of the Hamiltonian (158) found from the exact diagonalization for $U = 0.001$ (panel (a)) and $U = 1000$ (panel (b)). The number of particles is $N = 100$ for each component and $J = 1$. The parameter γ is varied by means of U_{ab} changes (see (159)).

Figs. 27 and 28)

- $\frac{NU}{J} \ll 1$: the square overlap between the Bogoliubov vacuum is close to 1 in a wide range except for a close vicinity of the critical point. As we will show in the next sections estimates of critical fluctuations (density and number fluctuations) based upon the Bogoliubov theory can be made in this regime.
- $\frac{NU}{J} \approx 1$: there appear significant deviations of the Bogoliubov predictions from exact results. The square overlap (Fig. 27) e.g. for $\gamma = 0.5$ is equal to 0.8 whereas in the previous case it approaches 1.
- $\frac{NU}{J} \gg 1$: a new analytical approximation is required to describe a shift of the critical point to lower values of γ. As can be seen in Fig. 28, for $N = 100$, $J = 1$ and $U = 1000$, the phase separation occurs at $\gamma_c = 0.1$ (so $U_{ab}^{(c)} = 1000.001$ instead of 1000.01 which would be the case if the mean field result $\gamma_c = 1$ were correct).

16 Critical fluctuations

16.1 Density fluctuations in the weakly interacting regime

Approaching the critical point we can expect growing density fluctuations of the condensate mixture. To estimate them we will use the method introduced in section 6.1. First, for $\gamma \to 1_-$ we can write the Bogoliubov vacuum state as a gaussian superposition over perfect condensate

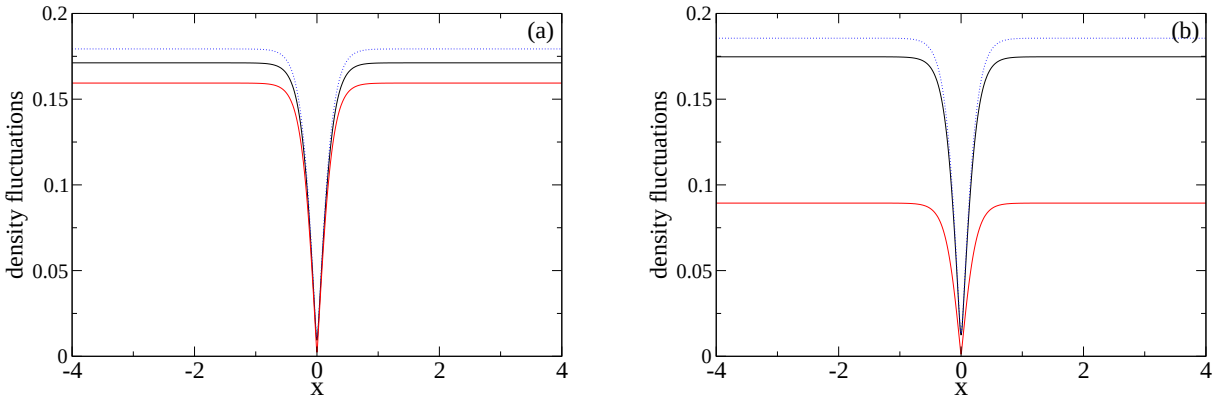

Figure 29: Standard deviation of the density fluctuations of one of the condensates divided by the average density for $N = 100$, $U = 0.001$ (a) and $U = 0.1$ (b). Solid lines correspond to results for $\gamma = 0.99$ (black lines - exact; red lines - Bogoliubov estimates based upon (176)). Dashed blue lines depict exact results for $\gamma = 1$.

states

$$|0_b\rangle \sim \int dq_a dq_b \exp\left(-\frac{q_a^2}{2\Lambda_a}\right) \exp\left(-\frac{q_b^2}{2\Lambda_b}\right) |N : \phi_q^{(a)}\rangle |N : \phi_q^{(b)}\rangle, \tag{173}$$

where $|N : \phi_q^{(a)}\rangle$ and $|N : \phi_q^{(b)}\rangle$ are N-body states where N particles occupy single particle wavefunctions

$$\phi_q^{(a)} = \frac{\phi_{a0} + \frac{q_a}{\sqrt{N}}\phi_{a1}}{\sqrt{1 + \frac{q_a}{N}}}, \quad \phi_q^{(b)} = \frac{\phi_{b0} + \frac{q_b}{\sqrt{N}}\phi_{b1}}{\sqrt{1 + \frac{q_b}{N}}}, \tag{174}$$

and

$$\Lambda_b = \Lambda_a = \frac{\lambda_a}{1 - \lambda_a}. \tag{175}$$

Note that $\lambda_a = \lambda_b$ for our choice of the system parameters. Density profiles as we approach the critical point from the "symmetric" side ($\gamma \to 1_-$) can be estimated from the densities

$$\begin{aligned} \sigma_a(x) &\sim \phi_{a0}^2(x) + 2\frac{q_a}{\sqrt{N}}\phi_{a0}(x)\phi_{a1}(x), \\ \sigma_b(x) &\sim \phi_{b0}^2(x) + 2\frac{q_b}{\sqrt{N}}\phi_{b0}(x)\phi_{b1}(x), \end{aligned} \tag{176}$$

In Fig. 29 we show standard deviation of the density fluctuations divided by the average density, i.e. the quantity $\sqrt{\mathrm{var}(\rho_q^{(a)})}/\langle\rho_q^{(a)}\rangle$ corresponding to the condensate a, where

$$\mathrm{var}(\rho_q^{(a)}) = \frac{2\Lambda_a}{N}\phi_{a0}^2\phi_{a1}^2. \tag{177}$$

and for the calculation we have taken the localized modes as

$$\psi_{1,2}(x) = \left(\frac{2}{\pi}\right)^{1/4}\exp\left[-(x\pm 2)^2\right]. \tag{178}$$

We can see that the Bogoliubov theory can provide us with reliable results only if we stay in the weakly interacting regime, $\frac{NU}{J} \ll 1$, which is the case for $N = 100$, $J = 1$ and $U = 0.001$.

The standard deviation of the fluctuations scales as

$$\sqrt{\frac{\Lambda^a}{N}} \sim \frac{1}{(\gamma_c - \gamma)^{1/4}}. \tag{179}$$

On the other side of the critical point the density fluctuations will be also present. For a superposition of the Bogoliubov vacuum states (171) we cannot simulate density measurements with the aid of the above method.

16.2 Order parameter and number fluctuations

Knowing the order parameter for an attractive condensate in the double well we can define it for the two component condensate in a completely analogous way. For the condensate a it is

$$\hat{\mathcal{B}} = \left|\hat{a}_1^\dagger\hat{a}_1 - \hat{a}_2^\dagger\hat{a}_2\right|. \tag{180}$$

Fig. 30 shows the order parameter at different interaction regimes. We can see the critical point shift as we increase the intra-component interactions. Fluctuations of the order parameter $(var(\hat{\mathcal{B}}))$ are maximal at the critical point, which can be seen in Fig. 31. The Bogoliubov predictions were obtained on the basis of the particle representation of the Bogoliubov vacuum state, Eqs. (167) and (171).

17 Entanglement in the double well system

The degree of entanglement between the two species is measured by the entropy of entanglement calculated as the von Neumann entropy of one of the reduced states

$$S = -Tr(\rho_a \ln \rho_a) = -Tr(\rho_b \ln \rho_b), \tag{181}$$

where ρ_a and ρ_b are reduced density matrices of the respective subsystems, i.e., $\rho_a = Tr_b\rho_{ab}$ and $\rho_b = Tr_a\rho_{ab}$ with $\rho_{ab} = |\Psi\rangle\langle\Psi|$ being the density matrix of the whole system. Its value for the

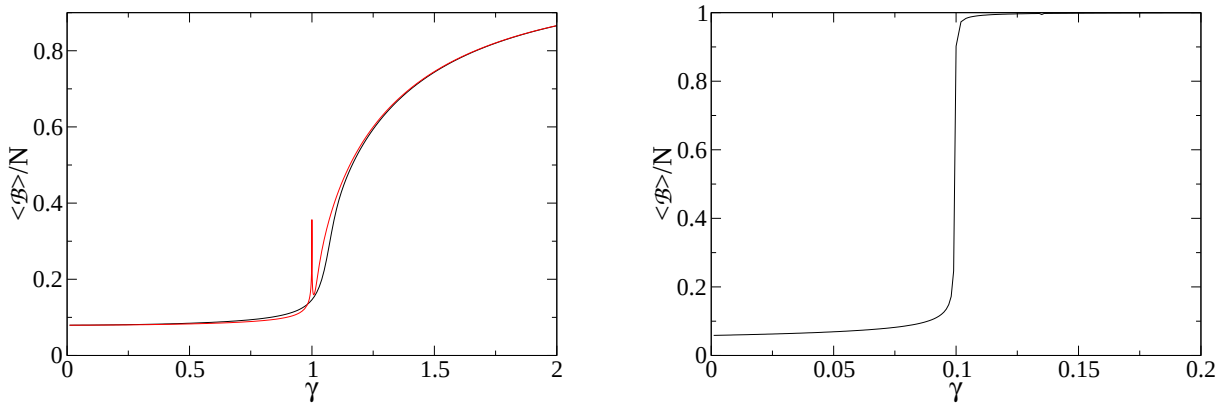

Figure 30: The order parameter, i.e. average value of the operator $\hat{B}$ (180) for a two component condensate with $N = 100$ in each component in the weak interacting, $U = 0.001$, (panel (a)) and strong interacting regime, $U = 1000$ (panel (b)). Black lines show results of the exact diagonalization. The red line in panel (a) corresponds to the Bogoliubov prediction. The parameter γ is varied by means of U_{ab} changes (see (159)). Here $J = 1$.

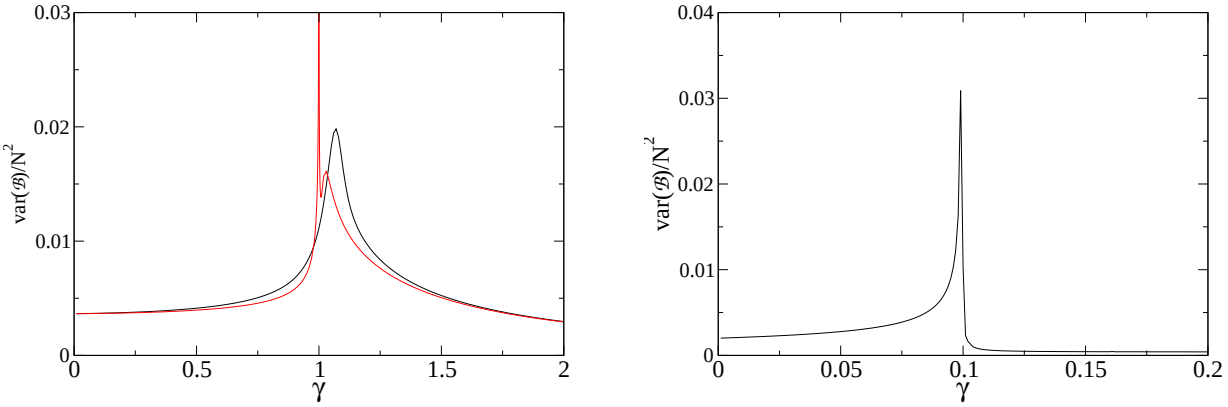

Figure 31: Variance of the $\hat{B}$ operator, (180) for a two component condensate with $N = 100$ in each component in the weak interacting, $U = 0.001$, (panel (a)) and strong interacting regime, $U = 1000$ (panel (b)). Black lines show results of the exact diagonalization. The red line in panel (a) corresponds to the Bogoliubov prediction. The parameter γ is varied by means of U_{ab} changes (see (159)). Here $J = 1$.

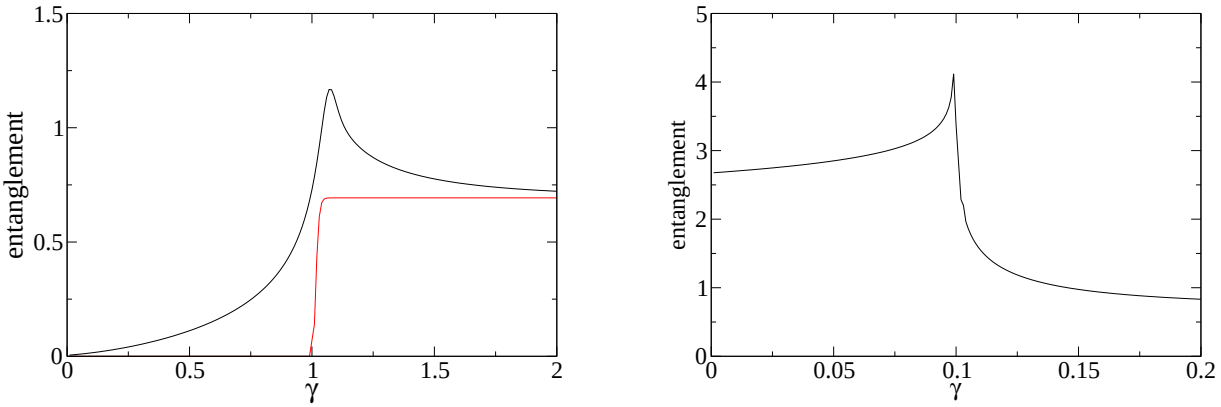

Figure 32: Entropy of entanglement for a two component condensate with $N = 100$ in each component in the weak interacting, $U = 0.001$, (panel (a)) and strong interacting regime, $U = 1000$ (panel (b)). The red line in panel (a) corresponds to the Bogoliubov prediction. The parameter γ is varied by means of U_{ab} changes (see (159)). Here $J = 1$.

double condensate under consideration is within the range between $S = 0$ for a separable and $S = \ln N$ for a maximally entangled system.

The Bogoliubov theory (167) predicts the decomposition of the ground state into two parts, responsible for condensates a and b, respectively. The entanglement entropy of its ground state is therefore (except for a very narrow transition region) equal to $S = 0$ (for $\gamma < 1$) and $S = \ln 2$ (for $\gamma > 1$), regardless of the regime of interactions we are in. Already in the weak interaction regime this prediction shows significant discrepancies from the exact result (see Fig. 32) In fact the entropy of entanglement has a maximum at the critical point and could be another signature of the phase transition. There is a significant entanglement of particles already in the miscible phase of the two condensates. Far away from the critical point the Bogoliubov results approach, however, the exact ones. When we switch to the strong interaction regime, the entropy of entanglement approaches the maximum entanglement value $S = \ln N$ at the critical point.

Part VII
Self-localization of impurity atoms in a trapped condensate

An impurity atom immersed in a condensate can have a bound state where it is self-localized [144]. It can distort the density of the surrounding BEC creating an effective trapping potential, both for repulsive and attractive interactions. This localizing potential was derived for an impurity interacting with a homogeneous as well harmonically trapped condensate in a strong coupling approach that assumes a product state of the condensate-impurity system [144]. In case of attractive boson-impurity interactions two critical values of the interaction were found. The first marks the onset of localization, and the higher one signals a transition to a short range physics regime where the mean field theory predicts collapse of the condensate cloud [145]. It was found however that the strong coupling approximation underestimates the latter critical value [146]. In addition, a high peak density of the BEC near the impurity can enhance inelastic collisions that lead to two- and three-body losses of the condensate atoms.

An impurity in a homogeneous condensate exhibits a parametric soliton behavior [57]. Quantum fluctuations around the product state that describe entanglement of the impurity and boson degrees of freedom were studied in such system. The quasiparticle excitation spectrum reveals two clear branches. Each excitation of the lower branch, except for the very lowest level, delocalizes an impurity atom, while the upper energy branch is nearly identical to the Hartree-Fock BEC spectrum in the absence of impurities [57].

An analysis of N impurity fields immersed in a condensate reveals an attractive condensate-mediated interaction between two impurities. Different localized phases can occur within various parameter regimes, including a crystal of impurity fields that can form spontaneously in the condensate. The superfluid system that simultaneously breaks the translational symmetry exhibits a supersolid behaviour [147].

An experimental signature of a self-localized state could be the modified condensate density due to the impurity presence. One needs, however, a significant number of impurity atoms in order to make the effect observable in an experiment. A kinetic energy accumulated in an impurity self-localized in the center of a condensate trapped in a 3D harmonic trap and then released should be manifest by a halo of impurity particles expanding much faster than the condensate cloud.

We will consider a subsystem of bosonic impurities that can form a small condensate immersed in a larger one. In a condensate trapped by a spherically symmetric trap the impurities can self-localize in the center without an impurity trapping potential. If we study the dynamical stability of such a configuration, it turns out that an unstable mode with the angular momentum $l = 1$ will cause an exponential escape from the symmetric state. We introduce therefore a potential that traps the impurity subsystem, such that its profile does not change much with respect to

the former case, but the spherically symmetric solution is now stable.

Symmetry breaking mean field solutions were found in a two component trapped condensate [148]. It was shown that the combined density profile of the two species looks very much like a single-species condensate, even though the individual density profiles of each species are greatly modified [84, 149]. Imaginary quasiparticle excitation energies leading to such a transition were identified within the Thomas-Fermi approximation [86].

We will investigate the condensate - impurity system using the number conserving Bogoliubov theory (see chapter III). We will study properties of the Bogoliubov quasiparticle spectrum and excitations and search for localized excitations of the impurity subsystem. In the end we will simulate the above mentioned experimental scenario of detecting the self-localized state.

Production of a self-localized state requires a very strong condensate-impurity interaction. This can in principle be achieved by means of a Feshbach resonance.

18 Bosonic impurities in a trapped condensate

18.1 Phase separation and self-localization of impurity atoms

We will describe the impurity - condensate system assuming that the impurity atoms form a small condensate immersed in the larger one. We will use a familiar model of a two component condensate with $N_I = 100$ impurity atoms and $N_B = 10^4$ atoms belonging to the large condensate [96]

$$\begin{aligned}\hat{H} &= \int d^3r \left(\hat{\psi}_I^\dagger \left[-\frac{\hbar^2}{2m}\nabla^2 + V_I(\vec{r}) + \frac{g_I}{2}\hat{\psi}_I^\dagger\hat{\psi}_I \right] \hat{\psi}_I \right. \\ &\left. + \hat{\psi}_B^\dagger \left[-\frac{\hbar^2}{2m}\nabla^2 + V_B(\vec{r}) + \frac{g_B}{2}\hat{\psi}_B^\dagger\hat{\psi}_B \right] \hat{\psi}_B + g_{IB}\hat{\psi}_I^\dagger\hat{\psi}_B^\dagger\hat{\psi}_I\hat{\psi}_B \right), \end{aligned} \tag{182}$$

where we have assumed equal masses of both species. The spherically symmetric trapping potentials are

$$V_I(\vec{r}) = \frac{1}{2}m\omega_I^2(x^2+y^2+z^2), \quad V_B(\vec{r}) = \frac{1}{2}m\omega_B^2(x^2+y^2+z^2), \tag{183}$$

and the interactions are given by

$$g_I = \frac{4\pi\hbar^2 a_I}{m}, \quad g_B = \frac{4\pi\hbar^2 a_B}{m}, \quad g_{IB} = \frac{2\pi\hbar^2 a_{IB}}{m}, \tag{184}$$

where a_I, a_B and a_{IB} are, respectively, scattering lengths of the impurity, condensate and condensate-impurity interactions. First, we will solve the Gross-Pitaevskii equations written in the spherical coordinates, assuming the following form of solutions

$$\phi_I(\vec{r}) = R^{(I)}(r)Y_{l,m}(\theta,\varphi), \quad \phi_B(\vec{r}) = R^{(B)}(r)Y_{l,m}(\theta,\varphi), \tag{185}$$

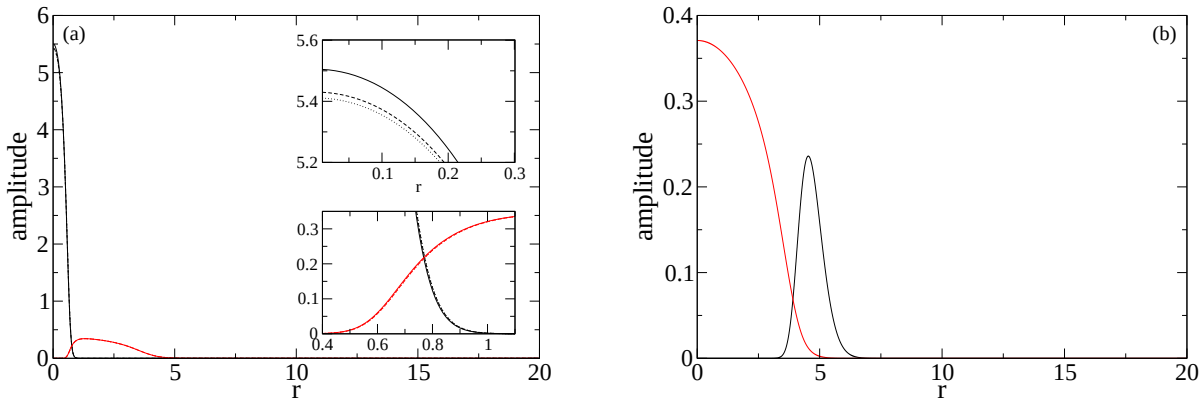

Figure 33: Stationary solutions to Eqs. (186), i.e. radial amplitudes ψ_I/r (black lines) and ψ_B/r (red lines). The scattering lengths are $a_I = 108.8a_0$, $a_B = 109.1a_0$ and $a_{IB} = 5000a_0$. Panel (a) shows a self-localized impurity for $\omega_s = 5$ (solid lines), $\omega_s = 1$ (dashed lines) and for $\omega_s = 0$ (dotted lines). The insets show a magnified region near $r = 0$ and a region of the overlapping condensates. The functions are practically the same in all the three cases. Panel (b) shows a ground state of the system for $\omega_s = 1$.

where $Y_{l,m}(\theta, \varphi)$ are spherical harmonic functions. Upon defining $R^{(i)} = \psi_i(\vec{r})/r$ and using $\sqrt{\hbar/m\omega_B}$ and $\hbar\omega_B$ as the length and energy units, respectively, we end up with stationary mean field equations that depend only on the radial variable. For a ground state we can take the angular momentum $l = 0$,

$$\begin{aligned} \mu_I \psi_I(r) &= \left(-\frac{1}{2}\frac{d^2}{dr^2} + \frac{1}{2}\omega_s r^2 + 4\pi N_I a_I \frac{\psi_I^2(r)}{r^2} + 4\pi N_B a_{IB} \frac{\psi_B^2(r)}{r^2} \right) \psi_I(r) \\ \mu_B \psi_B(r) &= \left(-\frac{1}{2}\frac{d^2}{dr^2} + \frac{1}{2} r^2 + 4\pi N_B a_B \frac{\psi_B^2(r)}{r^2} + 4\pi N_B a_{IB} \frac{\psi_I^2(r)}{r^2} \right) \psi_B(r), \end{aligned} \tag{186}$$

where we have defined

$$\omega_s = \frac{\omega_I^2}{\omega_B^2}. \tag{187}$$

In the following we will consider a ^{87}Rb system with $|2, 1\rangle$ impurities immersed in a $|1, -1\rangle$ condensate. The scattering lengths are, respectively, $a_I = 108.8a_0$ and $a_B = 109.1a_0$ (a_0 is the Bohr length) [78]. The trapping frequency in the calculations is $\omega_B = 2\pi \times 100$ Hz.

We have studied self-localized states obtained with the scattering length set in the range between $a_{IB} = 4000a_0$ and $a_{IB} = 30000a_0$. We can speak about a self-localized state if an impurity is focused in the center only by means of the interactions, i.e. $\omega_s = 0$. We have studied,

however, also situations where the impurity trapping is present, looking for configurations where the densities are not modified in a significant way with respect to the former case. Such states we will also call self-localized. For given interactions a_{IB} the trapping potential was varied between $\omega_s = 0$ and $\omega_s = 100$.

The equations (186) were solved by means of the method of the imaginary time relaxation to a ground state. Note that if an initial state in that method has a zero overlap with the ground state, we converge to one of excited states of our system. Starting with different initial states we were able to obtain stationary states plotted in Fig. 33.

As expected, self-localized states occurred at very strong repulsive interactions between the impurity and condensate atoms. In the case where the impurity trapping is absent ($\omega_s = 0$) we have found such states for $a_{IB} \geq 4000a_0$, a value much higher than the one needed for phase separation ($a_{IB}^c \approx 108.95a_0$). Panel (a) in Fig. 33 shows stationary solutions to Eqs. (186) for $\omega_s = 0$, $\omega_s = 1$ and $\omega_s = 5$. They almost fully overlap but as we will argue in the next section, their stability properties are different. The state with impurity atoms located in the center is a ground state in a steep impurity trap, $\omega_s = 5$, whereas (if we restrict to the spherical symmetry) for a weaker trapping it is an excited state, with a ground state e.g. at $\omega_s = 1$ revealing impurity atoms being outside, see Fig. 33. In fact, at $\omega_s < 5$ we need to look for ground states relaxing the assumption of their spherical symmetry [84, 149].

18.2 Bogoliubov quasiparticle excitations

We have applied the number conserving Bogoliubov theory to test the stability of mean field ground states and study the character of quasi-particle excitations. Investigating the self-localized states we are very far from the critical point for the phase separation so we can expect that the Bogoliubov approach should give reliable results. The ground state wavefunctions in the perturbative expansion used in the method are spherically symmetric. The matrix $\mathcal{L}$ (34) factorizes into blocks with different angular momenta l that can be diagonalized separately. We can assume the variable separation in the quasi-particle functions (eigenmodes of $\mathcal{L}$)

$$\begin{aligned} U_I(\vec{r}) &= \frac{u_I(r)}{r} Y_{l,m}(\theta,\varphi), \quad U_B(\vec{r}) = \frac{u_B(r)}{r} Y_{l,m}(\theta,\varphi), \\ V_I(\vec{r}) &= \frac{v_I(r)}{r} Y_{l,m}(\theta,\varphi), \quad V_B(\vec{r}) = \frac{v_B(r)}{r} Y_{l,m}(\theta,\varphi), \end{aligned} \tag{188}$$

so the diagonalization of $\mathcal{L}$ amounts to diagonalizing blocks corresponding to different angular momenta and depending only on the radial variable r. Hence in the following we will plot only the radial functions $u_I(r)$, $v_I(r)$, $u_B(r)$, $v_B(r)$.

The quasi-particle excitation spectrum (eigenvalues of $\mathcal{L}$) provides us with information about stability properties of a mean field stationary state. An imaginary eigenvalue is a signature that the system is unstable and under a weak perturbation will evolve to a new stable configuration. Negative eigenvalues imply an excited state, which is dynamically stable and can persist in a time evolution. Such a state is, however, thermodynamically unstable.

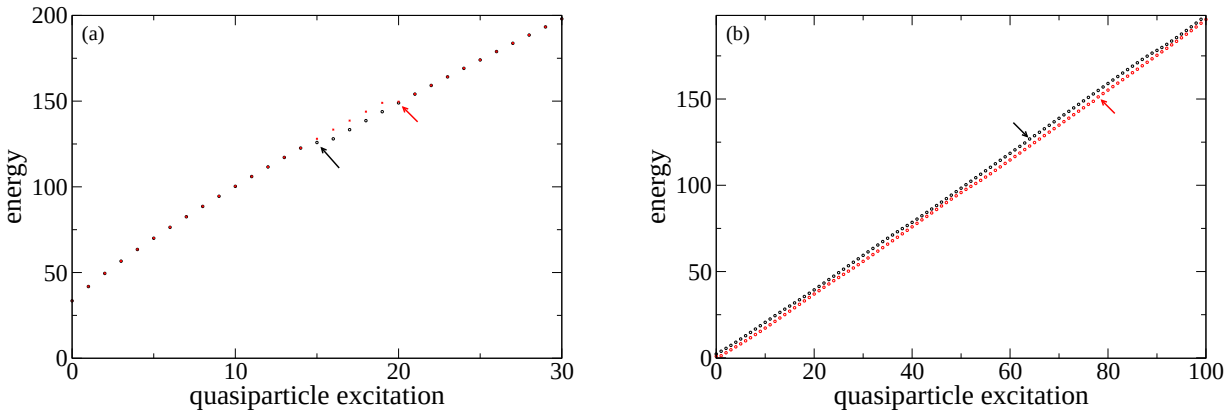

Figure 34: Quasiparticle excitation branch of the impurity (panel (a)) and of the large condensate (panel (b)). See the text for the method of distinguishing the branches. The angular momenta are $l = 0$ (black) and $l = 1$ (red circles). The arrows in panel (a) mark localized quasi-particle excitations of the impurity (with excitation energies $E = 125.9$ for $l = 0$ and $E = 149.7$ for $l = 1$), whereas in panel (b) the lowest condensate excitations higher than the above mentioned localized ones, i.e. corresponding to the energies $E = 126.8$ for $l = 0$ and $E = 151.2$ for $l = 1$. The scattering lengths are $a_I = 108.8a_0$, $a_B = 109.1a_0$ and $a_{IB} = 5000a_0$ and the trapping $\omega_s = 5$.

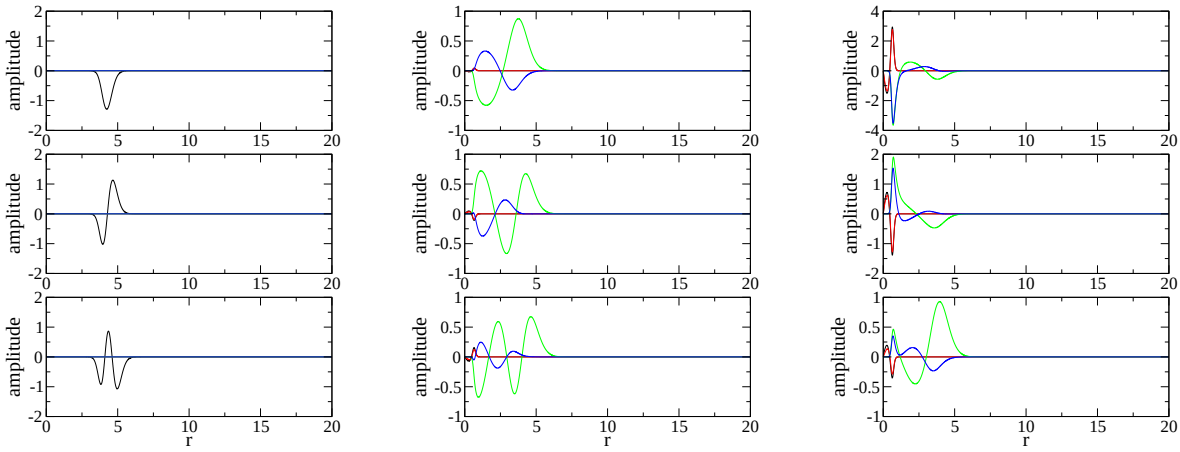

Figure 35: Three lowest excitations from the impurity branch ($l = 0$) – the left column, and from the condensate branch corresponding to $l = 0$ (the middle column) and to $l = 1$ (the right column), with $\omega_s = 5$. The scattering lengths are $a_I = 108.8a_0$, $a_B = 109.1a_0$ and $a_{IB} = 5000a_0$. The impurity functions are u_I (black), v_I (red), and the large condensate quasi-particle functions are u_B (green) and v_B (blue). In the left column only u_I is different than zero.

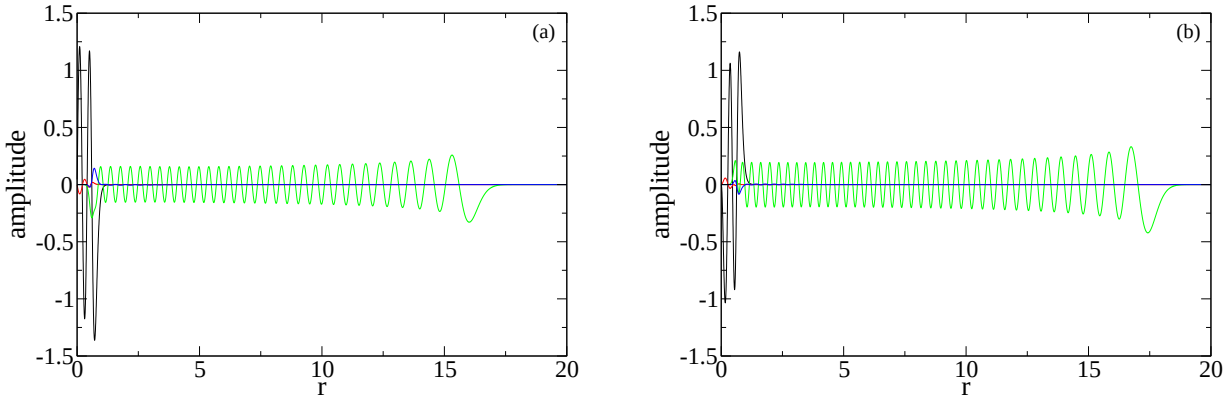

Figure 36: Localized quasiparticle excitations of the impurity (see Fig. 34 panel (a)) in the trapped system ($\omega_s = 5$) for the angular momentum $l = 0$ (panel (a)) and $l = 1$ (panel (b)). The scattering lengths are $a_I = 108.8a_0$, $a_B = 109.1a_0$ and $a_{IB} = 5000a_0$. The impurity functions are u_I (black), v_I (red), and the large condensate quasi-particle functions are u_B (green) and v_B (blue). The excitation energies are 125.86 and 149.7.

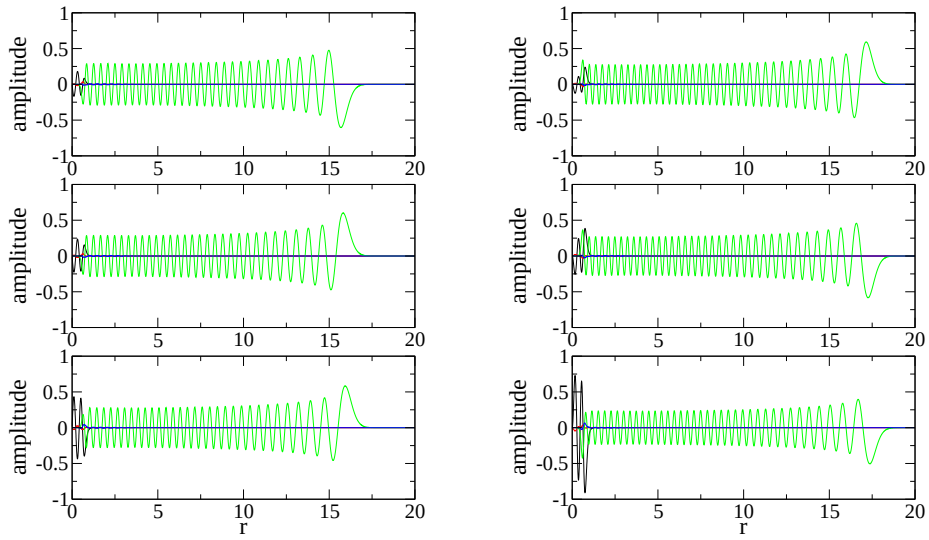

Figure 37: Three quasiparticle excitations from the condensate branch that precede the localized excitation in the impurity branch (see spectra in Fig. 34). The left column corresponds to $l = 0$ and the right one to $l = 1$. The system is trapped, $\omega_s = 5$. The scattering lengths are $a_I = 108.8a_0$, $a_B = 109.1a_0$ and $a_{IB} = 5000a_0$. The impurity functions are u_I (black), v_I (red), and the large condensate quasi-particle functions are u_B (green) and v_B (blue).

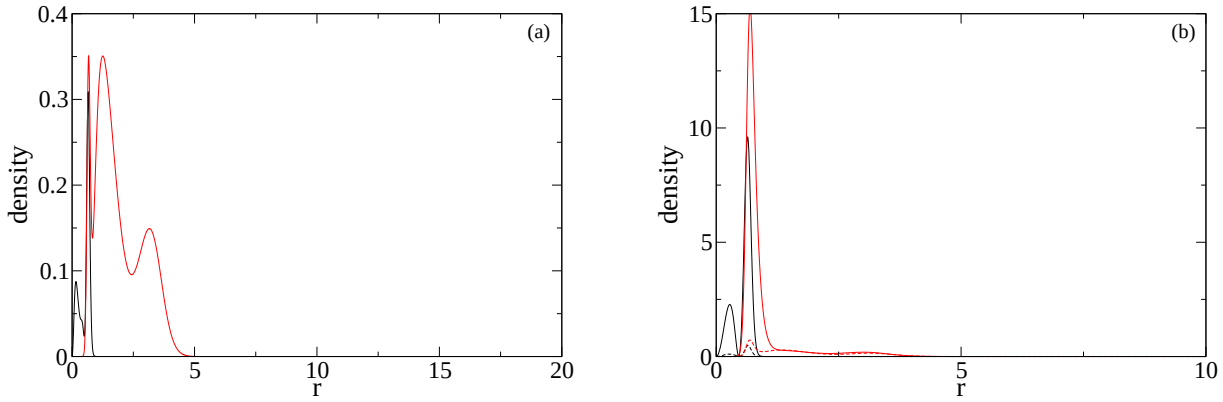

Figure 38: Density of depleted atoms of the impurity (black) and the condensate (red lines) for $l = 0$ (panel (a)) and $l = 1$ (panel (b)). The scattering lengths are $a_I = 108.8a_0$, $a_B = 109.1a_0$ and $a_{IB} = 5000a_0$. The impurity trapping is such that $\omega_s = 5$.

We have studied the quasi-particle spectra for mean field stationary states found for all mentioned above interaction values and trapping potentials. In the following we will concentrate on the case with $a_{IB} = 5000a_0$. If we trap only the larger condensate, and the impurity is focused in the middle only by the interactions ($\omega_s = 0$), there are many negative quasi-particle energies, both for $l = 0$ and higher. The corresponding excitations would delocalize the impurity. A self-localized state obtained at $\omega_s < 5$ has an unstable $l = 1$ mode that has an imaginary frequency, which is a signature of the trap symmetry breaking of the mean field ground state.

Results for $\omega_s = 5$ are shown in Figs. 34 - 38. We have split the quasi-particle spectrum into an impurity and a condensate excitation branch using the criterion whether the norm $\int dr|u_I(r)|^2$ is higher than $\int dr|u_B(r)|^2$ or not. This follows from the fact that if we excite a quasi-particle, a subsystem which has a higher value of $\langle u_i|u_i\rangle$ will get more excited. The situation where the above norms are comparable and both subsystems can acquire a similar excitation happens only for a few points in the spectra in Fig. 34. Note that all energies are positive, which implies that we have found the ground state. If we increase the angular momentum, subsequent spectra are except for the case $l = 1$ shifted upwards.

Subsequent quasi-particle excitations of the impurity are localized in the trap but outside of the large condensate (see Fig. 35). The impurity functions u_I reveal an increasing number of nodes with the growing quasi-particle number, and for most of them $|u_B(r)|^2 = 0$. The excitation branch of the larger condensate is linear for low lying quasi-particles. The lowest excitations from that branch are plotted in the middle and right column of Fig. 35. If we look at the quasi-particles for $l = 1$, we notice that they acquire high amplitudes at the impurity - condensate boundary. The density of depletion becomes high in that region. In fact, we are close to the $l = 1$ instability, which would occur for a self-localized state trapped by $\omega_s < 5$.

Note that the impurity excitation branch in Fig. 34 reveals several "jumps" where one of the lines gets shifted with respect to the other one. At those points there occurs a special kind of an excitation, the impurity subsystem remaining localized in the trap center (see Fig. 36). A closer look at modes corresponding to the branch of the large condensate excitations reveals that each of such localized states is preceded by a series of quasi-particles whose norms of $u_I(r)$ and $u_B(r)$ are comparable, and $\langle u_I|u_I\rangle < \langle u_B|u_B\rangle$, see Fig. 37.

The density of depletion, plotted in Fig. 38, is the highest at the boundary of the two condensates. The remarkable grow for $l = 1$ is due to the fact that we are close to the symmetry breaking instability.

19 Signatures of self-localization

In addition to the high impurity density, another experimental signature of a self-localized state could be its time evolution after release from the trap. We have taken the self-localized ground state found for $a_{IB} = 5000a_0$ and $\omega_s = 5$ and simulated its evolution with the traps turned off

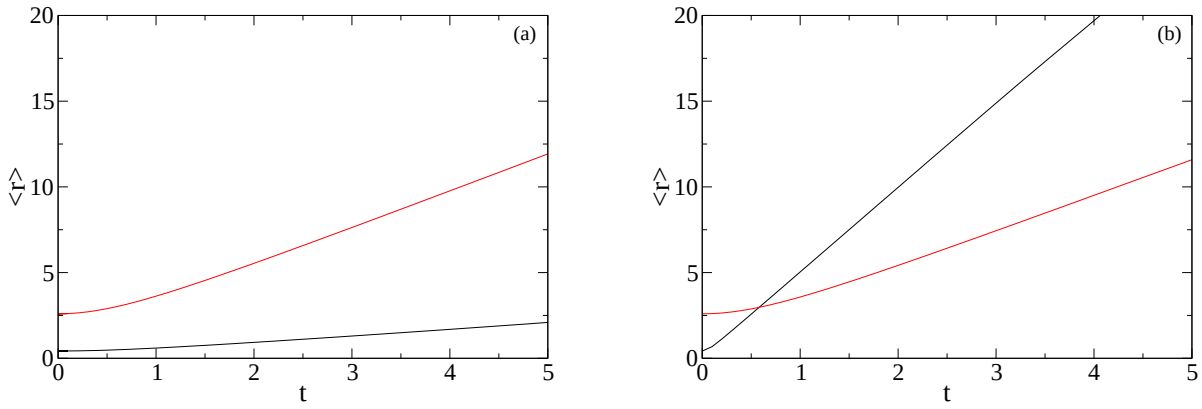

Figure 39: Time evolution (measured in units of $1/\omega_B$) of the self-localized ground state after releasing both condensates from the trap. The mean radial position $< r >$ of the impurity cloud is marked with black and of the larger condensate with red. Panel (a) corresponds to $a_{IB} = 5000a_0$ during the time evolution while the scattering length was set to $a_{IB} = 0$ in panel (b). The intra-condensate interactions are $a_I = 108.8a_0$ and $a_B = 109.1a_0$.

integrating the mean field equations

$$\begin{aligned} i\frac{\partial\psi_I(r)}{\partial t} &= \left(-\frac{1}{2}\frac{\partial^2}{\partial r^2} + 4\pi N_I a_I \frac{|\psi_I(r)|^2}{r^2} + 4\pi N_B a_{IB}\frac{|\psi_B(r)|^2}{r^2}\right)\psi_I(r) \\ i\frac{\partial\psi_B(r)}{\partial t} &= \left(-\frac{1}{2}\frac{\partial^2}{\partial r^2} + 4\pi N_B a_B \frac{|\psi_B(r)|^2}{r^2} + 4\pi N_B a_{IB}\frac{|\psi_I(r)|^2}{r^2}\right)\psi_B(r). \end{aligned} \tag{189}$$

The results are summarized in Fig. 39. We can see that in order to observe the halo of impurity particles surrounding the larger condensate one needs to tune the intercomponent scattering length to zero before the particle release. Otherwise the strong repulsive interactions prohibit the impurities to escape.

Part VIII
Conclusions

Let us now briefly review the main results of the thesis.

Soliton-like states that are supported by a strong coupling between an atomic and molecular condensate close to a Feshbach resonance were found. Nonlinearities that occur due to elastic scattering were included in the mean field model and their relative role was investigated. The soliton states are supported by a strong quasi-one-dimensional trapping. Simulations of an experimental production of the molecular condensate were performed. For optimized evolution time we obtained the solitonic ground states, whereas for shorter timescales trains of solitons. Behaviour of solitonic states in a magnetic field gradient was tested. It turns out that the atom-molecule coupling can prohibit the states from spreading, also splitting of an initial solitonic state to a soliton train is possible.

A more quantitative analysis of atom losses can be done in future, provided more experimental data on the Feshbach resonance under study is available. Bogoliubov theory of the coupled atom-molecule condensate can be developed to find whether the assumption of the two condensates is affected by the presence of non-condensed atoms.

The Bogoliubov vacuum state in the particle representation was derived for a two component condensate. Its form was proved analytically for a condensate in a homogeneous system and in the double well trapping potential. Density fluctuations corresponding to a long wavelength quasiparticle excitation were studied in a finite system with interactions approaching a phase separation condition. Even for a small number of depleted atoms they can be remarkable, and are especially pronounced if the total number of atoms is not too high.

A critical point against formation of a symmetry breaking, localized mean field solution was studied for a condensate with attractive interactions. The quantum phase transition was studied within a continuous model that reveals an effective potential resembling the one from the Landau Ginzburg theory. An order parameter was defined both for the double well case and for a condensate trapped in a finite box. In the former case it is related to the population difference between the two potential minima. In the latter it corresponds to a number of atoms depleted to two modes unstable in the Bogoliubov theory. Fluctuations of the order parameter are maximal at the critical point. For the double well system the above predictions were compared to exact results obtained by means of diagonalization of the two mode Hamiltonian. In addition, in the region of applicability of the Bogoliubov theory density fluctuations were shown for interactions approaching a critical value.

A quantum phase transition involving the symmetry breaking on the mean field level was investigated also for the double well trapped two component condensate. Here, the critical point marks the onset of the phase separation. Currently only numerical results of the exact diagonalization are available. The system behaviour is much richer than for the attractive single condensate because the intercomponent interaction provides an additional parameter.

Consequently the critical point can be achieved both at weak and strong interactions with respect to the tunnelling. The mean field critical parameter can be used only in the former case since at strong interactions the instability is shifted towards lower values than the mean field would suggest. Critical fluctuations of an order parameter defined in an analogous way as for the single component system are in both regimes maximal at the critical point. The Bogoliubov approximation was tested. It provided estimates of the density fluctuations.

Current and future research will be concentrated on a new analytical model describing the phase transition for the above mentioned various parameter regimes.

Impurity atoms immersed in a trapped condensate were studied on the basis of the Bogoliubov theory. Strong repulsive interactions between the impurity field and the condensate are responsible for the existence of self-localized states. Dynamical stability properties as well as the character of quasiparticle excitations were investigated. Possibility of observing the self-localization in an experiment was discussed. The main line of future research on this project would be to investigate time evolution of quasiparticles. We could obtain in that way information about behaviour of the particle depletion, which would make the analysis of the time evolution complete. Also trap symmetry breaking states can be studied. This would require a simulation of the system without the assumption about the spherical symmetry.

Acknowledgements

We would like to thank Krzysztof Sacha, Jakub Zakrzewski, Roman Marcinek, Jakub Prauzner - Bechcicki, Jacek Dziarmaga, Bogdan Damski, Andreas Buchleitner, Hannah Venzl and Henning Fehrmann for their help at different stages of this work.

We acknowledge support of the Faculty of Physics, Astronomy and Applied Computer Science at the Jagiellonian University, Polish Ministry of Science (scientific funds for the years 2005-2008 and 2008-2011), EU (Marie Curie ToK project COCOS MTKD-CT-2004-517186) and European Science Foundation.

References

[1] L.P. Pitaevskii, Zh. Eksp. Teor. Fiz. 40, 646 (1961).

[2] L.P. Pitaevskii, Sov. Phys.JETP **13**, 451 (1961).

[3] E.P. Gross, Nuovo Cimento **20**, 454 (1961).

[4] F. Dalfovo, S. Giorgini, L.P. Pitaevskii, and S. Stringari, Rev. Mod. Phys. **71**, 463 (1999).

[5] *Bose-Einstein Condensation in Atomic Gases*, Proceedings of the International School of Physics "Enrico Fermi", course 140, edited by M. Inguscio, S. Stringari, and C. Wieman (IOS Press, Amsterdam, 1999).

[6] B. Oleś and K. Sacha, J. Phys. A: Math. Theor. **41**, 145005 (2008).

[7] S. L. Sondhi, S. M. Girvin, J. P. Carini, and D. Shahar, Rev. Mod. Phys. **69**, 315 (1997).

[8] S. Sachdev, *Quantum Phase Transitions*, Cambridge University Press 1999.

[9] P. Ziń, J. Chwedeńczuk, B. Oleś, K. Sacha and M. Trippenbach, Europhys. Lett. **83**, 64007 (2008).

[10] P. Ziń, B. Oleś, M. Trippenbach, and K. Sacha, Phys. Rev. A **78**, 023620 (2008).

[11] B. Oleś, K. Sacha, J. Phys. B: At. Mol. Opt. Phys. **40**, 1103 (2007).

[12] H. Feshbach, Ann. Phys. (N.Y.) **5**, 357 (1958).

[13] C. Chin, R. Grimm, P. Julienne and E. Tiesinga, arXiv: 0812.1496v1.

[14] K. M. Jones, E. Tiesinga, P. D. Lett, and P. S. Julienne, Rev. Mod. Phys. **78**, 483 (2006).

[15] T. Köhler, K. Góral, P. S. Julienne, Rev. Mod. Phys. **78**, 1311 (2006).

[16] K. Góral, T. Köhler, S. A. Gardiner, E. Tiesinga and P. S. Julienne, J. Phys. B: At. Mol. Opt. Phys. **37** 3457 (2004).

[17] S. Inouye, M. R. Andrews, J. Stenger, H.-J. Miesner, D. M. Stamper-Kurn, and W. Ketterle, Nature **392**, 151 (1998).

[18] S. L. Cornish, N. R. Claussen, J. L. Roberts, E. A. Cornell, and C. E. Wieman, Phys. Rev. Lett. **85**, 1795 (2000).

[19] T. Weber, J. Herbig, M. Mark, H.-Ch. Naägerl, and R. Grimm, Science **299**, 232 (2003).

[20] G. Roati, M. Zaccanti, C. D'Errico, J. Catani, M. Modugno, A. Simoni, M. Inguscio, and G. Modugno, Phys. Rev. Lett. **99**, 010403 (2007).

[21] J. L. Roberts, N. R. Claussen, S. L. Cornish, E. A. Donley, E. A. Cornell, and C. E. Wieman, Phys. Rev. Lett. **86**, 4211 (2001).

[22] E. A. Donley, N. R. Clausen, S. L. Cornish, J. L. Roberts, E. A. Cornell, and C. E. Wieman, Nature **412**, 295 (2001).

[23] M. Gustavsson, E. Haller, M. J. Mark, J. G. Danzl, G. Rojas-Kopeinig, and H.-C. Naägerl, Phys. Rev. Lett. **100**, 080404 (2008).

[24] M. Fattori, C. D'Errico, G. Roati, M. Zaccanti, M. Jona-Lasinio, M. Modugno, M. Inguscio, and G. Modugno, Phys. Rev. Lett. 100, 080405 (2008).

[25] M. Inguscio, W. Ketterle, and C. Salomon (eds.), "Ultracold Fermi Gases" (IOS Press, Amsterdam), Proceedings of the International School of Physics "Enrico Fermi", 2008, Course CLXIV, Varenna, 20-30 June 2006.

[26] M. Greiner, C. A. Regal, and D. S. Jin, Nature **412**, 537 (2003).

[27] H. Suno, B. D. Esry, and Chris H. Greene, Phys. Rev. Lett. **90**, 053202 (2003).

[28] Q. Chen, J. Stajic, S. Tan, K. Levin, Physics Reports, **412**, 1 (2005).

[29] E. A. Donley, N. R. Claussen, S. T. Thompson, and C. E. Wieman, Nature **417**, 529 (2002).

[30] J. Herbig, T. Kraemer, M. Mark, T. Weber, C. Chin, H.-Ch. Nägerl, R. Grimm, Science **301**, 1510 (2003).

[31] S. Dürr, T. Volz, A. Marte, and G. Rempe, Phys. Rev. Lett. **92**, 020406 (2004).

[32] F. Dalfovo and S. Stringari, Phys. Rev. A **53**, 2477 (1996).

[33] M. R. Matthews, B. P. Anderson, P. C. Haljan, D. S. Hall, C. E. Wieman, and E. A. Cornell, Phys. Rev. Lett. **83**, 2498 (1999).

[34] J. R. Abo-Shaeer, C. Raman, J. M. Vogels, and W. Ketterle, Science **292**, 476 (2001).

[35] L. Deng, E. W. Hagley, J. Wen, M. Trippenbach, Y. Band, P. S. Julienne, J. E. Simsarian, K. Helmerson, S. L. Rolston, and W. D. Phillips, Nature **398**, 218 (1999).

[36] M. Trippenbach, Y. B. Band, and P. S. Julienne, Phys. Rev. A **62**, 023608 (2000).

[37] A. Smerzi, S. Fantoni, S. Giovanazzi, and S. R. Shenoy, Phys. Rev. Lett. **79**, 4950 (1997).

[38] M. Albiez, R. Gati, J. Fölling, S. Hunsmann, M. Cristiani, and M. K. Oberthaler, Phys. Rev. Lett. **95**, 010402 (2005).

[39] L. Khaykovich, F. Schreck, G. Ferrari, T. Bourdel, J. Cubizolles, L. D. Carr, Y. Castin, and C. Salomon, Science **296**, 1290 (2002).

[40] K. S. Strecker, G. B. Partridge, A. G. Truscott, and R. G. Hulet, Nature **417**, 150 (2002).

[41] S. Burger, K. Bongs, S. Dettmer, W. Ertmer, K. Sengstock, A. Sanpera, G. V. Shlyapnikov, and M. Lewenstein, Phys. Rev. Lett. **83**, 5198 (1999).

[42] J. Denschlag, J. E. Simsarian, D. L. Feder, C. W. Clark, L. A. Collins, J. Cubizolles, L. Deng, E. W. Hagley, K. Kelmerson, W. P. Reinhardt, S. L. Rolston, B. I. Schneider, and W. D. Phillips, Science **287**, 97 (2000).

[43] P. G. Kevrekidis, G. Theocharis, D. J. Frantzeskakis, and B. A. Malomed, Phys. Rev. Lett. **90**, 230401 (2003).

[44] F. Kh. Abdullaev, A. M. Kamchatnov, V. V. Konotop, and V. A. Brazhnyi, Phys. Rev. Lett. **90**, 230402 (2003).

[45] T. G. Vaughan, K. V. Kheruntsyan, and P. D. Drummond, Phys. Rev. A **70**, 063611 (2004).

[46] M. Matuszewski, E. Infeld, B. A. Malomed, and M. Trippenbach, Phys. Rev. Lett. **5**, 050403 (2005).

[47] T. Karpiuk, M. Brewczyk, S. Ospelkaus-Schwarzer, K. Bongs, M. Gajda, K. Rzążewski, Phys. Rev. Lett. **93**, 100401 (2004).

[48] B. Eiermann, Th. Anker, M. Albiez, M. Taglieber, P. Treutlein, K.-P. Marzlin, and M. K. Oberthaler, Phys. Rev. Lett. **92**, 230401 (2004).

[49] Yu.S. Kivshar and G.P. Agrawal, *Optical Solitons: From Fibers to Photonic Crystals* (Academic Press 2003).

[50] E. Timmermans, P. Tommasini, M. Hussein, A. Kerman, Phys. Rep. **315** (1999).

[51] Y. Castin, in *Les Houches Session LXXII*, "Coherent atomic matter waves", 1999, edited by R. Kaiser, C. Westbrook and F. David, (Springer-Verlag Berlin Heilderberg New York 2001).

[52] A. Marte, T. Volz, J. Schuster, S. Dürr, G. Rempe, E. G. M. van Kempen, B. J. Verhaar, Phys. Rev. Lett. **89**, 283202 (2002).

[53] V. A. Yurovsky and A. Ben-Reuven, Phys. Rev. A **70**, 013613 (2004).

[54] M. A. Karpierz, Opt. Lett. **16**, 1677 (1995).

[55] H. He, M. J. Werner, and P. D. Drummond, Phys. Rev. E **54**, 896 (1996).

[56] P. D. Drummond, K. V. Kheruntsyan, and H. He, Phys. Rev. Lett. **81**, 3055 (1998).

[57] K. Sacha and E. Timmermans, Phys. Rev. A **73**, 063604 (2006).

[58] R. Wynar, R. S. Freeland, D. J. Han, C. Ryu, and D. J. Heinzen, Science **287**, 1016 (2000).

[59] N. R. Claussen, S. J. J. M. F. Kokkelmans, S. T. Thompson, E. A. Donley, E. Hodby, and C. E. Wieman, Phys. Rev. A **67**, 060701(R) (2003).

[60] K. Xu, T. Mukaiyama, J. R. Abo-Shaeer, J. K. Chin, D. E. Miller, and W. Ketterle, Phys. Rev. Lett. **91**, 210402 (2003).

[61] J. L. Roberts, N. R. Claussen, S. L. Cornish, and C. E. Wieman, Phys. Rev. Lett. **85**, 728 (2000).

[62] E. Braaten and H.-W. Hammer, Phys. Rev. Lett. **87**, 160407 (2001).

[63] B. D. Esry, C. H. Greene and J. P. Burke Jr., Phys. Rev. Lett. **83**, 1751 (1999).

[64] V. A. Yurovsky and A. Ben-Reuven, Phys. Rev. A **67**, 050701 (2003).

[65] G. Theocharis, P. Schmelcher, P. G. Kevrekidis, and D. J. Frantzeskakis, Phys. Rev. A **72**, 033614 (2005).

[66] M. H. Anderson, J. R. Ensher, M. R. Matthews, C. E. Wieman, and E. A. Cornell, Science **269**, 198 (1995).

[67] K. B. Davis, M. -O. Mewes, M. R. Andrews, N. J. van Druten, D. S. Durfee, D. M. Kurn, and W. Ketterle, Phys. Rev. Lett. **75**, 3969 (1995).

[68] C. C. Bradley, C. A. Sackett, and R. G. Hulet, Phys. Rev. Lett. **78**, 985 (1997).

[69] C. J. Myatt, E. A. Burt, R. W. Ghrist, E. A. Cornell, and C. E. Wieman, Phys. Rev. Lett. **78**, 586 (1997).

[70] J. Stenger, S. Inouye, D. M. Stamper-Kurn, H.-J. Miesner, A. P. Chikkatur, and W. Ketterle, Nature **396**, 345 (1998).

[71] D. M. Stamper-Kurn, H.-J. Miesner, A. P. Chikkatur, S. Inouye, J. Stenger, and W. Ketterle, Phys. Rev. Lett. **83**, 631 (1999).

[72] M. Lewenstein, A. Sanpera, V. Ahufinger, B. Damski, A. Sen, U. Sen, Adv. in Phys. **56**, 243 (2007).

[73] G. Modugno, M. Modugno, F. Riboli, G. Roati, and M. Inguscio, Phys. Rev. Lett. **89**, 190404 (2002).

[74] K. Günter, T. Stöferle, H. Moritz, M. Köhl, and T. Esslinger, Phys. Rev. Lett. **96**, 180402 (2006).

[75] S. Ospelkaus, C. Ospelkaus, O. Wille, M. Succo, P. Ernst, K. Sengstock, and K. Bongs, Phys. Rev. Lett. **96**, 180403 (2006).

[76] D. S. Hall, M. R. Matthews, C. E. Wieman, and E. A. Cornell, Phys. Rev. Lett. **81**, 1543 (1998).

[77] A. Sinatra, P. O. Fedichev, Y. Castin, J. Dalibard, and G. V. Shlyapnikov, Phys. Rev. Lett. **82**, 251 (1999).

[78] D. S. Hall, M. R. Matthews, J. R. Ensher, C. E. Wieman, and E. A. Cornell, Phys. Rev. Lett. **81**, 1539 (1998).

[79] T.-L. Ho and V. B. Shenoy, Phys. Rev. Lett. **77**, 3276 (1996).

[80] B. D. Esry, C. H. Greene, J. P. Burke, Jr., and J. L. Bohn, Phys. Rev. Lett. **78**, 3594 (1997).

[81] H. Pu and N. P. Bigelow, Phys. Rev. Lett. **80**, 1130 (1998).

[82] H. Pu and N. P. Bigelow, Phys. Rev. Lett. **80**, 1134 (1998).

[83] B. D. Esry and C. H. Greene, Phys. Rev. A **59**, 1457 (1997).

[84] M. Trippenbach, K. Góral, K. Rzążewski, B. Malomed, Y. B. Band, J. Phys. B **33**, 4017 (2000).

[85] F. Riboli and M. Modugno, Phys. Rev. A **65**, 063614 (2002).

[86] A. A. Svidzinsky and S. T. Chui, Phys. Rev. A **67**, 053608 (2003).

[87] Ph. Nozieres and D. Pines, *The Theory of Quantum Liquids*, (Addison Wesley, New York, 1990), Vol.II; A.L. Fetter, Ann. Phys. (N.Y.), **70**, 67 (1972).

[88] M. Lewenstein and L. You, Phys. Rev. Lett. **77**, 3489 (1996).

[89] Y. Castin and R. Dum, Phys. Rev. A **57**, 3008 (1998).

[90] C. W. Gardiner, Phys. Rev. A **56**, 1414 (1997);

[91] M. D. Girardeau Phys. Rev. A **58**, 775 (1998).

[92] J. Dziarmaga and K. Sacha, Phys. Rev. A **67**, 033608 (2003).

[93] D. M. Larsen, Ann. Phys. (N.Y.) **24**, 89 (1963).

[94] W. H. Bassichis, Phys. Rev. **134**, A543 (1964).

[95] A. S. Sørensen, Phys. Rev. A **65**, 043610 (2002).

[96] A. J. Leggett, Rev. Mod. Phys. **73**, 307 (2001).

[97] J. Dziarmaga and K. Sacha, J. Phys. B: At. Mol. Opt. Phys. **39**, 57 (2006).

[98] M. Rodríguez, S. R. Clark, and D. Jaksch, Phys. Rev. A **75**, 011601 (2007).

[99] J. Javanainen and S. M. Yoo, Phys. Rev. Lett. **76**, 161 (1996).

[100] M. R. Andrews, C. G. Townsend, H.-J. Miesner, D. S. Durfee, D. M. Kurn, and W. Ketterle, Science **275**, 637 (1997).

[101] Y. Shin, C. Sanner, G.-B. Jo, T. A. Pasquini, M. Saba, W. Ketterle, D. E. Pritchard, M. Vengalattore, and M. Prentiss, Phys. Rev. A **72**, 021604(R) (2005).

[102] Y. Castin and J. Dalibard, Phys. Rev. A **55**, 4330 (1997).

[103] A. Dragan and P. Ziń, Phys. Rev. A **76**, 042124 (2007).

[104] J. Chwedeńczuk, P. Ziń, K. Rzążewski, and M. Trippenbach, Phys. Rev. Lett. **97**, 170404 (2006).

[105] J. Dziarmaga, Z. P. Karkuszewski and K. Sacha, J. Phys. B: At. Mol. Opt. Phys. **36**, 1217 (2003).

[106] E. V. Goldstein and P. Meystre, Phys. Rev. A **55**, 2935 (1997).

[107] C. P. Search, A. G. Rojo, and P. R. Berman, Phys. Rev. A **64**, 013615 (2001).

[108] P. Tommasini, E. J. V. de Passos, A. F. R. de Toledo Piza, M. S. Hussein, and E. Timmermans, Phys. Rev. A **67**, 023606 (2003).

[109] E. Timmermans, Phys. Rev. Lett. **81**, 5718 (1998).

[110] A. S. Alexandrov, V. V. Kabanov, J. Phys.: Condens. Matter **14** L327 (2002).

[111] R. Gati and M. K. Oberthaler, J. Phys. B **40**, R61 (2007).

[112] S. Raghavan, A. Smerzi, S. Fantoni, and S. R. Shenoy, Phys. Rev. A **59**, 620 (1999).

[113] E. A. Ostrovskaya, Y. S. Kivshar, M. Lisak, B. Hall, F. Cattani, and D. Anderson, Phys. Rev. A 61, 031601(R) (2000).

[114] J. R. Anglin, P. Drummond, and A. Smerzi, Phys. Rev. A **64**, 063605 (2001).

[115] M. Saba, T. A. Pasquini, C. Sanner, Y. Shin, W. Ketterle, and D. E. Pritchard, Science **307**, 1945 (2005).

[116] R. W. Spekkens and J. E. Sipe, Phys. Rev. A **59**, 3868 (1999).

[117] L. Pitaevskii and S. Stringari, Phys. Rev. Lett. **87**, 180402 (2001).

[118] R. Gati, B. Hemmerling, J. Folling, M. Albiez, and M. K. Oberthaler, Phys. Rev. Lett **96**, 130404 (2006).

[119] C. Orzel, A. K. Tuchman, M. L. Fenselau, M. Yasuda and M. A. Kasevich, Science **291**, 2386 (2001).

[120] J. Javanainen and M. Yu. Ivanov, Phys. Rev. A **60**, 2351 (1999).

[121] T. Schumm, S. Hofferberth, L. M. Andersson, S. Wildermuth, S. Groth, I. Bar-Joseph, J. Schmiedmayer and P. Kruger, Nature Physics **1**, 57 (2005).

[122] G.-B. Jo, Y. Shin, S. Will, T. A. Pasquini, M. Saba, W. Ketterle, D. E. Pritchard, M. Vengalattore, and M. Prentiss, Phys. Rev. Lett. **98**, 030407 (2007).

[123] G. J. Milburn, J. Corney, E. M. Wright and D. F. Walls, Phys. Rev. A **55**, 4318 (1997).

[124] K. W. Mahmud, J. N. Kutz, and W. P. Reinhardt, Phys. Rev. A **66**, 063607 (2002).

[125] E. Infeld, P. Ziń, J. Gocałek and M. Trippenbach, Phys. Rev. E **74**, 026610 (2006).

[126] P. Ziń, E. Infeld, M. Matuszewski, G. Rowlands and M. Trippenbach, Phys. Rev. A **73**, 022105 (2006).

[127] J. I. Cirac, M. Lewenstein, K. Mölmer, and P. Zoller, Phys. Rev. A **57**, 1208 (1998).

[128] D. Gordon and C. M. Savage, Phys. Rev. A **59**, 4623 (1999).

[129] D. A. R. Dalvit, J. Dziarmaga, and W. H. Żurek, Phys. Rev. A **62**, 013607 (2000).

[130] D. Jaksch, C. Bruder, J. I. Cirac, C. W. Gardiner, and P. Zoller, Phys. Rev. Lett. **81**, 3108 (1998).

[131] V. V. Ulyanov and O. B. Zaslavskii, Phys. Rep. **216**, 179 (1992).

[132] R. Botet and R. Jullien, Phys. Rev. B **28**, 3955 (1983).

[133] M. Girardeau, Phys. Fluids **5**, 1468 (1962).

[134] M. Girardeau, J. Math. Phys. **6**, 1083 (1965).

[135] L. D. Carr, Charles W. Clark, and W. P. Reinhardt, Phys. Rev. A **62**, 063611 (2000).

[136] R. Kanamoto, H. Saito and M. Ueda, Phys. Rev. Lett. **94**, 090404 (2005).

[137] I. Castin and C. Herzog, arXiv:cond-mat/0012040v2.

[138] R. Kanamoto, H. Saito, and M. Ueda, Phys. Rev. A **73**, 033611 (2006).

[139] F. Takano, Phys. Rev. **123**, 699 (1961).

[140] H. T. Ng, C. K. Law, and P. T. Leung, Phys. Rev. A **68**, 013604 (2003).

[141] J. Chen, Y. Guo, H. Cao and H. Song, arXiv:quant-ph/0507191v1 (2005).

[142] H. T. Ng and P. T. Leung, Phys. Rev. A **71**, 013601 (2005).

[143] W. Li, W. Yang, X. Xie, J. Li and X. Yang, J. Phys. B: At. Mol. Opt. Phys. **39**, 3097 (2006).

[144] F. M. Cucchietti and E. Timmermans, Phys. Rev. Lett. **96**, 210401 (2006).

[145] R. M. Kalas and D. Blume, Phys. Rev. A **73**, 043608 (2006).

[146] M. Bruderer, W. Bao and D. Jaksch, Europhys. Lett. **82**, 30004 (2008).

[147] D. C. Roberts and S. Rica, Phys. Rev. Lett. **102**, 025301 (2009).

[148] P. Öhberg and S. Stenholm, Phys. Rev. A **57**, 1272 (1998).

[149] D. Gordon and C. M. Savage, Phys. Rev. A **58**, 1440 (1998).